PNNL-13681

Pacific Northwest National Laboratory
Operated by Battelle for the U.S. Department of Energy

Evaluation and Testing of Noble Metals Surrogates

S.K. Sundaram
A.R. Cooper
J. Holbrock
B. MacIsaac
C. Tschauner

September 2002

Prepared for the U.S. Department of Energy
under Contract DE-AC06-76RL01830

PACIFIC NORTHWEST NATIONAL LABORATORY
operated by
BATTELLE MEMORIAL INSTITUTE
for the
UNITED STATES DEPARTMENT OF ENERGY
under Contract DE-AC06-76RLO 1830

Printed in the United States of America

Available to DOE and DOE contractors from the
Office of Scientific and Technical Information, P.O. Box 62, Oak Ridge, TN 37831;
prices available from (615) 576-8401.

Available to the public from the National Technical Information Service,
U.S. Department of Commerce, 5285 Port Royal Rd., Springfield, VA 22161

PNNL-13681

Evaluation and Testing of Noble Metals Surrogates

S. K. Sundaram
Brett C. MacIsaac
Alan R. Cooper
Candice H. Trader
Jeremy J. Holbrook
Pacific Northwest National Laboratory, Richland, WA 99352

September 2002

Prepared for the U.S. Department of Energy
under Contract DE-AC06-76RLO 1830.

Pacific Northwest National Laboratory
Richland, Washington 99352

Abstract

This report summarizes the results of testing and evaluation of noble metal surrogates that will support testing of noble metals in melters. The candidate system, potential surrogates, model glass systems, and test conditions have been chosen based on the existing reported data in literature as well as expertise existing at various sites, thermodynamics, physical properties, and cost of materials. The methodology involves testing interaction of RuO_2 and WO_3 and other surrogates in the test melt followed by characterization of the bulk glass and oxide-glass melt interfaces. The report explains different techniques used for studying settling, crystallization, rheology, and partitioning of noble metals or surrogates or spinel phases in the selected systems. The report presents and discusses how these results support the selection of the suitable surrogate for RuO_2. Finally the report concludes with identification of the best-suited surrogate (solubility and redox surrogate WO_3 and conductivity surrogate Cr_2O_3) proposed and makes suitable recommendations for the follow up melter test activities.

Summary

The formation and settling of noble metals in high-level waste (HLW) glass melts poses a major challenge to the vitrification technology. Precipitation of noble metals in these joule-heated melters can lead to operational difficulties and premature failure of the melter through electrical shorting and enhanced corrosion of the electrodes. Additionally, the noble metals are known to act as nucleation sites for the precipitation and growth of spinel (crystalline) phases, which in turn will settle to the bottom of the melter and cause the viscosity of the melt to increase in that region. Use of actual noble metals and compounds for melter testing is not cost effective. Pacific Northwest National Laboratory (PNNL) and Savannah River Technology Center (SRTC) have undertaken efforts to identify suitable surrogates for noble metals to facilitate extensive melter testing that will provide key processing data. This report summarizes the results of the experimental testing evaluation of noble metal surrogates performed at PNNL.

Initial selection of model glass test systems, noble metals, potential surrogates, and test conditions was done based on the existing data and expertise at DOE various sites (West Valley, Savannah River, and Hanford), thermodynamics, physical properties, and cost of materials. A simplified version of HLW glass (MS-7) and a modified neutralized caustic acid waste (NCAW) glass compositions were used in this study. Overview of existing literature on noble metals in waste melts and melter testing indicated that RuO_2 was the most commonly detected phase present. Hence, the present testing was focused at RuO_2 and its potential suitable surrogates. The potential surrogates considered and studied were WO_3, Cr_2O_3, $NiCr_2O_4$, and Inconel 600. From chemical stability and density perspectives, the W-O system showed the promise of serving as a surrogate for Ru as well as RuO_2. WO_2 (12.11 g/cm^3) could act as a surrogate for Ru (12.30 g/cm^3) under reducing conditions. Alternatively, WO_3 (7.20 g/cm^3) could act as a surrogate for RuO_2 (6.97 g/cm^3) under oxidizing conditions. Therefore, the surrogate testing was focused at WO_3. The testing included: 1) double-crucible settling study, 2) viscosity and rheology, 3) crystallization study, 4) high temperature optical microscopy, and 5) partition study.

Double crucible settling studies indicated more spinel crystals formed at 950ºC and started settling at 1000ºC, with RuO_2 as well as WO_3 in MS-7 glass. Figure S.1 compares the thin section of the inner crucibles with RuO_2 and WO_3 heat-treated at 900-1000ºC for 19-13h. SEM, EDS, and XRD data have supported this observation. XRD data confirmed formation of Trevorite ($NiFe_2O_4$) phase. No other major phase was detected. Ru was found to partition readily in the spinel phase, as compared to W.

Figure S.1. RuO_2 vs. WO_3 – Temperature Effect (0.5 wt.% in MS-7)

Crystallization study (heat-treatment followed by XRD measurements) showed that addition (0.5 wt.%) of RuO_2 or WO_3 to MS-7 resulted in formation of Trevorite. Residual undissolved RuO_2 was detected in the glass containing RuO_2. No WO_3 was detected by XRD in the glass containing WO_3. The difference was attributed to higher solubility of WO_3 in the glass, as compared to RuO_2.

An order of magnitude increase in viscosity values was observed as addition of $NiCr_2O_4$ (one of potential surrogates studied in this project) increased from 1 wt.% to 10 wt.% in modified NCAW glass melts, as shown in Figure S.2. This also resulted in an increase in shear stress of rotating spindle in rheology testing. This data clearly established the consequences of increased spinel formation and accumulation in this system.

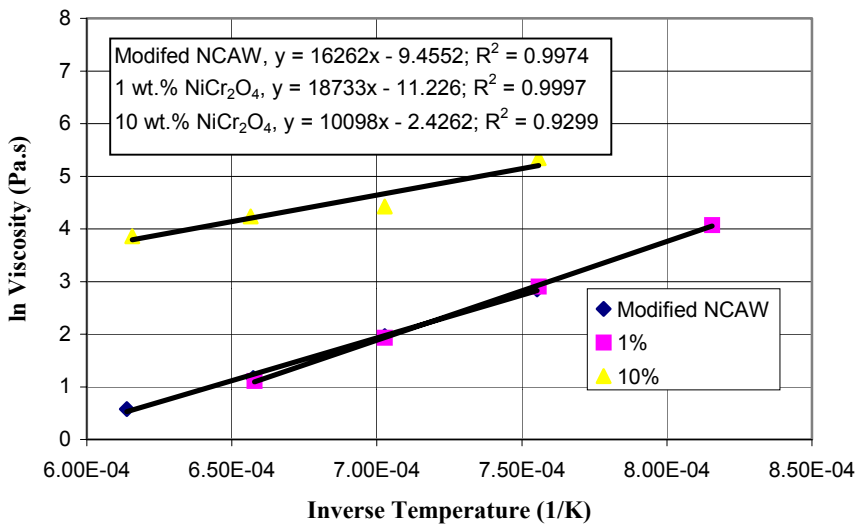

Figure S.2. Effect of Addition of $NiCr_2O_4$ on Viscosity of the Modified-NCAW Melt

High temperature optical microscopy results showed floating nodular aggregates of RuO_2 at higher temperature (> 900ºC) due to its insolubility in the MS-7 melt (Figure S.3 (a)). On the contrary, $NiCr_2O_4$ dissolved completely in the test melt (Figure S.3 (b)).

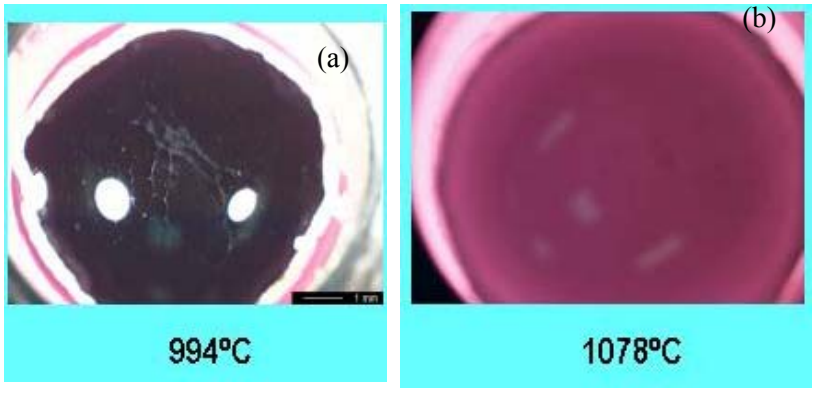

Figure S.3. High Temperature Optical Microscopy of (a) RuO_2 and (b) $NiCr_2O_4$ in MS-7 Melt

Partitioning study of noble metal species (Ru and RuO_2) and the surrogate species (W and WO_3) between spinel (nonstoichiometric $MgAl_2O_4$) and model glass melt (MS-7) indicated striking similarity between RuO_2 and WO_3, as shown in Figure S.4 (a) and (b), respectively. The sequence of the events was:

1) The glass melt reacted with the spinel forming a reaction layer at the spinel-glass interfacial region. Some Ru or W partitioned in spinel in this reaction layer.
2) Excess Ru or W remained near the interfacial region and in bulk glass.
3) Spinel segments began to dislodge from the bulk spinel, drifted into the melt and eventually dissolved into the glass melt.
4) Some Ru-containing and W-rich regions remained in the glass side of the interfacial region.
5) Spinel (either $MgAl_2O_4$ or Trevorite or a combination of these two) recrystallized in the glass melt.

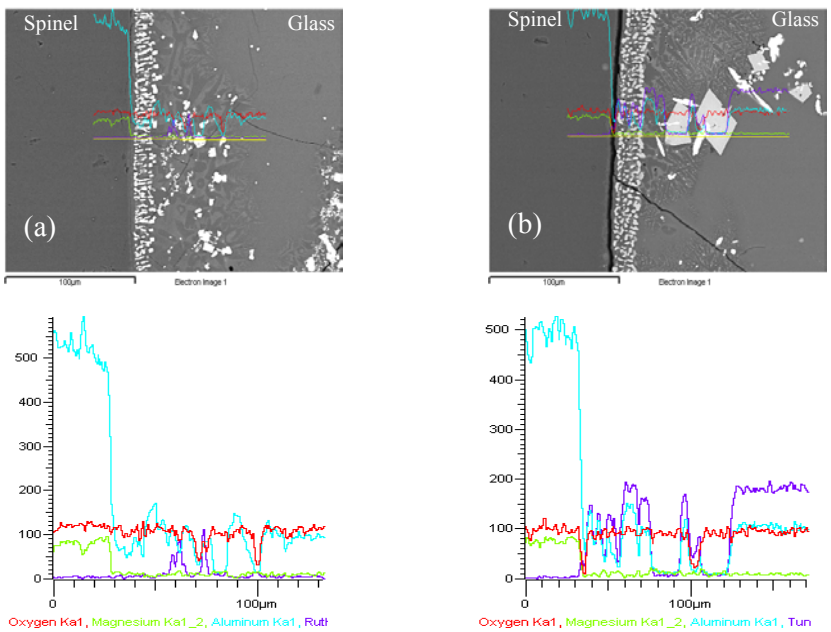

Figure S.4. SEM-EDS of (a) RuO_2 and (b) WO_3 in MS-7 Melt (0.5 wt.%, 1000ºC, 23h)

Top: Back-scattered SEM image with line EDS superimposed, Bottom: Line EDS scan

AC conductivity data clearly indicated that Cr_2O_3 showed conductivity data closely matched that of RuO_2, as shown in Figure S.5. Cr_2O_3 was recommended as a conductivity surrogate.

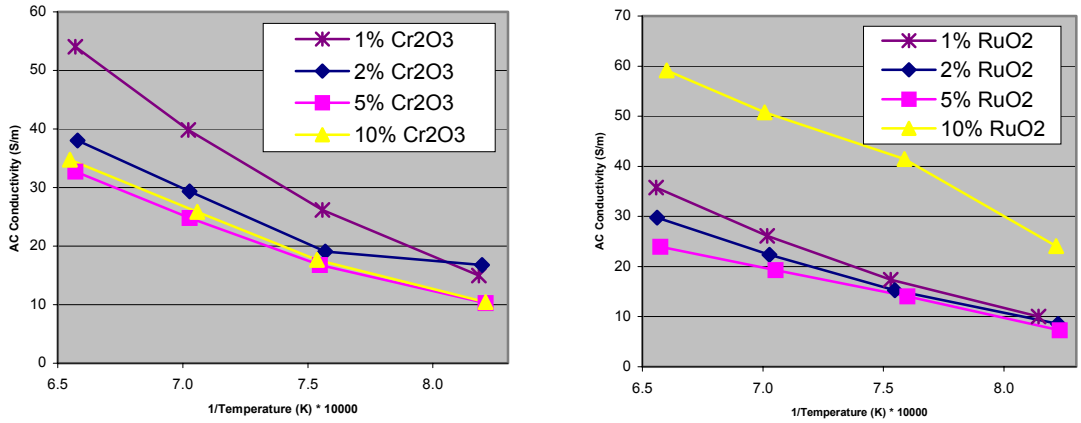

Figure S.5. AC conductivity of Cr_2O_3 (left) and RuO_2 (right)

From the thermodynamic stability and density perspectives, RuO_2 and WO_3, showed a good match. Based on our results on these aspects, WO_3 was recommended as a chemical surrogate for RuO_2. A research-scale melter (RSM) test was also recommended before testing the surrogate in an engineering scale melter.

Glossary

η	viscosity
ASTM	American Society for Testing and Materials
DOE	U.S. Department of Energy
DWPF	Defense Waste Processing Facility
EA	Environmental Assessment
EDS	energy dispersive spectroscopy
FY	Fiscal Year
HAW	high-activity waste
HLW	high-level waste
NCAW	neutralized caustic acid waste
OES	optical emission spectroscopy
RSM	research-scale melter
SEM	scanning electron microscopy
T	temperature
TFA	Tanks Focus Area
XRD	X-ray diffraction

Acknowledgments

The authors would like to acknowledge Denny Bickford for technical guidance, Joe Perez and Pavel Hrma for useful discussion, Michael Schweiger and Jarrod Crum for helping the students Candice Trader, Alan Cooper, and Jeremy Holbrook, Craig Habeger for particle size measurements, Jim Coleman for SEM-EDS work, and Nat Canfield and Dave McCready for XRD work. The authors would also like to acknowledge Ron Goles for technical review, Nancy Foote for prompt editing, and William Holtzscheiter for management and guidance. This study was funded by the Department of Energy's Office of Science and Technology through the Tanks Focus Area. Pacific Northwest National Laboratory is operated for the U.S. Department of Energy by Battelle under Contract DE-AC06-76RLO 1830.

Contents

Figures

Tables

1.0 Introduction

The noble metals rhodium (Rh), ruthenium (Ru), and palladium (Pd) are fission products that partition to the waste sludges after the acid wastes from the processing of spent fuel are made alkaline. In some cases these metals can approach concentrations on the order of 0.1 mass % in the waste sludges, while the solubilities of the metal or metal oxide in glass melts are reported to be about 0.01 mass %. The actual solubility in the melt depends on the glass composition, redox, and temperature of the melt. The densities of the metal and oxides are substantially higher than the glass melt [~ $10 \cdot 10^3$ kg/m^3 vs. $2.5 \cdot 10^3$ kg/m^3] and tend to settle to the bottom of the melter. If the accumulation of these metals becomes great enough, a low resistance path for electrical current is established and an electrical short results in premature failure of the melter if no method is present to remove the accumulated metals. This early failure has been a concern at the Savannah River Site, West Valley, and Hanford. In the case of West Valley operations, the power fluctuations observed have been attributed to noble metals accumulation in the melter. A sludge sampler was designed and deployed by Pacific Northwest National Laboratory (PNNL) team.

Actual failure of a glass melter at Dessel, Belgium was attributed to noble metal accumulation and subsequent shorting of the electrodes. Additionally, these noble metals and metal oxides usually precipitate as very fine particles, which serve as excellent nucleation sites for other species in the glass melt that are at their solubility limits, e.g. spinels. Solubility limits of oxides are presented in Figure 1.1. It is known the solubility of noble metals in the glass melts is small (shown as 0 in Figure 1.1). But, solubility studies of noble metals in waste glass melts are limited.

Figure 1-1. Solubility Limits of Oxides

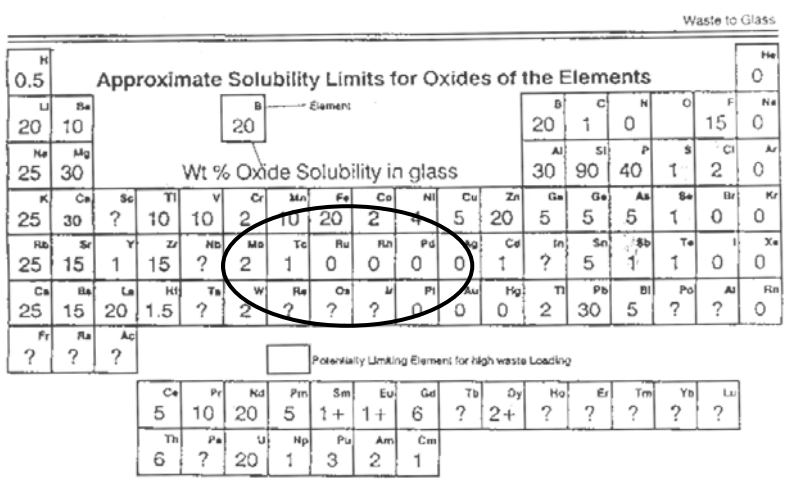

While fundamental understanding of dissolution and structural incorporation of noble metals is still mostly qualitative in nature, significant level of testing has been done in melters in the USA and other countries. The melter data are valuable in the sense they emulate conditions that are close to the actual melter processing conditions and they also provide guidelines for design and scale-up studies. Therefore, it is worthwhile to conduct melter tests to collect necessary processing data.

Use of actual expensive noble metals in melter tests will result in significant impact on cost of tests. Additionally, the noble metals may not be available in a timely manner for testing. Therefore, one

needs to use inexpensive surrogates for noble metals. In response to this need, the Tanks Focus Area (TFA) supports the present effort. The main objectives of the present task are: 1) Identify potential noble metals surrogates, 2) Evaluate their performances in representative waste glass melts in the laboratory, and 3) Recommend suitable surrogates for testing in melters. This report summarizes the results of the task.

2.0 Identification and Evaluation of Surrogates

A suitable noble metals surrogate needs to meet stringent requirements. Table 2.1 shows a summary of the properties of the noble metals. In identifying and evaluating a surrogate, attempt will be taken to meet as many requirements as possible. We have listed the basic requirements of a suitable noble metals surrogate here:

1. Density of the surrogate
2. Thermodynamic stability of the surrogate
3. Solubility of the surrogate in glass melts
4. Partitioning of the surrogate between glass and crystalline phases
5. Chemical interaction of the surrogate with other waste constituents
6. Interaction of the surrogate with other crystalline phases (e.g., spinels)
7. Availability
8. Cost

Given the above list of requirements, it is less likely there exists a surrogate that meets all these requirements. Our identification and evaluation processes are described in the following sections. The requirement 4 is briefly addressed. The requirements 5 and 6 have not been considered for simplicity and budget considerations.

2.1 Summary of Past Melter Data

A summary of past melter testing data is presented in this section to establish the state of knowledge in this area as well as to determine the technical scope of the present task. Three major melter test campaigns testing noble metals have been completed in the past: 1) PNNL test, 2) German melter test, and 3) Integrated DWPF (Defense Waste Processing Facility) Melter System (IDMS). Noble metals have been included in glass development studies since some of the earliest waste solidification and vitrification work at PNNL (Sundaram and Perez, 2000). The insolubility of noble metals in glasses was observed at those early stages and was also known from the literature; however, the effect this insolubility could have on melter operation was not known. Early works in 1970s included crucible and laboratory-scale tests. Since then, five major studies, gradient furnace testing (GFT), research scale melter (RSM) testing, engineering scale melter (ESM) testing, modeling, and engineering analysis, were completed at PNNL. German melter tests (1980s and 1990s) showed that the accumulation of noble metals could be greatly decreased by increasing the slope of the melter floor. When using a flat-bottom melter with a bottom drain, approximately 65 percent of the noble metals fed were retained in the melter. However, with a 75º/60º sloped melter floor, net deposits of noble metals were not detected by measuring changes in electrical resistance at the end of each pour through the bottom drain. After comparing two systems for glass pouring, the bottom drain was found to be more efficient than the overflow system in discharging noble metals. For Ru, retention was 10.3 percent using the bottom drain and 41.4 percent with the overflow system. Air sparging was also tested to determine its effects on noble metals accumulation. With a melter having 45º-sloped floor, agitating the molten glass resulted in a decrease of Ru retention from 38 percent to 24 percent, and a decrease of Pd retention from 45 percent to 3 percent. However, in tests with a 75º/60º sloped floor, it was found that air sparging was not effective enough at suspending noble metal particles to allow discharge through the overflow system. A thorough investigation of the behavior of noble metal deposits and a complete analysis of the individual particles was also performed. It was concluded that the removal of Rh from the simulant waste stream had no effect on the size and sedimentation of other noble metals.

The IDMS was designed as a pilot-scale test facility for the DWPF. Before testing with the IDMS, two short-term noble metals campaigns with a 1/100th scale mini-melter revealed a need for extended noble metals testing. Numerous test runs with the IDMS melter addressed the designs of the DWPF feed preparation system, offgas system, and the melter itself. The IDMS engineering-scale melter is prototypic of the DWPF melter. It was designed with a melt surface area of 0.29 m^2 (approximately 1/9th of the DWPF surface area), and a melt volume of 0.20 m^3. The IDMS has conducted a total of 16 noble metal-related runs with four different types of wastes sludges (Blend, HM, PUREX, and NCAW) containing various amounts of noble metals. Some of the sludge compositions were modified in order to judge the effects of components such as mercury and nitrite (Hutson et al. 1991; Hutson 1992; Hutson 1993).

Table 2.2 summarizes the noble metals found in various melter runs. The summary clearly indicates that the most commonly found species is RuO_2 in the melter. Ru has always been found in association with RuO_2 and other noble metals. Therefore, Ru-RuO_2 system was studied for surrogate evaluation and testing.

2.2 Density

As the settling is a physical phenomenon, density criterion is first considered. In order to closely simulate and study the suspension and settling characteristics, the surrogate must have density values comparable to that of the noble metal or oxide. The density of RuO_2 is 6.97 g/cm^3 and Ru, 12.30 g/cm^3.

The down-selection was done in two or three steps. First the elements and compounds with density values within ± 10% of the density values of Ru and RuO_2 were listed. The candidates were evaluated for hazards and stability. The next stage was to narrow the range down to ± 5% and the evaluation was repeated. In the case of Ru, third stage narrowed the range down to ± 3%. The results are summarized in Tables 2.3 (RuO_2) and 2.4 for Ru. WO_3 (7.20 g/cm^3) and WO_2 (12.11 g/cm^3) were selected as surrogates for RuO_2 and Ru, respectively.

Table 2-1 Properties of Noble Metals

Property	Iron	Cobalt	Nickel	Ruthenium	Rhodium	Palladium	Osmium	Iridium	Platinum
Atomic Weight	55.845	58.9332	58.6934	101.07	102.9055	106.42	190.23	192.217	195.087
mp (^{o}C)	1538	1495	1455	2334	1964	1554.9	3033	2446	1768.4
bp (^{o}C)	2861	2927	2913	4150	3695	2963	5012	4428	3825
Density (g/cm^3)	7.87	8.86	8.9	12.1	12.4	12	22.59	22.5	21.5
Density (g/cm^3) @ mp	6.98	7.75	7.81	10.65	10.7	10.38	20	19	19.77
Heat Capacity (J/g K) @ 25°C	0.449	0.421	0.444	0.328	0.243	0.246	0.13	0.131	0.133
Thermal Conductivity (cal/s.cm.^{o}C)	0.19	0.1653	0.198		0.36				
Spec. Heat (J/g K)	0.449	0.421	0.444	0.238	0.243	0.246	0.13	0.131	0.133
Enthalpy of Fusion (kJ/mol)	13.81	16.2	17.48	38.59	26.59	16.74	57.85	41.12	22.17
Heat of Vaporization (kcal/g-atom)	84.6	1500	91	148	127	90	162	152	122
Electrical Resistivity ($10^{-8}\Omega$) @273K	8.57	5.6	6.16	7.1	4.3	9.78	8.1	4.7	9.6
Electronegativity (Paulings)	1.83	1.88	1.91	2.2	2.28	2.2	2.2	2.2	2.2
Covalent Radius (Angstroms)	1.17	1.16	1.15	1.25	1.25	1.28	1.26	1.27	1.3
Linear Coefficient of Expansion (k^{-1})	11.8×10^{-6}	13.0×10^{-6}	13.4×10^{-6}	6.4×10^{-6}	8.2×10^{-6}	11.8×10^{-6}	5.1×10^{-6}	6.4×10^{-6}	8.8×10^{-6}
Electrical Resistivity ($\mu\Omega$-cm)	9.71	6.34	6.844	7.2	4.5	9.93	8.12	5.11	9.85
Crystal Structure	cubic, bc	hexagonal	cubic, fc	hexagonal	cubic, fc	cubic, fc	hexagonal	cubic, fc	cubic, fc

CRC Handbook, 81st Edition
Alfa Aesar: Research Chemicals, Metals and Materials……1997-98

Table 2-2. Summary of Melter Tests

Metal or Compound	PNNL Findings (1)		German Findings (2)		IDMS Findings (3)	
	Particle Size	Composition	Particle Size	Composition	Particle Size	Composition
Ru	Submicron, spheres	30 -70% retention, present as RuO_2	2.0 - 5.0 micron spheres	11 wt%		Between 0.16-7.74 wt. %, present as
Rh	<10 micron, spheres	1 to 2 microns	1.5 - 2.0 micron spheres	6 wt%		Between 0.026-1.21 wt%
Pd	Submicron to 10 micron, spheres	1.0 wt%	1.5 - 2.0 micron spheres	5 wt%		Between 0.031-0.17 wt%
RuO_2	<10 micron, needles	1.4 wt%	2.0 - 5.0 micron, needles	0.05 - 0.1 wt%,		Between 0.16-7.74 wt%
Spinels	2 to 4 micron, cubic					Between 27-66 wt. %, Cr-rich

(1) - Vitrification studies conducted at PNL (Jensen et al. 1983) from "Preliminary Melter Performance Assessment Report", PNL-9822/UC-721.
(2) - From "Virtification of Noble Metals Containing NCAW Simulant with an Engineering Scale Melter (ESM)" (W. Grunwald et al. 1993).
(3) - From "Inspection and Analysis of the Integrated DWPF Melter System (IDMS) After Seven Years of Continuous Operation", WSRC-MS-99-0036 (C.M. Jantzen and D. Lambert, 1994).

Table 2-3. Potential Surrogates For RuO_2 Based On Density (6.97 g/cm^3± 10%)

Metal or Compound	Density (g/cm^3)
Americium (III) Bromide	6.85
Americium (IV) Fluoride	7.23
Antimony	6.68
Antimony (III, V) Oxide	6.64
Arsenic (III) Telluride	6.50
Barium Stannate	7.24
Bismuth Basic Carbonate	6.86
Bismuth Oxychloride	7.72
Bismuth Selenide	7.50
Bismuth Sulfide	6.78
Bismuth Telluride	7.74
Cadmium Antimonide	6.92
Cadmium Iodide	6.48
Cadmium Titanate	6.50
Cerium	6.77
Cerium (III) Carbide	6.90
Cerium (IV) Oxide	7.65
Chromium Arsenide	7.04
Chromium Carbide	6.68
Chromium Nitride	6.80
Chromium (III) Telluride	7.00
Cobalt Arsenide ($CoAs_2$)	7.20
Cobalt Arsenide ($CoAs_3$)	6.84
Cobalt Boride (CoB)	7.25
Cobalt (II) Selenide	7.65
Copper (I) Selenide	6.84
Copper (II) Telluride	7.09
Copper (II) Tungstate	7.50
Dysprosium Boride	6.98
Dysprosium (III) Hydride	7.10
Erbium Boride	7.00
Erbium Silicide	7.26
Erbium Telluride	7.11
Europium (III) Oxide	7.42
Gadolinium (III) Oxide	7.07
Halfnium Fluoride	7.10
Halfnium Silicide	7.60
Holmium Fluoride	7.66
Holmium Silicide	7.10
Indium (III) Oxide	7.18
Indium (III) Iodide	7.40
Iron Boride (Fe_2B)	7.30
Iron Boride (FeB)	7.00
Iron Phosphide	6.80
Iron Tungstate	7.51
Lead (II) Bromide	6.69
Lead (II) Carbonate	6.60
Lead (II) Chloride Fluoride	7.05
Lead (II) Hydroxide	7.59
Lead (II) Molybdate	6.70
Lead (II) Oxide Hydrate	7.41
Lead (II) Phosphate	7.01
Lead (II) Selenite	7.00
Lead (II) Sulfide	7.60
Lead (IV) Fluoride	6.70
Lutetium Boride	7.00
Magnesium Tungstate	6.84
Manganese	7.30
Manganese Antimonide (MnSb)	6.90
Manganese Antimonide (Mn_2Sb)	7.00
Manganese Boride	7.20
Manganese Carbide	6.89
Manganese Tungstate	7.20
Mercury (I) Chloride	7.16
Molybdenum Phosphide	7.34
Molybdenum (IV) Selenide	6.90
Neodymium	7.01
Neodymium Oxide	7.24
Neodymium Telluride	7.00
Nickel Bromide	7.13
Nickel Phosphide	7.33
Nickel Selenide	7.20
Niobium (II) Oxide	7.30
Praseodymium Oxide	6.90
Praseodymium Telluride	7.00
Promethium	7.26
Rhenium (IV) Fluoride	7.49
Rhodium (IV) Oxide	7.20
Samarium	7.52
Samarium (III) Telluride	7.31
Silver (I) Oxide	7.20
Silver (I) Sulfide	7.23
Tantalum Aluminide	7.02
Tantalum (IV) Sulfide	6.86
Tellurium Dichloride	6.90
Thallium (I) Carbonate	7.11
Thallium (I) Chloride	7.00
Thallium (I) Iodide	7.10
Thallium (I) Selenide	6.88
Thorium Boride	6.99
Thorium Sulfide	7.30
Tin (white)	7.27
Tin (IV) Oxide	6.85
Tungsten (VI) Oxide	**7.20 (± 5%)**
Ytterbium	6.90
Zinc	7.14
Zirconium Nitride	7.09

Pink - Soluble in H_2O or Glass Melt
Blue – Toxic
Yellow – Radioactive
Green - Non-oxide (unlikely surrogate)

Table 2-4. Potential Surrogates For Ru Based On Density (12.30 g/cm^3 ± 10%)

Metal or Compound	Density (g/cm^3)
Halfnium	13.31
Halfnium Carbide	12.20
Palladium	12.02
Tungsten Dioxide	**12.11 (± 3%)**
Americium Dioxide	11.68
Iridium Dioxide	11.67
Lead	11.34
Neptunium Dioxide	11.11
Osmium Dioxide (brown)	11.37
Plutonium Dioxide	11.46
Rhenium Dioxide	11.40
Rhodium	12.40
Tantallum Diboride	11.15
Thallium	11.85
Thorium	11.70
Uranium Diboride	12.70
Uranium Dicarbide	11.28
Uranium Hydride	10.95
Uranium Dioxide	10.96

Red - Soluble in H_2O or Glass Melt
Blue – Toxic
Yellow – Radioactive
Green - Non-oxide (unlikely surrogate)

2.3 Thermodynamic Stability

The thermodynamic calculation was performed using F∗A∗C∗T[a]. The free energy of formation of the oxides as a function of temperature is shown in Figure 2.1. WO_2 and WO_3 are relatively more stable than RuO_2 over a temperature range of 0 – 1600ºC. Note that these free energy values are for ideal states at ambient pressure. With change in the melter atmosphere, the redox equilibrium will shift. W-O system shows the promise of serving as a surrogate for Ru as well as RuO_2. As shown below, WO_2 (12.11 g/cm^3) can act as a surrogate for Ru (12.30 g/cm^3) under reducing conditions. Alternatively, WO_3 (7.20 g/cm^3) can act as a surrogate for RuO_2 (6.97 g/cm^3) under oxidizing conditions.

Reduction	↔	Oxidation
Ru (12.30 g/cm^3)	↔	RuO_2 (6.97 g/cm^3)
WO_2 (12.11 g/cm^3)	↔	WO_3 (7.20 g/cm^3)

[a] F∗A∗C∗T = Facility for the Analysis of Chemical Thermodynamics, Ecole Polytechnique, UniversitJ of MontrJal, Canada.

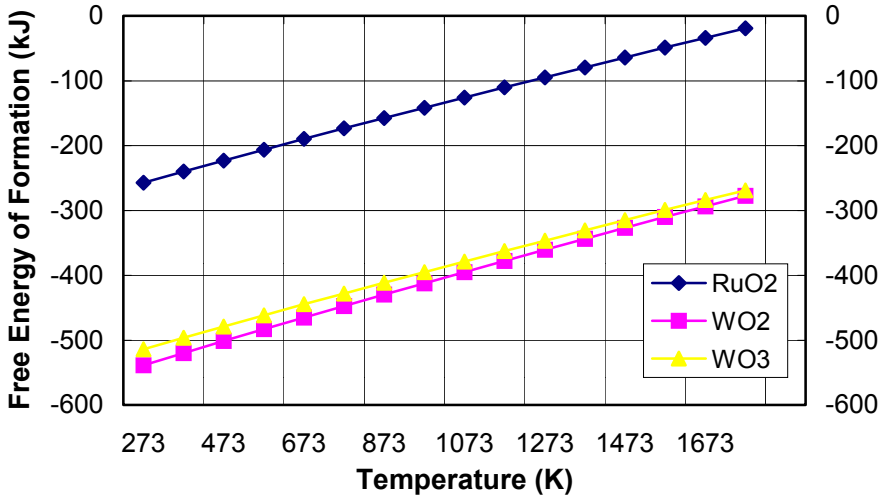

Figure 2-1. Thermodynamic Stability

2.4 Solubility

Ruthenium (Ru) and other platinum group of metals are sparingly soluble in glass-forming melts. However, measurable amounts of chemically dissolved Ru (about 100-2000 ppm) have been reported to dissolve in soda-silica glass melts (Mukerji and Biswas, 1967). The solubility appears to be enhanced with rising temperatures and higher Na_2O/SiO_2 compositional ratios. The solubility of ruthenium in phosphate glasses approaches 10 000 ppm of Ru at 1000ºC (Biswas and Mukerji, 1968). In these melts, the process by which Ru as RuO_2 goes into the melt solution has been first linked to the indirect reaction of the RuO_2 with singly bonded oxygens of the melt network.

The solubility of Ru has been then linked to the stabilization of certain oxidation states of Ru (redox chemistry) in simple glasses. Ru displays ten oxidation states in its compounds and complexes (Bailar et al., 1973). Every positive oxidation state to +8 is known as the neutral and –2 states. Absorption spectra of glasses colored by Ru indicate the presence of Ru(III) and Ru(IV) dissolved in acidic silicate glasses, Ru(IV) and Ru(VI) in basic silicate glasses, Ru(VI) and Ru(VII) in soda phosphate glasses, Ru(VI) and Ru(VI) in lead phosphate glasses as well as borophosphate glasses and Ru(III) and Ru(IV) in borosilicate glasses (Mukerji and Biswas, 1971; Mukerji, 1972). The colors of these glasses range from pink to yellow to green depending on the composition and synthesis conditions owing to the various Ru oxidation states. Electron spin resonance (ESR) data indicate the absence of Ru(V) and the presence of Ru(III) and Ru(IV) in borosilicates manufactured at 1500ºC (Mukerji, 1975). High Ru solubilities always correspond to the occurrence of Ru(VI) in the glasses, indicating that Ru(VI) is the species most easily accommodated within the glass melt structure. Schreiber and coworkers (Schreiber et al., 1986) have investigated the amount of Ru dissolved in a borosilcate glass system as a function of amount of Ru, redox additives, time, and melt temperature and atmosphere. In all the cases, the Ru solubility has been less than about 0.001 wt.%, the approximate limit of detection in the glasses. Insoluble RuO_2 has always been found in these glasses. These results have not substantiated the results by Muherji and Biswas ((Mukerji and Biswas, 1967; Biswas and Mukerji, 1968; Mukerji and Biswas, 1971; Mukerji, 1972; Mukerji, 1975).

Generally solubility is studied by dissolving the dopant in a glass melt characterizing the glass post mortem. Two somewhat different techniques used to obtain solubility of species in glass melts are: 1) the stirred crucible method (Dingwell et al., 1994) and 2) the wire loop method (Holzheid et al., 1994;

Borisov et al., 1994). The principal advantage of the stirred crucible technique is that changes in oxygen fugacity (fO_2) and temperature (or composition) can be performed in a stepwise fashion without interruption of the experiment, and the response of the samples can be monitored by taking samples at any time. This can be used to demonstrate the achievement of equilibrium by time series and by reversals both in temperature and in fO_2. However, the relatively long times needed to achieve equilibrium with this method makes its use undesirable at higher temperatures (> 1500ºC), where the time spent at temperature needs to be as short as possible to minimize the inevitable deterioration of the gas-mixing furnace under extreme conditions. Therefore, the conventional wire-loop technique is used at 1600 and 1700ºC. Ertel and coworkers (Ertel et al., 1996) have determined the solubility of tungsten (W) in a haplobasaltic melt as a function of fO_2 in the temperature range of 1300 – 1700ºC, using the above the two techniques. According to this work, W dissolves in the melt with a quadrivalent (4+) formal oxidation state over the entire range of fO_2 and temperature investigated. The solubility of W decreases strongly with increasing temperature at constant fO_2. W concentrations range form 20 ppm to 17 wt%. The solution of WO_2 in the melt may be described by Henry's Law (shown in Figure 2.2) up to remarkably high temperatures (e.g., 14 wt% at 1500ºC). In the Figure 2.2, the hatched area shows the range in which the Henry's Limit is obeyed.

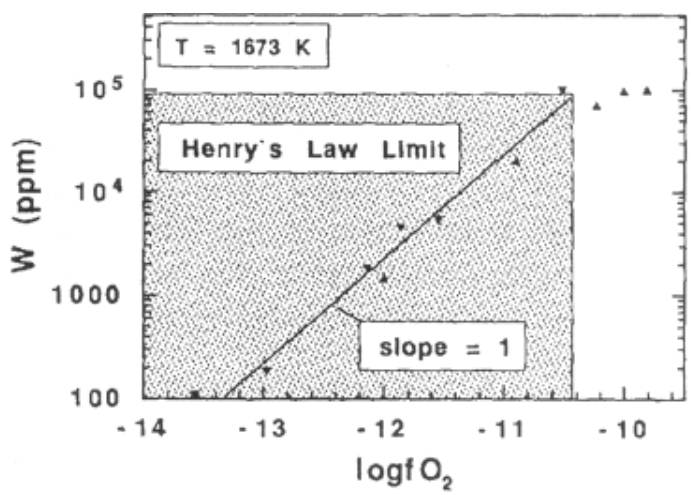

Figure 2-2. The Henry's Law Limit for W in Silicate Melt at 1400ºC (Ertel et al., 1996)

As the present task's main goal is to identify suitable surrogate for noble metals, the exact solubility of noble metals has not been determined. A systematic study of the Ru solubility in high-level waste glass compositions is needed to understand its precise role in processing HLW glass compositions.

2.5 Partitioning

Spinel phases are consistently found to be concentrators of platinum group of elements (PGE) in geochemistry. Capobianco and Drake have studied the partitioning of PGE between spinel and silicate melt. The experimental details are given elsewhere (Capobianco and Drake, 1990). The silicate melt is from the CaO-Al_2O_3-MgO-SiO_2 system. The bulk glass melt composition is temperature dependent because of the spinel capsule dissolves into the sample at higher temperature. The starting capsule material is a very non-stoichiometric spinel (approximately 90 wt% Al_2O_3, 10 wt% MgO), which at testing conditions exsolves into corundum and a spinel with less excess Al_2O_3. Table 2.5 summarizes experimentally determined spinel/melt partition coefficients for Pd, Ru, and Rh, the PGE contents of phases of interest, and experimental run conditions.

Table 2-5. Summary of Platinum-Group Element Spinel/Melt Partition Coefficients, Run Conditions, and Phase Concentrations (in ppm)

	$D^{xl/melt}$	T(ºC)	Spinel	Glass	Atmosphere
Ru	25(9)[1]	1450	7900(300)[2]	320(120)[2]	Air
	22(9)[1]	1290	5900(400)[2]	270(110)[2]	Air
Rh	78(15)[1]	1450	4300(460)[2]	55(9)[3]	Air
	90(10)[4]	1300	50*-73700†	50*-980†	Oxygen
Pd	< 0.02	1450	25*	1120(100)	Oxygen

[1]error in phase concentrations propagated through to quotient, D; [2]standard deviation of electron probe analyses; [3]single PIXE analysis and associated counting statistical error; [4]standard deviation of D's calculated from analyses of immediately adjacent phases; *electron probe detection limit; †range of concentrations within single run

In the case of these melts, RuO_2 is present in the 1300ºC runs, while at 1450ºC only Ru has been found in the run products. The amount of Ru in the spinel is not sensitive to temperature and is fairly uniform in the unattached euhedral spinels. The partition coefficients of D^{Ru} values of 22-25 ± 9 indicate that Ru is significantly compatible in spinel in these melts.

The results of a preliminary study of partition of Ru and W in contact with spinel and a model glass are summarized in this report. Further study of partition of Ru in high-level waste glass compositions is needed.

2.6 Cost and Availability

The RuO_2 and surrogate WO_3 were purchased from Johnson Matthey and Alfa Aesar, respectively. The costs are compared in Table 2.5. RuO_2 cost 25-30 times more than WO_3. For the quantities ordered (100-500 grams), availability was not a problem. Large amounts of RuO_2 could face supply problem.

2.7 Surrogates Selection

Thermodynamic and cost considerations clearly favor WO_3[b] as a potential surrogate for RuO_2[c]. In addition, Cr_2O_3, $NiCr_2O_4$, and Inconel 600 have also been considered[d]. Sources of Cr_2O_3[e] in melter environments are refractories and oxidation by-products of the electrode used (Inconel 690). $NiCr_2O_4$[f] is a basic spinel compound that has been identified in many melters and laboratory studies. Inconel 600[g] has chemical similarity to the electrode used in melters, Inconel 690.

[b] Alfa Aesar
[c] Johnson Matthey
[d] Personal communication with Mr. Denny Bickford at SRTC
[e] Fisher Scientific
[f] Alfa Aesar
[g] GNK Sinter Metals, 22501 Gohlmann Parkway, Richton Park, IL 60471

Table 2-6. Cost of RuO_2 and WO_3

Chemical Name:		**Ruthenium oxide**
Formula:	**RuO_2**	
	Description	**Typical Purity(%)**
	-100 mesh	99.9
Pricing:	**Quantity (g)**	**Price (U.S. $)**
	2	50.00
	10	166.00
	50	768.00
Chemical Name:		**Tungsten oxide**
Formula:	**WO_3**	
	Description	**Typical Purity (%)**
	3-12 mm pieces (sintered, yellow-green)	99.99 (vac. dep. grade)
Pricing:	**Quantity (g)**	**Price (U.S. $)**
	50	50.00
	200	130.00
	500	246.00

3.0 Surrogate Characterization and Testing

3.1 Characterization of Surrogate Powders

As-received powders were characterized using particle size analyzer, scanning electron microscopy (SEM), and energy dispersive spectrometry (EDS). No attempt was made to grind these materials down to specific particle size range or distribution due to preliminary nature of this investigation. These results are discussed in this section.

3.1.1 RuO_2

RuO_2 shows a narrow particle size range of about 100-400 µm with a peak around 275 µm. The spongy particulates show uniform distribution and some segregation.

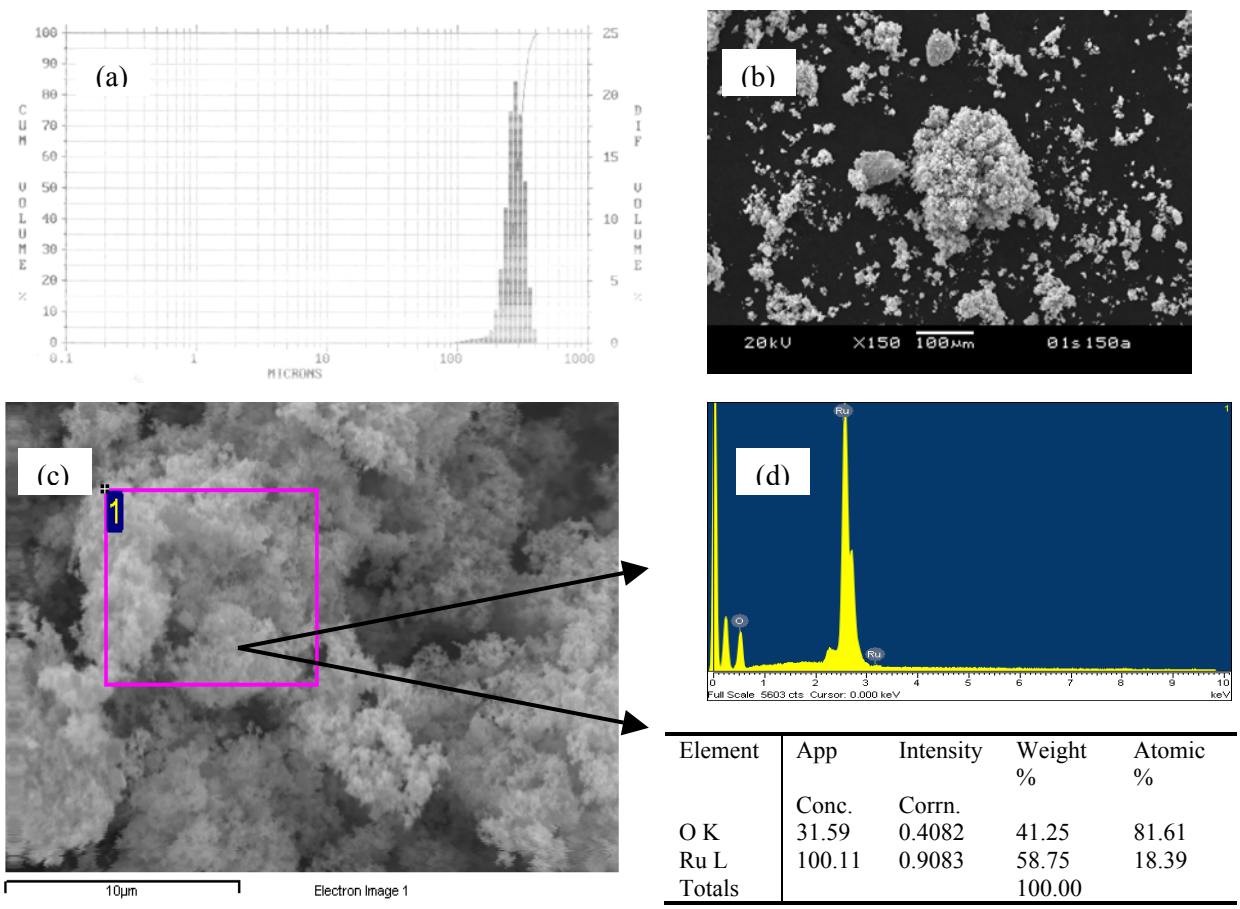

Element	App Conc.	Intensity Corrn.	Weight %	Atomic %
O K	31.59	0.4082	41.25	81.61
Ru L	100.11	0.9083	58.75	18.39
Totals			100.00	

Figure 3-1. a) Particle Size, b) SEM, c) Point EDS area, and d) EDS Data of RuO_2 Powder

3.1.2 WO_3

WO_3 shows a wide particle size range of about 10-500 µm with three peaks around 20, 60, and 300 µm. The particulates have finer granular texture.

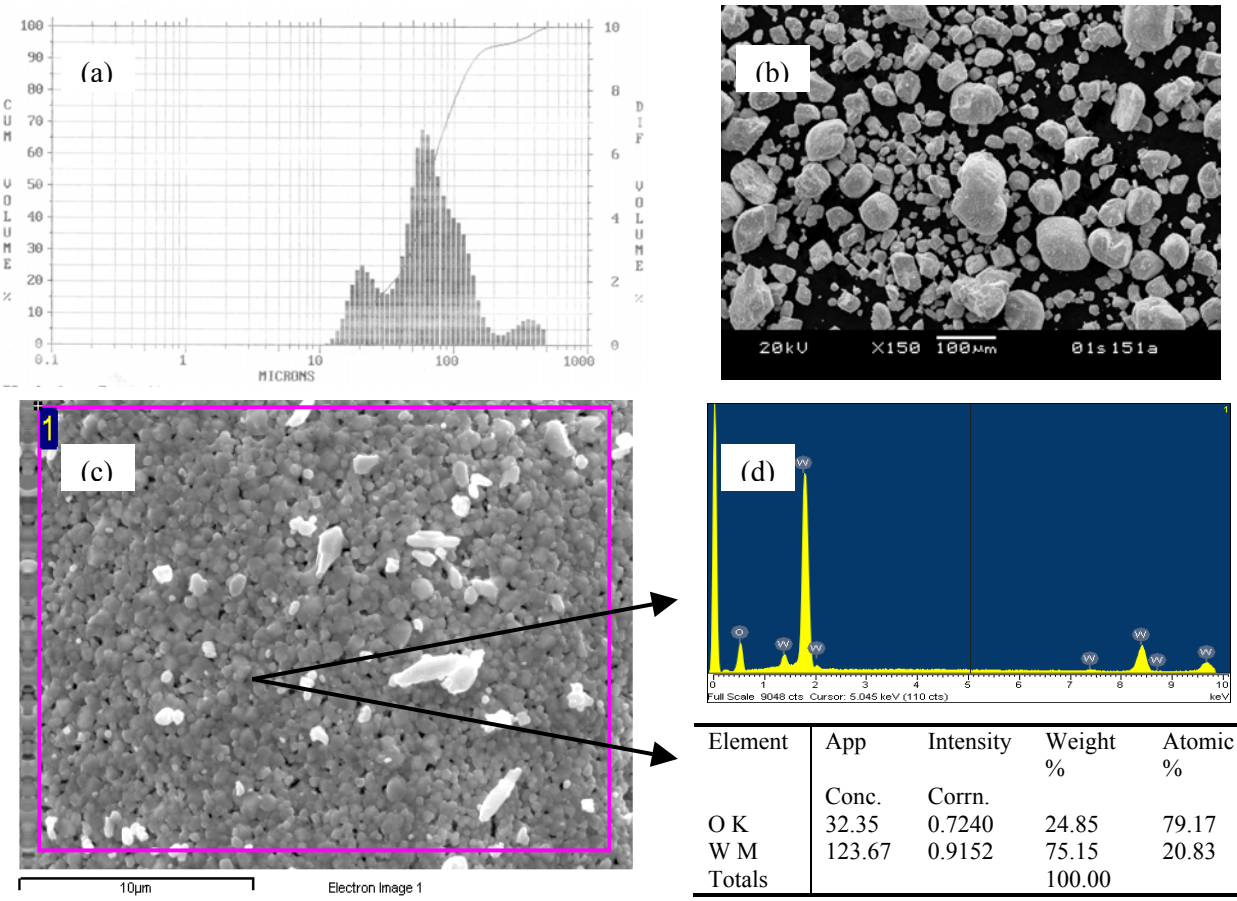

Element	App Conc.	Intensity Corrn.	Weight %	Atomic %
O K	32.35	0.7240	24.85	79.17
W M	123.67	0.9152	75.15	20.83
Totals			100.00	

Figure 3-2. a) Particle Size, b) SEM, c) Point EDS area, and d) EDS Data of WO_3 Powder

3.1.3 Cr_2O_3

Cr_2O_3 shows a particle size range of about 0.2-5 µm with two peaks around 0.8 µm. The spongy particulates show some segregation.

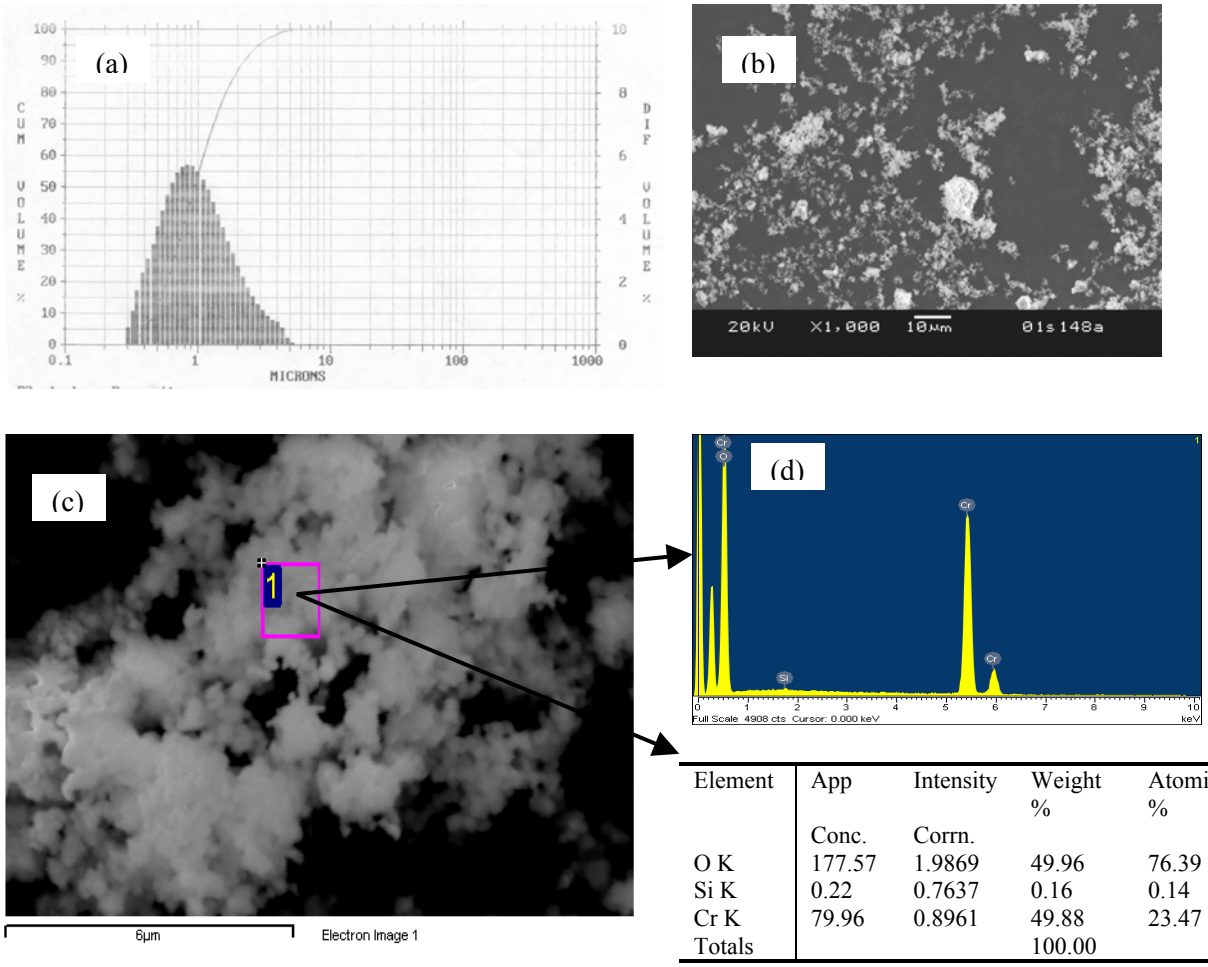

Element	App Conc.	Intensity Corrn.	Weight %	Atomic %
O K	177.57	1.9869	49.96	76.39
Si K	0.22	0.7637	0.16	0.14
Cr K	79.96	0.8961	49.88	23.47
Totals			100.00	

Figure 3-3. a) Particle Size, b) SEM, c) Point EDS area, and d) EDS Data of Cr_2O_3 Powder

3.1.4 $NiCr_2O_4$

$NiCr_2O_4$ shows the widest particle size range of about 0.25-500 µm with three distinct peaks around 0.4.5, 120, and 450 µm. The spongy particulates show some segregation.

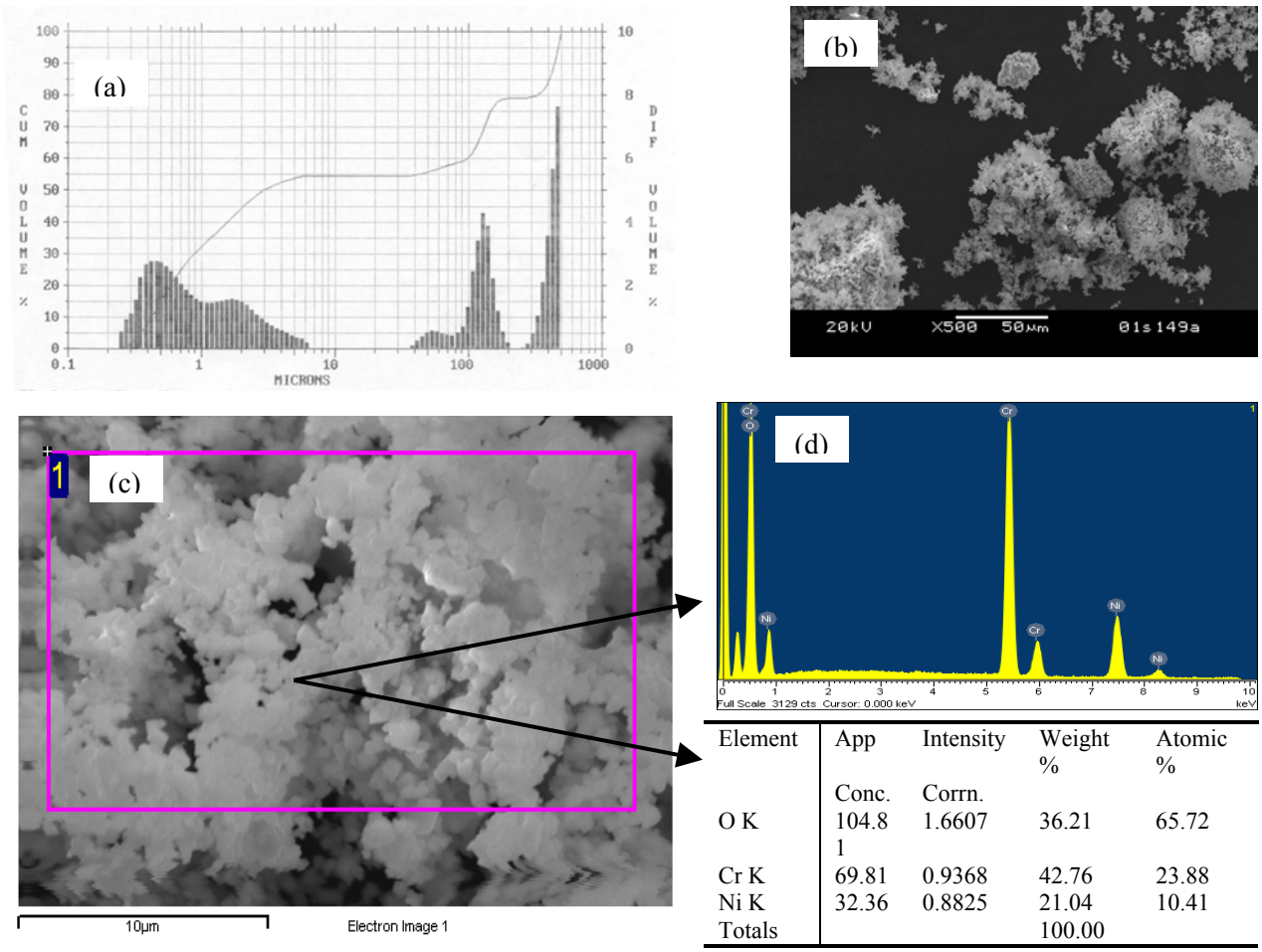

Element	App Conc.	Intensity Corrn.	Weight %	Atomic %
O K	104.81	1.6607	36.21	65.72
Cr K	69.81	0.9368	42.76	23.88
Ni K	32.36	0.8825	21.04	10.41
Totals			100.00	

Figure 3-4. a) Particle Size, b) SEM, c) Point EDS area, and d) EDS Data of $NiCr_2O_4$ Powder

3.1.5 Inconel 600

Inconel 600 shows a sharp particle size range of about 100-500 µm with one peak around 350 µm. The rounded particulates show granular texture.

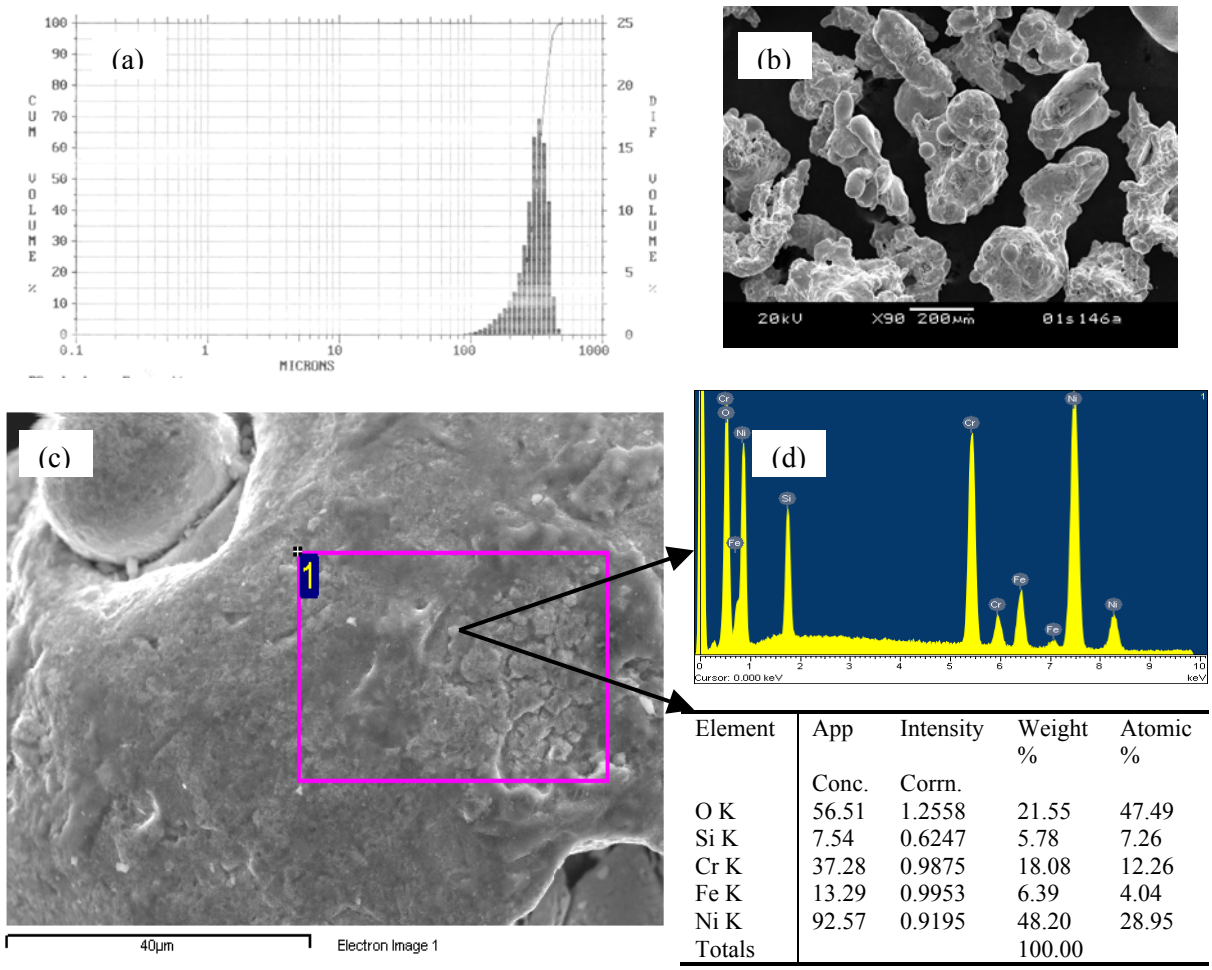

Element	App Conc.	Intensity Corrn.	Weight %	Atomic %
O K	56.51	1.2558	21.55	47.49
Si K	7.54	0.6247	5.78	7.26
Cr K	37.28	0.9875	18.08	12.26
Fe K	13.29	0.9953	6.39	4.04
Ni K	92.57	0.9195	48.20	28.95
Totals			100.00	

Figure 3-5. a) Particle Size, b) SEM, c) Point EDS area, and d) EDS Data of Inconel 600 Powder

3.2 Selection and Preparation of Glasses

Two glasses, shown in Table 3.1, were chosen for this study. MS-7 (a simplified version of a typical Hanford HLW glass with a liquidus temperature, T_L, of 1078ºC) was chosen as it had been used as a model high-level waste glass in recent spinel settling studies at PNNL. Modified NCAW was chosen as several melter studies had already reported using this composition.

Glasses were made from oxides, carbonates, and boric acid. These batch chemicals were milled for 5 min in an agate mill and melted for 1 h. The glass was quenched on a steel pour plate, then ground in a tungsten carbide mill for 4 min and remelted to ensure homogeneity.

Table 3-1. Target Glass Compositions

MS-7

Oxide	Wt %
Al_2O_3	8.00
B_2O_3	7.00
Cr_2O_3	0.30
Fe_2O_3	11.50
Li_2O	4.54
MgO	0.60
MnO	0.50
Na_2O	15.30
NiO	0.95
SiO_2	45.31
ZrO_2	6.00
Total	**100.00**

Modified NCAW

Oxide	Wt %
SiO_2	52.97
B_2O_3	14.99
Li_2O	5.34
Al_2O_3	2.57
CaO	0.23
CdO	0.87
CeO_2	0.18
Cl^-	0.08
Cr_2O_3	0.07
Cs_2O	0.17
CuO	0.07
Fe_2O_3	8.06
La_2O_3	0.19
MgO	0.10
MnO_2	0.61
MoO_3	0.16
Na_2O	6.10
Nd_2O_3	0.99
NiO	0.66
P_2O_5	0.25
PbO_2	0.20
ReO_2	0.10
RuO_2	0.11
SiO_2	0.14
SO_3	0.19
TiO_2	0.19
ZnO	0.10
ZrO_2	4.31
Total	**100.00**

3.3 Double Crucibles Test

Klouzek and coworkers (Klouzek et al. 2001) used a double crucible assembly, a smaller alumina crucible placed inside a larger silica crucible (shown in Figure 3.6). This assembly was used to minimize Marangoni convection and bubble generation within the inner crucible (LaMont and Hrma, 1998). MS-7 glass melt was poured into preheated crucibles until the top of the inner crucible was just covered with the

melt. The crucible assembly was then placed back into the furnace at 1220ºC. After 20 min., the temperature was lowered to the test temperatures, for increasing time intervals (up to 30 h), and then cooled. The test conditions are listed in Table 3.2. Vertical thin sections were prepared to investigate the area inside the alumna crucible. Crystals were studied using an Olympus PMG3 microscope and Clemex Image Analyzer.

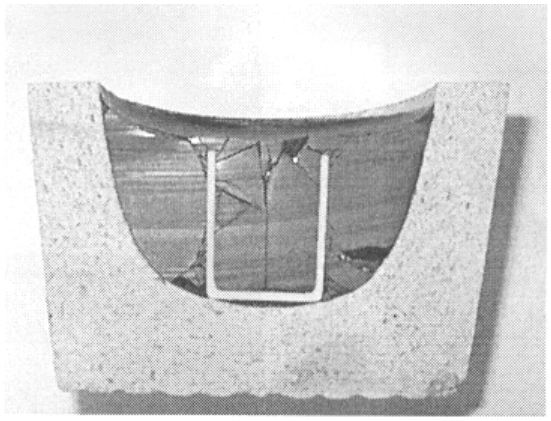

Figure 3-6. Double Crucible Test (Klouzek et al. 2001)

Table 3-2. Test Parameters

Parameters	Values
Oxides	RuO_2, WO_3
Concentrations (nominal wt %)	0.005, 0.5, 1.0
Temperature (ºC)	900, 950, 1000
Time (hours)	7, 15, 19, 23

In addition, $NiCr_2O_4$ was also tested to a limited extent (0.1 and 0.5 wt % at 950ºC and 1050ºC for 15-23 h.) in modified NCAW glass melt. Quick tests showed that Cr_2O_3 dissolved easily into the model systems and Inconel 600 powders settled shortly after their addition to the test melts. Therefore, Cr_2O_3 and Inconel 600 were not further investigated.

3.4 Crystallization Studies

In order to compare the role of RuO_2 and WO_3 in spinel crystallization (Plaisted et al. 2001), samples of MS-7 glass with 0.5 wt% of RuO_2 or WO_3 for crystallization studies were heat-treated in 2 × 2 × 2 cm platinum crucibles at 900, 950, and 1000ºC for 7-23 h. The heat-treated samples were characterized by using x-ray diffraction (XRD). Qualitative XRD data are presented in this report.

3.5 Viscosity Tests

Modified NCAW glass was used for these tests. The rheology of the melts containing 1 and 10 wt.% of $NiCr_2O_4$, was studied using a Brookfield digital rotating viscometer with a disk spindle (Mika and Hrma 2000). The temperature ranged from 1050ºC to 1350ºC, and the spindle speed, from 0.005 to 1 RPS. Before each measurement, the sample was held for 90 min at the measuring temperature. The idle time for spindle-speed change was 5 min and for temperature change 30 min. The lower surface of the

spindle was about 13 mm above the crucible bottom. The shear stress ($\tau = M/2\pi R_d L$, where M = torque, R_d = spindle radius, 7.3 mm, and L = spindle height, 2 mm) was determined[h].

3.6 High Temperature Optical Microscopy

High temperature optical microscopy was used to study the suspension of RuO_2 and $NiCr_2O_4$. The hot stage designed and developed in-house (shown in Figure 3.7) was used. The stage was place on the platform of the optical microscope (Metallux II, Leco Corporation) with the crucible with the test glass. Test melt (MS-7) with 1 wt.% of RuO_2 or $NiCr_2O_4$ powder added was observed from room temperature to about 1100ºC. The melt changes were photographed.

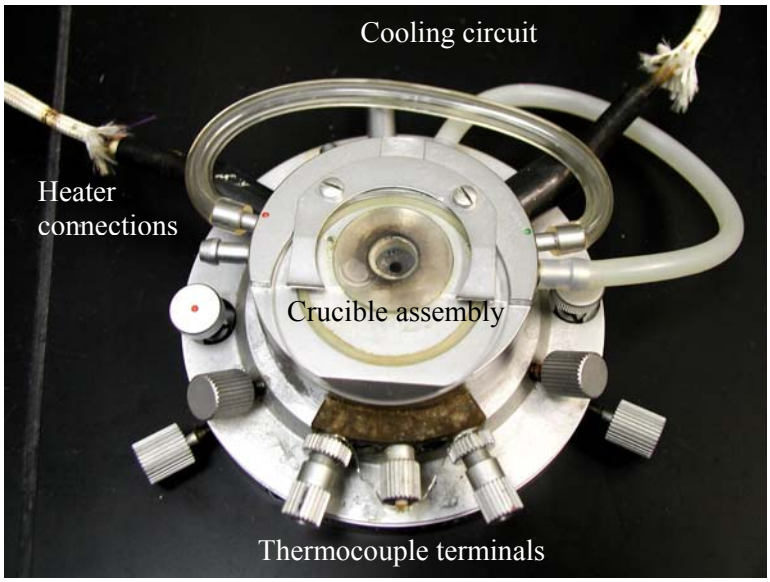

Figure 3-7. Hot Optical Microscopy Stage

3.7 Partition Stuides

Partitioning of noble metal species (Ru and RuO_2) and the surrogate species (W and WO_3) between spinel ($MgAl_2O_4$) and model glass melt (MS-7) was studied following the same technique followed by Capobianco and Drake (Capobianco and Drake, 1990). Capsules made from single crystal synthesized spinel boules (grown by the flame fusion method, i.e., Verneuil process) commercially available[i]. The capsule spinel was chosen for its easy availability and its prior use for partition study. The starting capsule is non-stoichiometric spinel (90 wt.% Al_2O_3 and 10 wt.% MgO). In the preparation of the spinel capsule, a slice was cut from the boule and a hole was drilled into the slice (Figure 3.8 (a) – (c)). Then, the hole was packed with the glass powder with suitable additive and suspended using platinum wire wound around an alumina rod (Figure 3.8(d)). Several samples were assembled in a ceramic trough, as shown in Figure 3.8(e).

About 2 gm of MS-7 glass was mixed with 0.5 wt.% of the species (Ru, RuO_2, W, WO_3) and placed into the capsule. The assembly of capsules were heated to 1220ºC and held at that temperature for

[h] Brookfield Viscometer Guide, Brookfield Engineering Laboratories, Brookfield, MA, USA.
[i] Supplier: Morion Company, Birghton, MA, USA.

20 min. Then, the temperature was decreased to the test temperatures (900ºC and 1000ºC) for 7 – 23 h. After the completion of the heat-treatment, the capsule was cooled to room temperature and sectioned at the middle. The cross section of the capsule with the glass melt was prepared for SEM and EDS. EDS scans (along a line at and across the spinel-melt interfacial region) were done to determine the extent of the spinel-melt interaction and chemistry change across the interface.

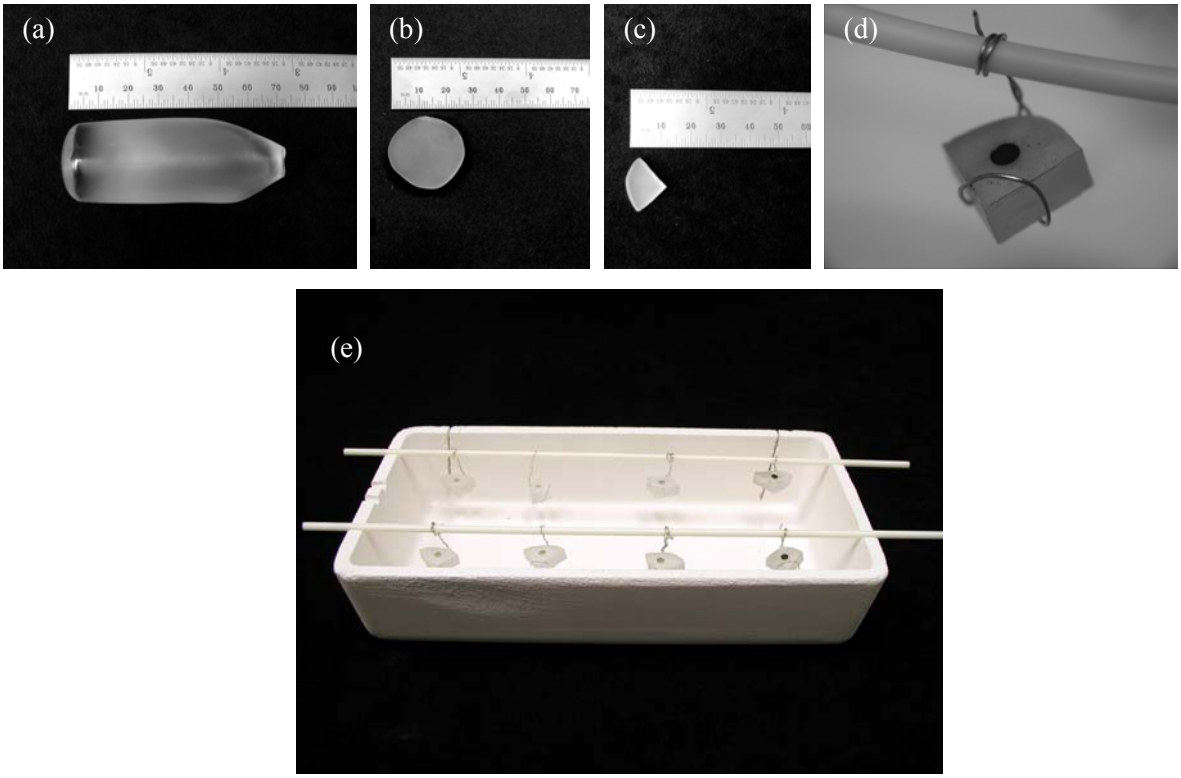

Figure 3-8. Capsule and Sample Preparation for Partition Study

3.8 AC Conductivity Test

AC electrical conductivity (at 60 Hz) of the DWPF frit glass samples with 1, 2, 5, and 10 wt.% of the conductivity surrogates (Inconel 600, Cr_2O_3, $NiCr_2O_4$), RuO_2 and WO_3 at 950-1250°C was measured using two-probe technique.

4.0 Results and Discussion

4.1 Double Crucible Tests

4.1.1 RuO_2 vs. WO_3 in MS-7

Figure 4.1 shows the thin sections of the inner crucible containing the test glasses with 0.5 wt.% RuO_2 or WO_3 at test temperatures for 7-23 h. At 900ºC, RuO_2, spinel crystals formed sparingly. In the case of WO_3, more spinel crystals (dark spots) were clearly seen at 950ºC, especially after 19 h. The temperature effect was more pronounced. In either case, more spinel crystals formed at 950ºC and started settling at 1000ºC, as shown in Figure 4.2.

Selected areas of the samples (especially near the wall of the inner crucible) were characterized using SEM and EDS. Figures 4.3 and 4.4 show features of sample containing 0.5 wt.% of RuO_2 heat-treated at 950ºC for 23 h. Area 1 in Figure 4.3 represents bulk glass region. No measurable Ru was detected in this region. This was interpreted to be due to low solubility of RuO_2 in glass as well as the detectability limit of the EDS technique. Spinel crystals (about 2-5μm size) were seen in the sample. The crystal on right side of Figure 4.3 was Fe-Ni spinel with about 3.56 wt.% of Ru. In Figure 4.4, the crystal on the left side was Fe-Ni spinel with no detectable Ru. The area marked 4 on the right side of Figure 4.4 was an alkali silicate phase containing Fe and Zr along with about 7.65 wt.% of Ru.

Figure 4.5 shows features of sample containing 0.5 wt.% of WO_3 heat-treated at 950ºC for 23 h. Area 1 represents bulk glass region. The crystal was Fe-Ni spinel (about 20-50μm size). No measurable W was detected in these regions. This was also interpreted to be due to low solubility of RuO_2 in glass as well as the detectability limit of the EDS technique. On comparing these observations with Figures 4.3 and 4.4, the data suggested RuO_2 partitioned in spinel more readily.

Figure 4.6 shows features of sample containing 1 wt.% of RuO_2 heat-treated at 950ºC for 23 h. Area 1 represents bulk glass region. Islands of segregated Ru-rich regions were observed. These regions clearly indicated supersaturation of the melt with Ru. Based on these results, all partition studies (section 4.5) used 0.5 wt.% of RuO_2 or WO_3.

4.1.2 $NiCr_2O_4$ in Modified NCAW

Figures 4.7, 4.8, and 4.9 show the thin sections of test glasses containing 0.1, 0.5, and 1 wt.% of $NiCr_2O_4$ at test temperatures for 15-25 h, respectively. In the case of 0.1 wt.% (Figure 4.7), the spinel crystals (dark spots) appeared after 15 h but reduced in number after 23 h, suggesting redissolution of the crystals in the melts. Relatively more spinel crystals were observed with 0.5 wt.% of $NiCr_2O_4$ (Figure 4.8). Addition of more $NiCr_2O_4$ (Figure 4.9) resulted in segregation of the crystals.

Figures 4.10-4.12 show SEM-EDS data of different regions for the sample containing 0.5 wt.% of $NiCr_2O_4$ heat-treated at 950ºC for 23 h. In Figure 4.10, region 1 represents the bulk glass. Several Ni-Cr spinel crystals clustered together. Different regions showed in Figures 4.11 and 4.12 contained various levels of Ru. As the test glass contained 0.11 wt.% RuO_2, these observations supported our conclusion in the previous section (4.1.1) that Ru precipitated more readily in the presence of spinel.

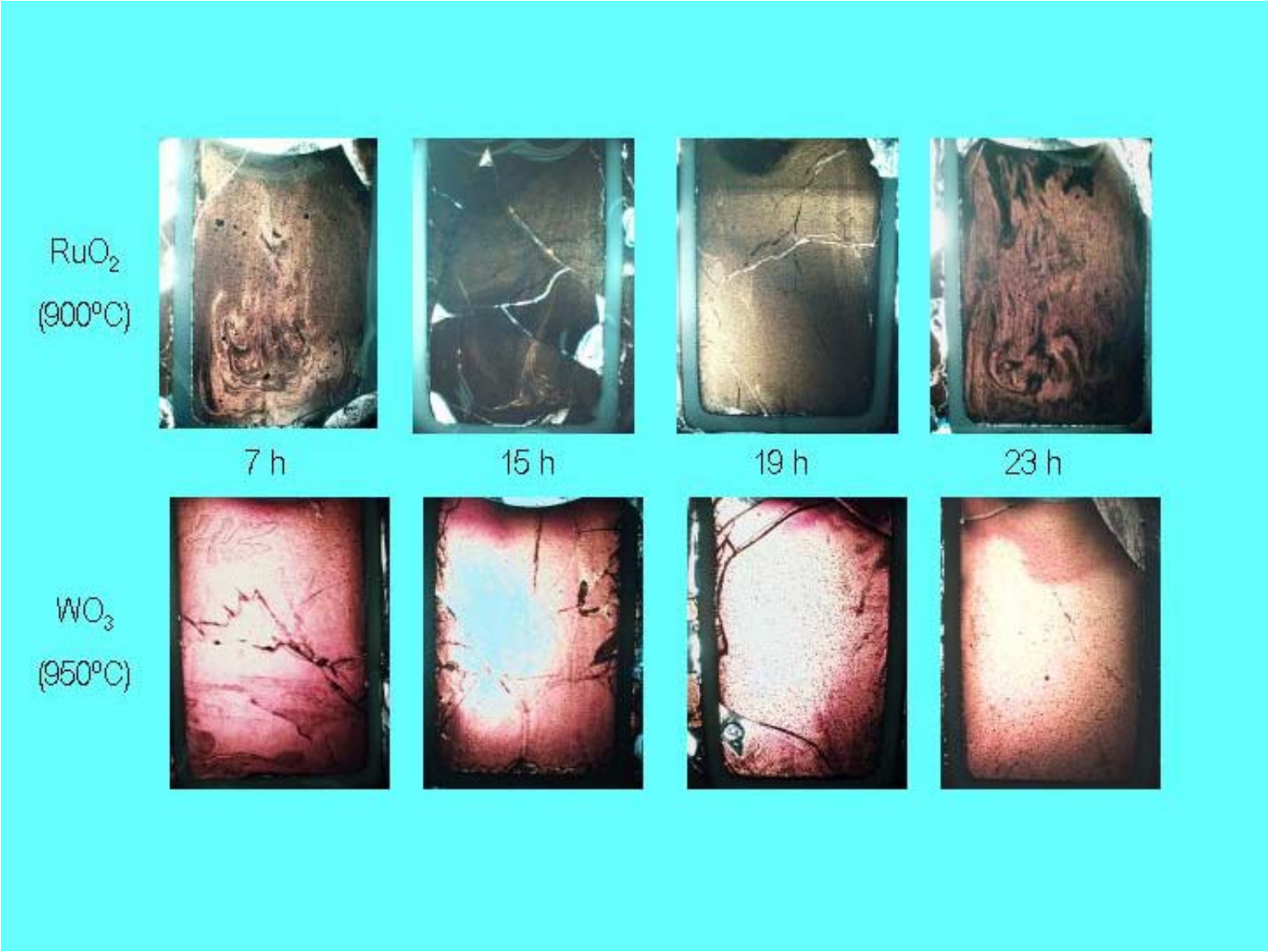

Figure 4-1. RuO_2 vs. WO_3 – Time Effect (0.5 wt.% in MS-7)

Figure 4-2. RuO_2 vs. WO_3 – Temperature Effect (0.5 wt.% in MS-7)

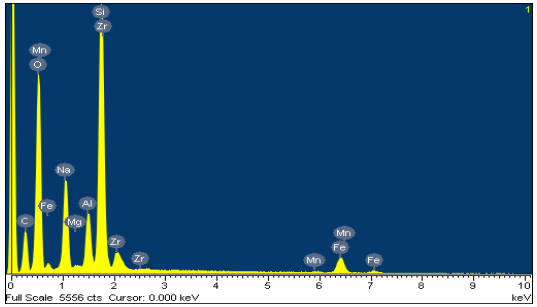

Element	App Conc.	Intensity Corrn.	Weight %	Atomic %
O K	74.12	1.0853	53.08	67.84
Na K	11.59	0.8044	11.20	9.97
Mg K	0.17	0.6318	0.21	0.17
Al K	4.20	0.7532	4.33	3.28
Si K	22.69	0.8062	21.88	15.93
Mn K	0.31	0.8190	0.30	0.11
Fe K	5.14	0.8358	4.79	1.75
Zr L	3.25	0.6006	4.21	0.94
Totals			100.00	

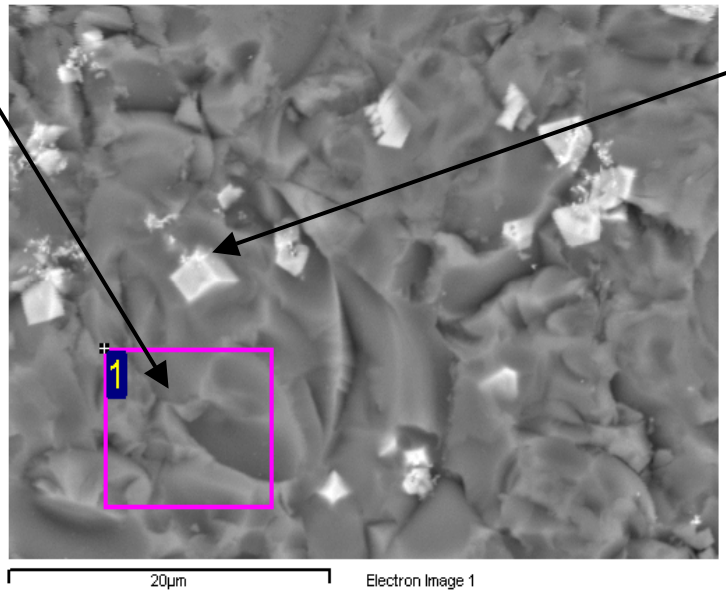

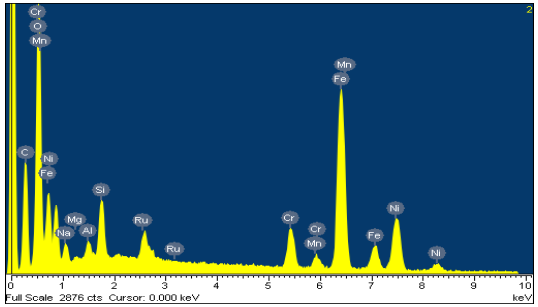

Element	App Conc.	Intensity Corrn.	Weight %	Atomic %
O K	47.00	1.2650	34.32	62.23
Na K	1.24	0.4297	2.66	3.36
Mg K	0.16	0.4307	0.35	0.41
Al K	0.65	0.5518	1.09	1.17
Si K	2.62	0.6721	3.60	3.72
Cr K	5.27	0.9986	4.87	2.72
Mn K	1.22	0.9101	1.24	0.65
Fe K	33.43	0.9289	33.24	17.27
Ni K	14.26	0.8740	15.06	7.44
Ru L	2.97	0.7710	3.56	1.02
Totals			100.00	

Figure 4-3. SEM –EDS of RuO_2 in MS-7 (0.5 wt.%, 950ºC/23h)

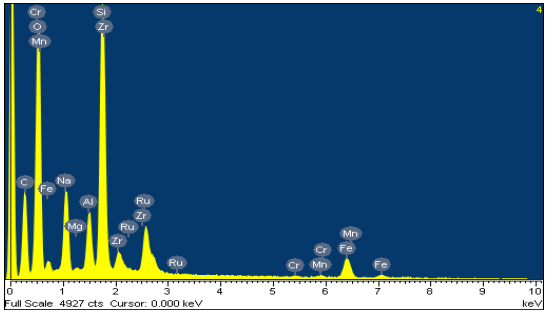

Element	App Conc.	Intensity Corrn.	Weight %	Atomic %
O K	79.23	0.9409	55.88	73.15
Na K	9.34	0.7471	8.30	7.56
Mg K	0.18	0.6269	0.19	0.16
Al K	3.86	0.7490	3.42	2.65
Si K	20.32	0.8161	16.52	12.32
Cr K	0.25	0.8439	0.20	0.08
Mn K	0.29	0.8237	0.24	0.09
Fe K	5.67	0.8417	4.47	1.68
Zr L	3.04	0.6436	3.14	0.72
Ru L	8.28	0.7185	7.65	1.58
Totals			100.00	

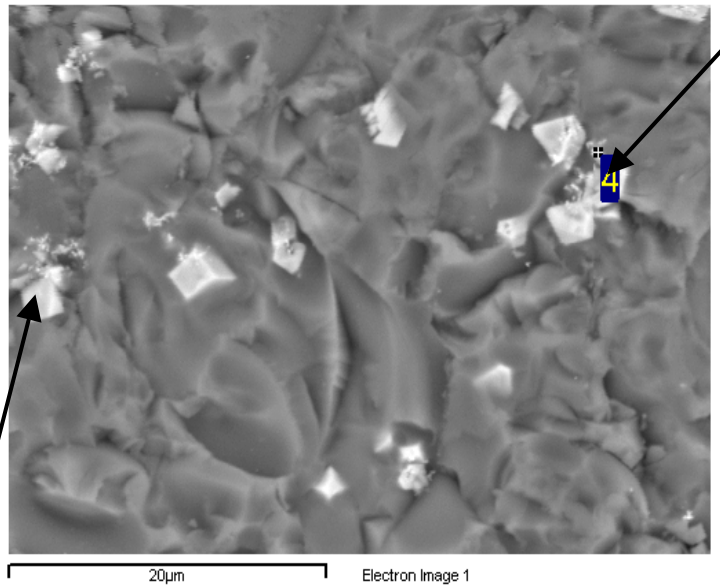

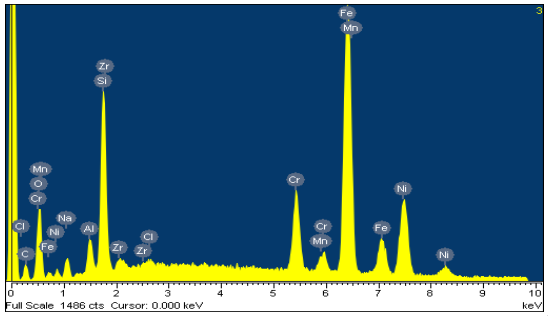

Element	App Conc.	Intensity Corrn.	Weight %	Atomic %
O K	7.27	1.1287	10.85	26.57
Na K	0.68	0.4109	2.77	4.72
Al K	0.66	0.5351	2.08	3.02
Si K	3.97	0.6514	10.26	14.32
Cl K	0.10	0.7455	0.24	0.26
Cr K	4.88	1.0446	7.87	5.93
Mn K	0.85	0.9459	1.51	1.08
Fe K	24.85	0.9615	43.51	30.52
Ni K	10.28	0.8939	19.36	12.92
Zr L	0.56	0.6049	1.56	0.67
Totals			100.00	

Figure 4-4. SEM –EDS of RuO_2 in MS-7 (0.5 wt.%, 950ºC/23h)

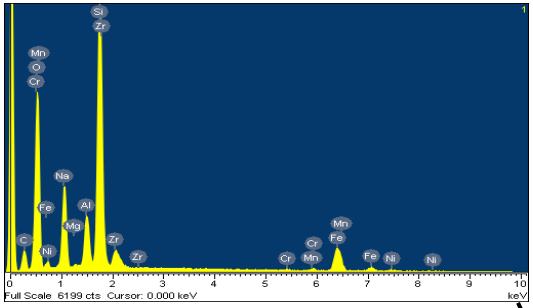

Element	App Conc.	Intensity Corrn.	Weight %	Atomic %
O K	62.38	1.0518	48.61	64.71
Na K	10.26	0.7765	10.83	10.03
Mg K	0.11	0.6205	0.15	0.13
Al K	3.93	0.7439	4.33	3.42
Si K	22.25	0.8004	22.79	17.28
Cr K	0.22	0.8585	0.21	0.08
Mn K	0.39	0.8271	0.39	0.15
Fe K	7.98	0.8448	7.74	2.95
Ni K	0.64	0.8450	0.62	0.22
Zr L	3.15	0.5951	4.34	1.01
Totals			100.00	

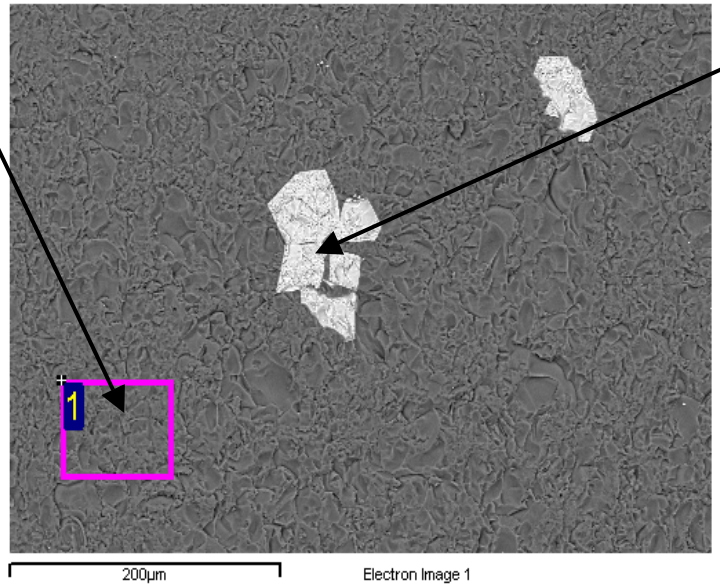

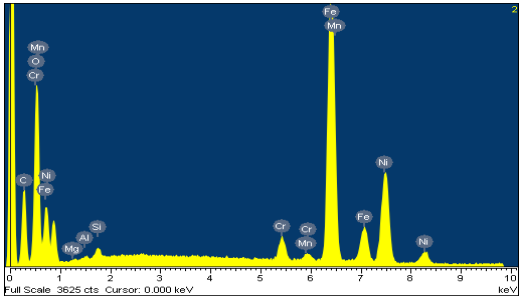

Element	App Conc.	Intensity Corrn.	Weight %	Atomic %
O K	36.65	1.3784	22.25	49.98
Mg K	0.07	0.3757	0.15	0.23
Al K	0.10	0.4920	0.17	0.23
Si K	0.49	0.6203	0.67	0.85
Cr K	3.19	1.0894	2.45	1.69
Mn K	0.84	0.9526	0.74	0.48
Fe K	55.83	0.9820	47.56	30.61
Ni K	27.66	0.8899	26.01	15.92
Totals			100.00	

Figure 4-5. SEM –EDS of WO_3 in MS-7 (0.5 wt.%, 950ºC/23h)

Figure 4-6. SEM –EDS of RuO_2 in MS-7

(1 wt.%, 950ºC/23h)

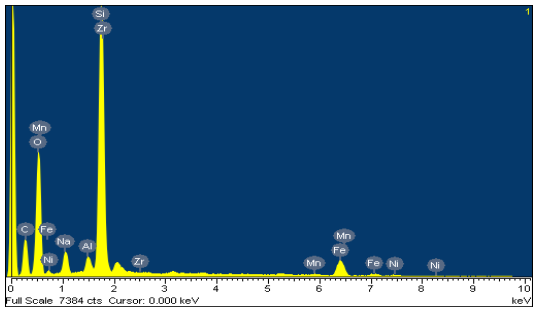

Element	App Conc.	Intensity Corrn.	Weight %	Atomic %
O K	53.30	1.0174	52.01	68.36
Na K	3.28	0.7540	4.32	3.95
Al K	1.30	0.7957	1.62	1.26
Si K	26.23	0.8684	29.99	22.46
Mn K	0.28	0.8215	0.34	0.13
Fe K	6.06	0.8396	7.17	2.70
Ni K	0.58	0.8404	0.68	0.25
Zr L	2.28	0.5828	3.88	0.89
Totals			100.00	

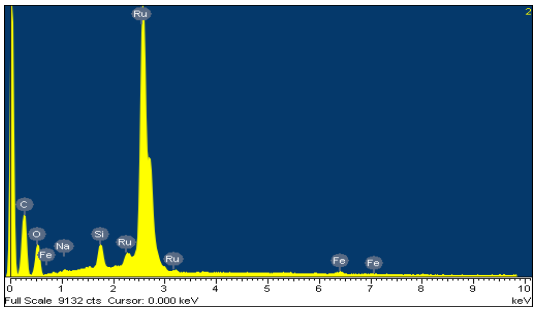

Element	App Conc.	Intensity Corrn.	Weight %	Atomic %
O K	16.90	0.3824	33.43	73.69
Na K	0.44	0.6843	0.48	0.74
Si K	2.97	0.9034	2.48	3.12
Fe K	1.08	0.9173	0.89	0.56
Ru L	75.14	0.9053	62.72	21.89
Totals			100.00	

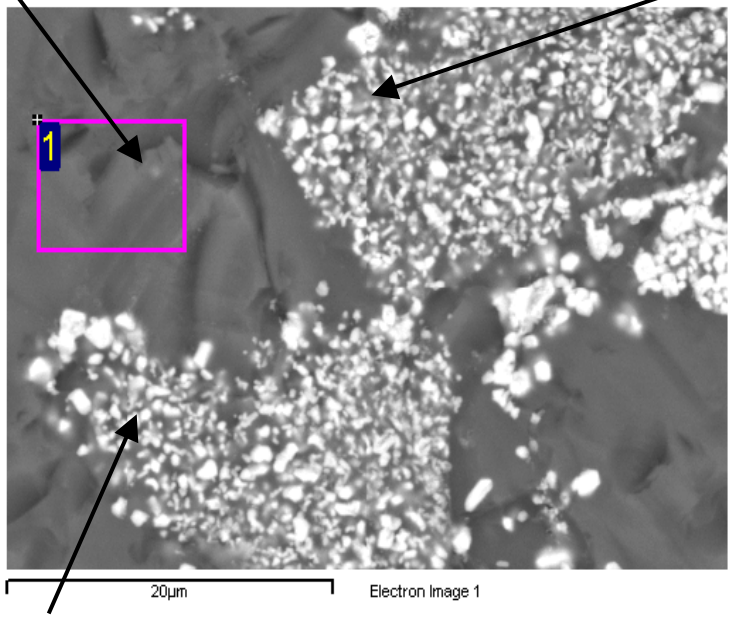

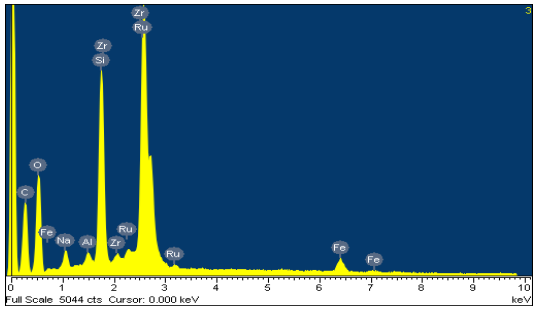

Element	App Conc.	Intensity Corrn.	Weight %	Atomic %
O K	30.34	0.5100	44.66	74.97
Na K	1.73	0.7033	1.84	2.16
Al K	0.70	0.7826	0.67	0.67
Si K	12.88	0.8865	10.91	10.43
Fe K	3.23	0.8800	2.75	1.32
Zr L	1.33	0.7416	1.35	0.40
Ru L	41.02	0.8146	37.81	10.05
Totals			100.00	

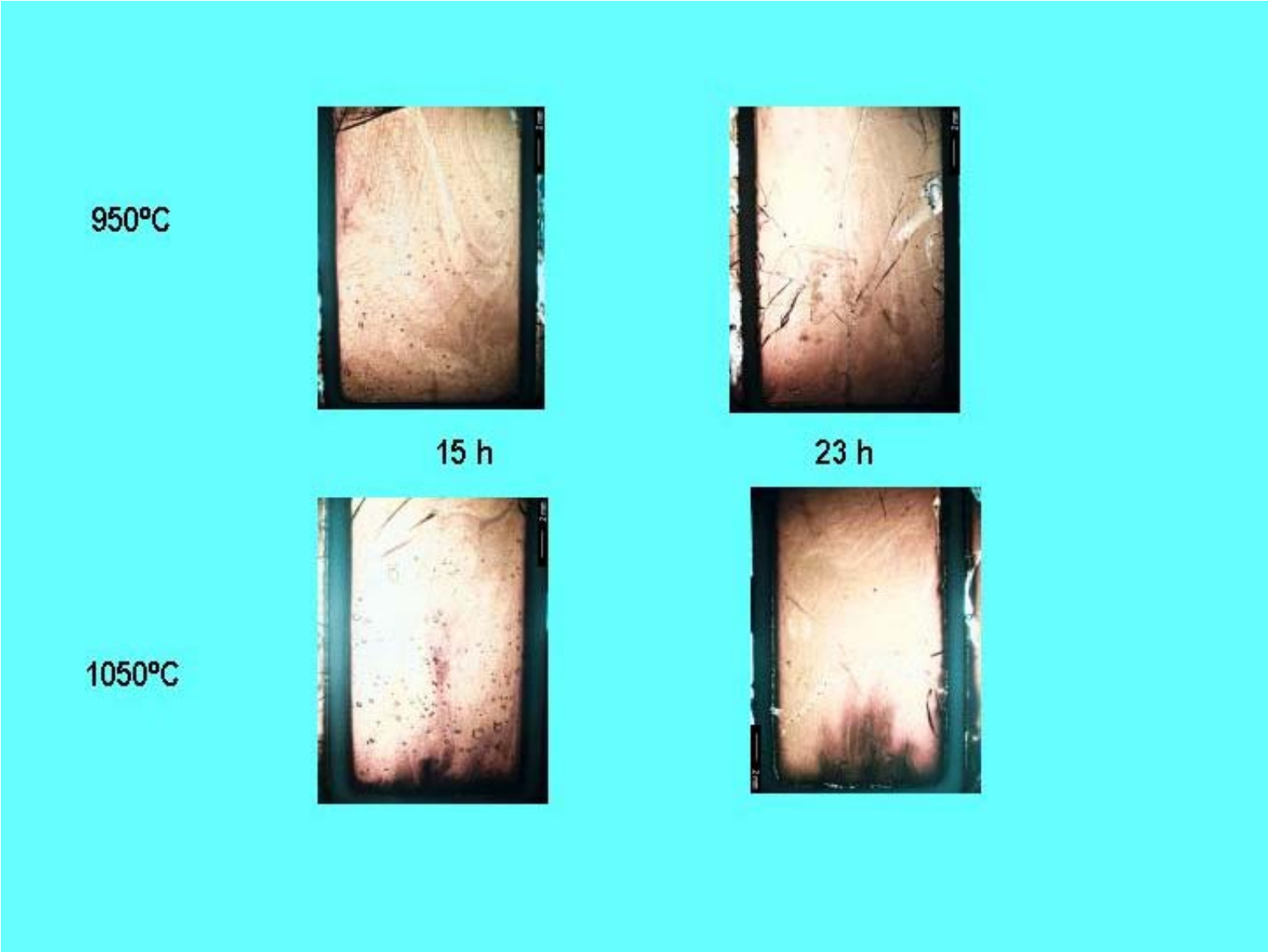

Figure 4-7. 0.1% $NiCr_2O_4$ in Modifed NCAW

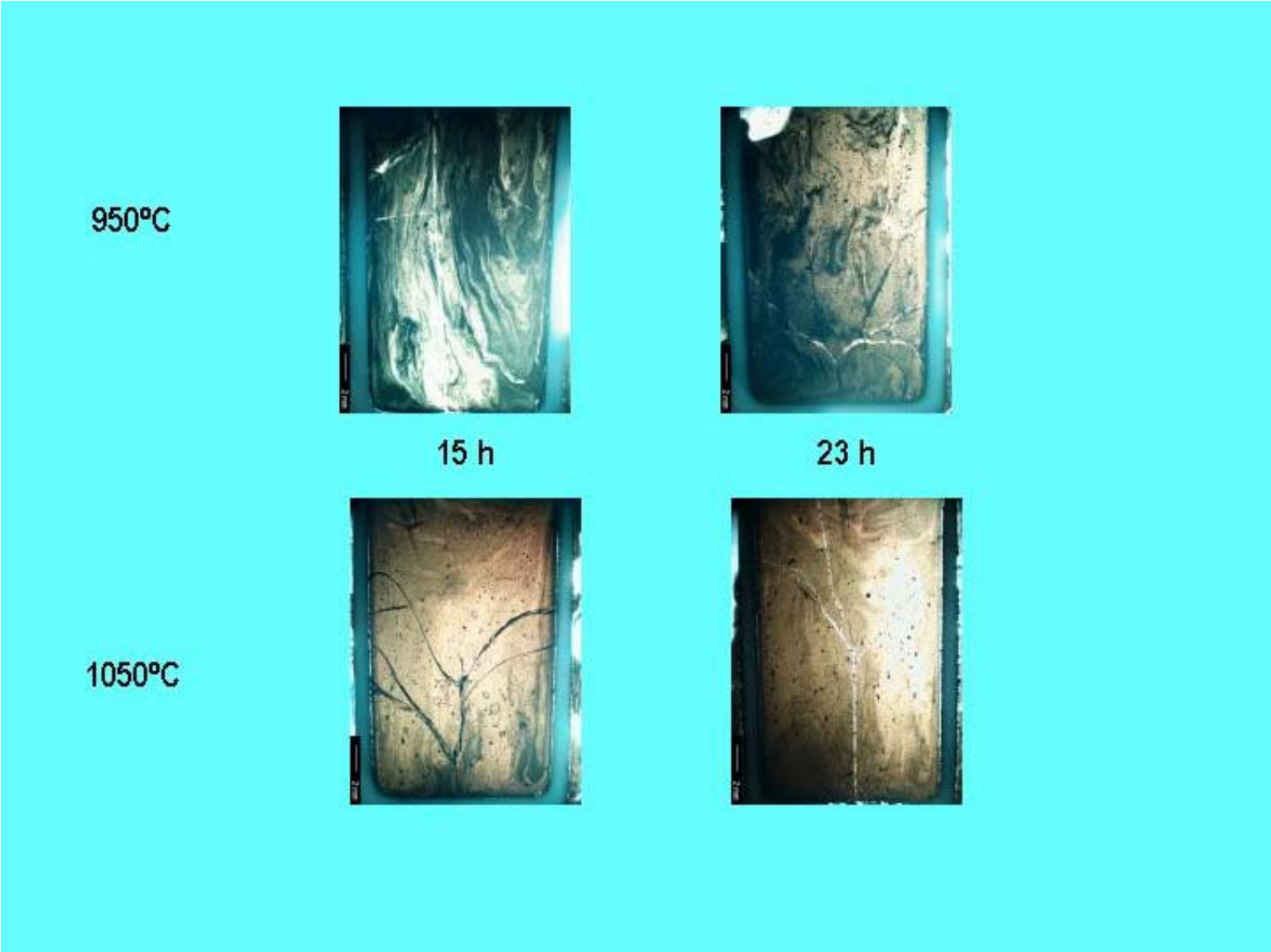

Figure 4-8. 0.5% $NiCr_2O_4$ in Modified NCAW

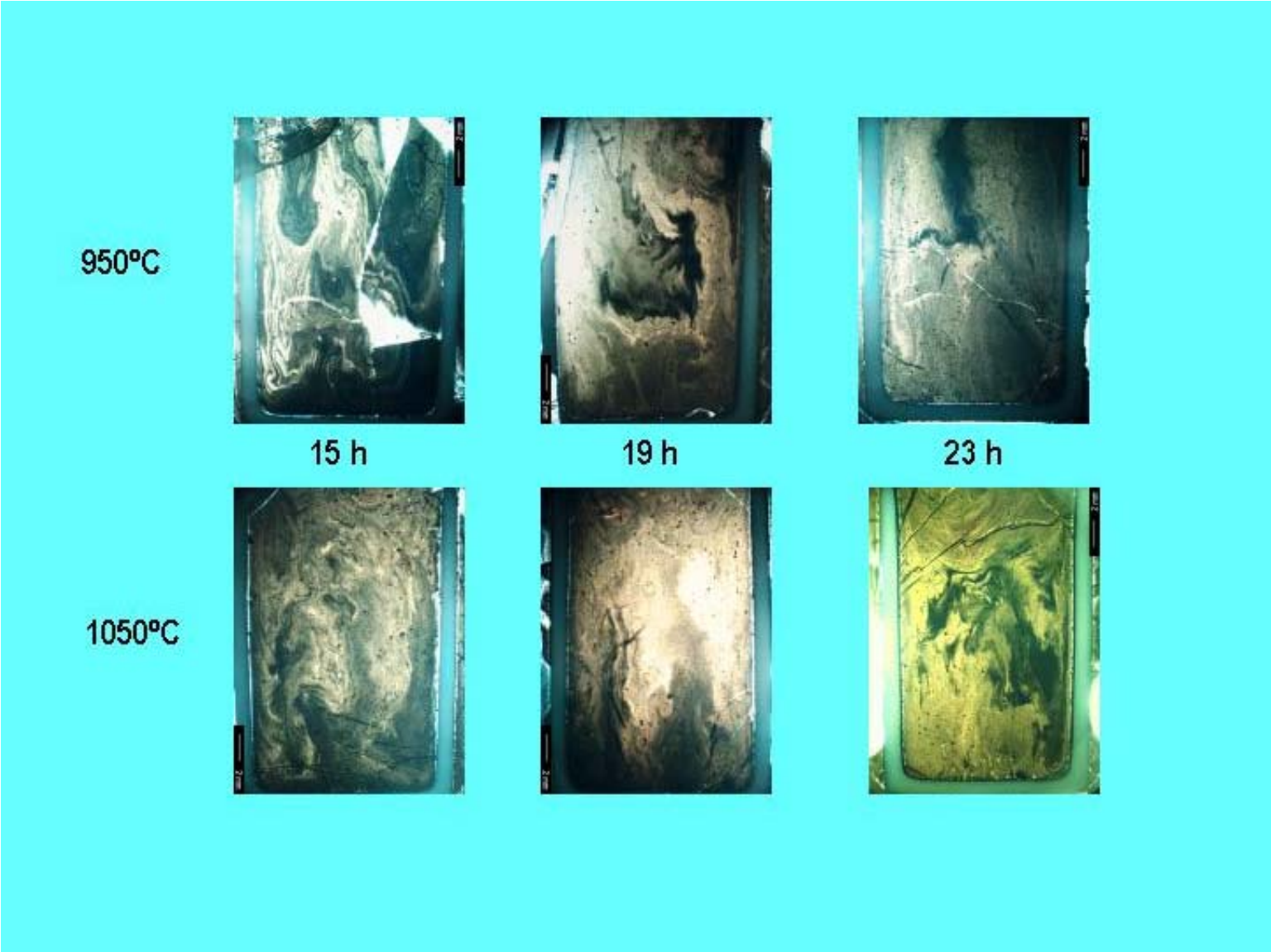

Figure 4-9. 1% $NiCr_2O_4$ in Modifed NCAW

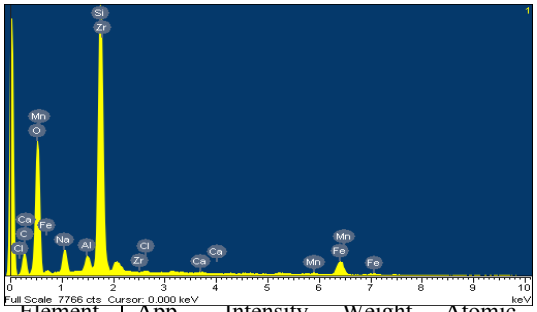

Element	App Conc.	Intensity Corrn.	Weight %	Atomic %
O K	65.18	1.0245	54.45	70.23
Na K	3.80	0.7612	4.27	3.83
Al K	1.48	0.8006	1.58	1.21
Si K	29.37	0.8724	28.82	21.18
Cl K	0.20	0.6831	0.24	0.14
Ca K	0.26	0.9491	0.24	0.12
Mn K	0.28	0.8170	0.29	0.11
Fe K	6.06	0.8341	6.22	2.30
Zr L	2.67	0.5898	3.87	0.88
Totals			100.00	

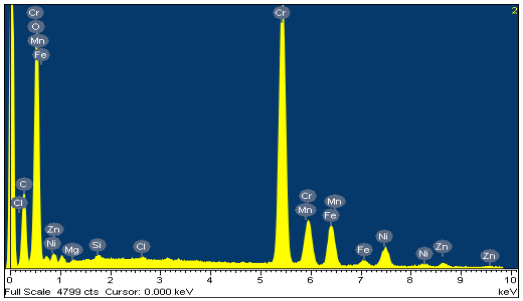

Element	App Conc.	Intensity Corrn.	Weight %	Atomic %
O K	71.48	1.6751	32.57	61.60
Mg K	0.14	0.4489	0.23	0.29
Si K	0.30	0.7063	0.33	0.35
Cl K	0.15	0.8271	0.14	0.12
Cr K	55.82	0.9477	44.95	26.16
Mn K	3.11	0.9208	2.58	1.42
Fe K	11.55	0.8613	10.23	5.55
Ni K	7.79	0.8760	6.79	3.50
Zn K	2.42	0.8432	2.19	1.01
Totals			100.00	

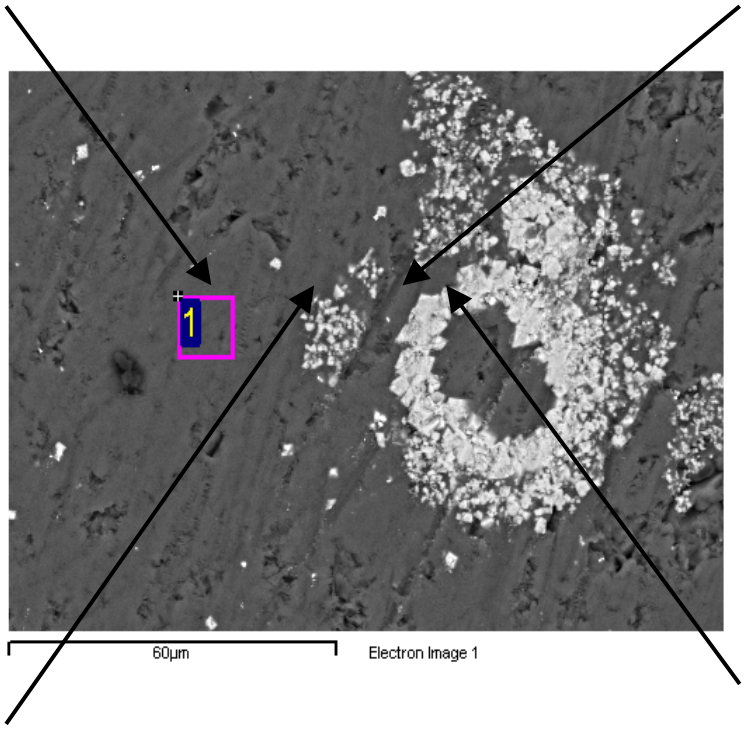

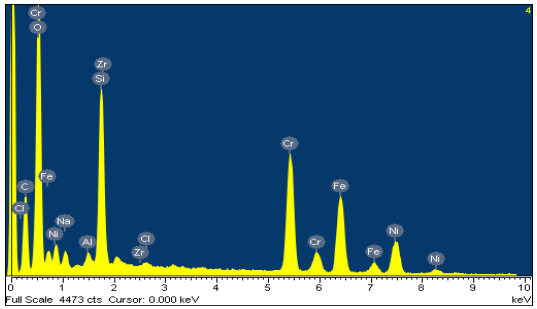

Element	App Conc.	Intensity Corrn.	Weight %	Atomic %
O K	76.59	1.3477	40.42	65.44
Na K	1.41	0.4915	2.04	2.30
Al K	0.67	0.6172	0.77	0.74
Si K	11.26	0.7342	10.91	10.06
Cl K	0.28	0.7590	0.26	0.19
Cr K	22.66	0.9291	17.35	8.64
Fe K	20.52	0.8787	16.61	7.70
Ni K	12.50	0.8617	10.32	4.55
Zr L	1.19	0.6436	1.31	0.37
Totals			100.00	

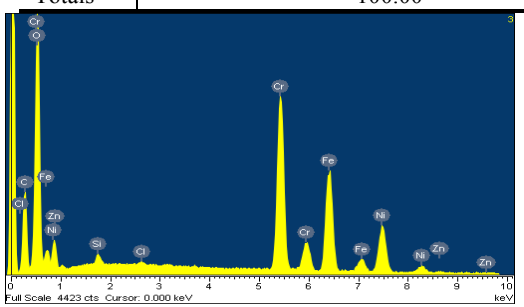

Element	App Conc.	Intensity Corrn.	Weight %	Atomic %
O K	72.02	1.5776	33.82	63.43
Si K	0.60	0.6773	0.66	0.70
Cl K	0.18	0.8051	0.17	0.14
Cr K	35.13	0.9743	26.71	15.41
Fe K	27.42	0.8987	22.60	12.14
Ni K	18.18	0.8758	15.37	7.86
Zn K	0.76	0.8346	0.67	0.31
Totals			100.00	

Figure 4-10. 0.5% $NiCr_2O_4$ in Modifed NCAW (950°C/23h)

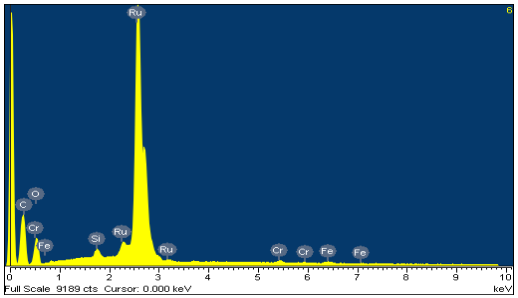

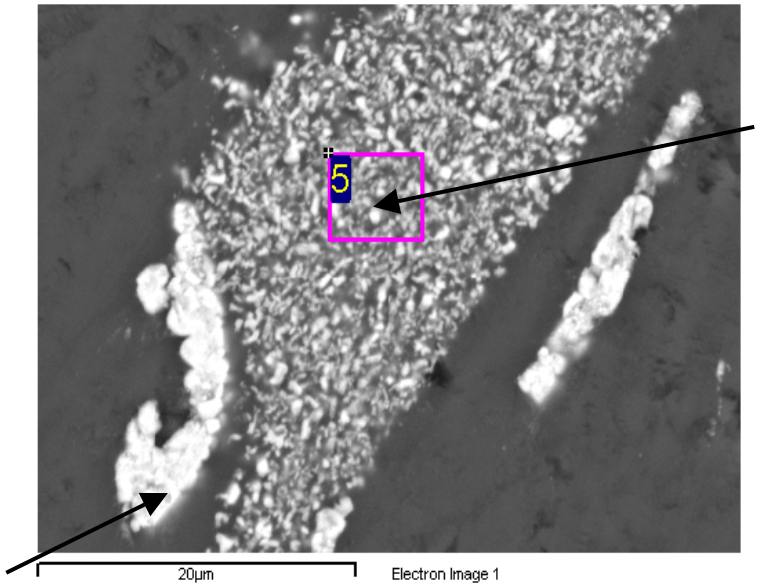

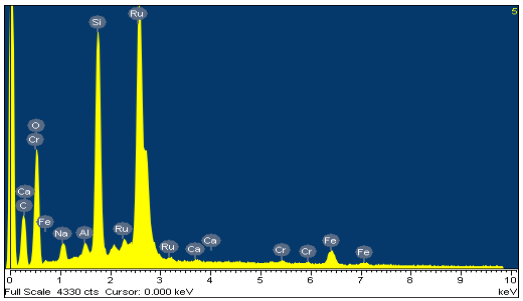

Element	App Conc.	Intensity Corrn.	Weight %	Atomic %
O K	31.47	0.5295	45.31	74.30
Na K	1.77	0.7024	1.93	2.20
Al K	0.70	0.7813	0.68	0.66
Si K	14.61	0.8837	12.60	11.77
Ca K	0.20	0.8862	0.17	0.11
Cr K	0.38	0.8534	0.34	0.17
Fe K	3.61	0.8752	3.15	1.48
Ru L	38.23	0.8135	35.83	9.30
Totals			100.00	

Element	App Conc.	Intensity Corrn.	Weight %	Atomic %
O K	15.10	0.3674	30.66	72.59
Si K	1.18	0.9053	0.98	1.32
Cr K	0.85	0.8780	0.72	0.53
Fe K	0.93	0.9251	0.75	0.51
Ru L	82.60	0.9209	66.89	25.06
Totals			100.00	

Figure 4-11. 0.5% $NiCr_2O_4$ in Modifed NCAW (950ºC/23h) – Different Region

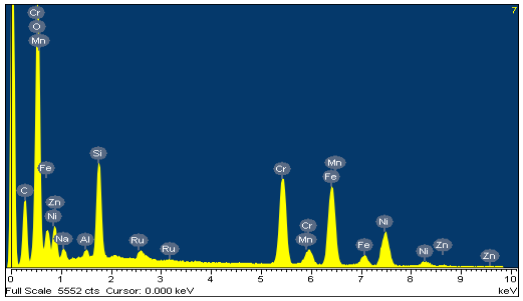

Element	App Conc.	Intensity Corrn.	Weight %	Atomic %
O K	84.28	1.3870	40.93	67.82
Na K	0.49	0.4565	0.72	0.83
Al K	0.54	0.5905	0.62	0.61
Si K	7.75	0.7112	7.34	6.92
Cr K	21.31	0.9456	15.18	7.74
Mn K	1.20	0.8961	0.90	0.43
Fe K	26.21	0.8925	19.78	9.39
Ni K	15.97	0.8660	12.42	5.61
Zn K	0.74	0.8230	0.61	0.25
Ru L	1.72	0.7670	1.51	0.40
Totals			100.00	

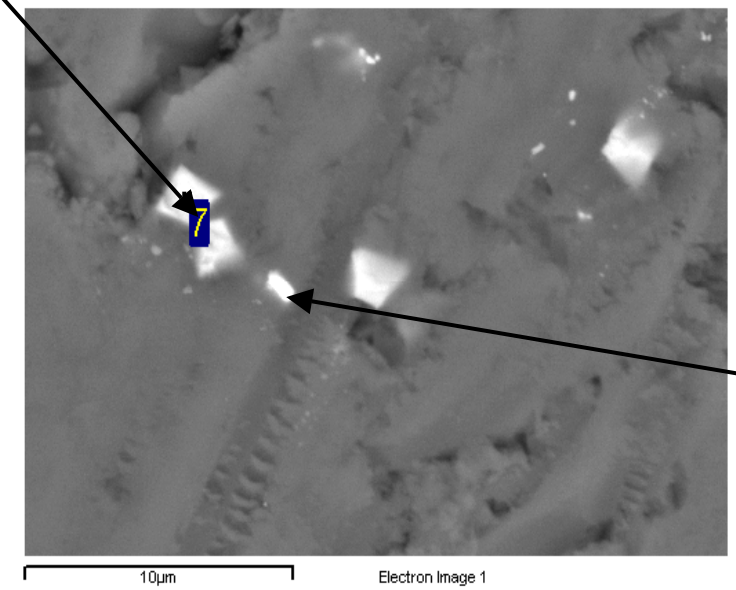

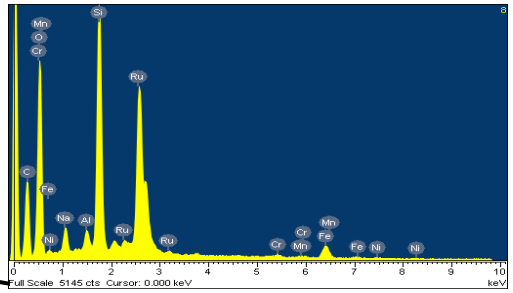

Element	App Conc.	Intensity Corrn.	Weight %	Atomic %
O K	61.77	0.6807	55.40	78.82
Na K	2.89	0.6946	2.54	2.51
Al K	1.32	0.7698	1.05	0.89
Si K	19.09	0.8642	13.48	10.93
Cr K	0.49	0.8429	0.35	0.15
Mn K	0.27	0.8333	0.20	0.08
Fe K	3.70	0.8556	2.64	1.08
Ni K	0.50	0.8718	0.35	0.13
Ru L	30.92	0.7871	23.99	5.40
Totals			100.00	

Figure 4-12. 0.5% $NiCr_2O_4$ in Modifed NCAW (950°C/23h) – Different Region

4.2 Crystallization Studies

XRD was used to compare the effect of RuO_2 and WO_3 on crystals formed in the MS-7 glass melt. Figures 4.13 and 4.14 showed that RuO_2 as well as WO_3 formed mainly spinel (Trevorite – $NiFe_2O_4$) crystals under comparable test conditions (0.5 wt.%, 1000ºC). Undissolved RuO_2 was detected. No other prominent phase could be detected within the detectability of the XRD technique. Further investigation of effects of temperature (950°C) and time (Figure 4.15) on the crystallization confirmed formation of various amounts of Trevorite. These results indicated that WO_3 addition did not crystallize any new phase in the test melt.

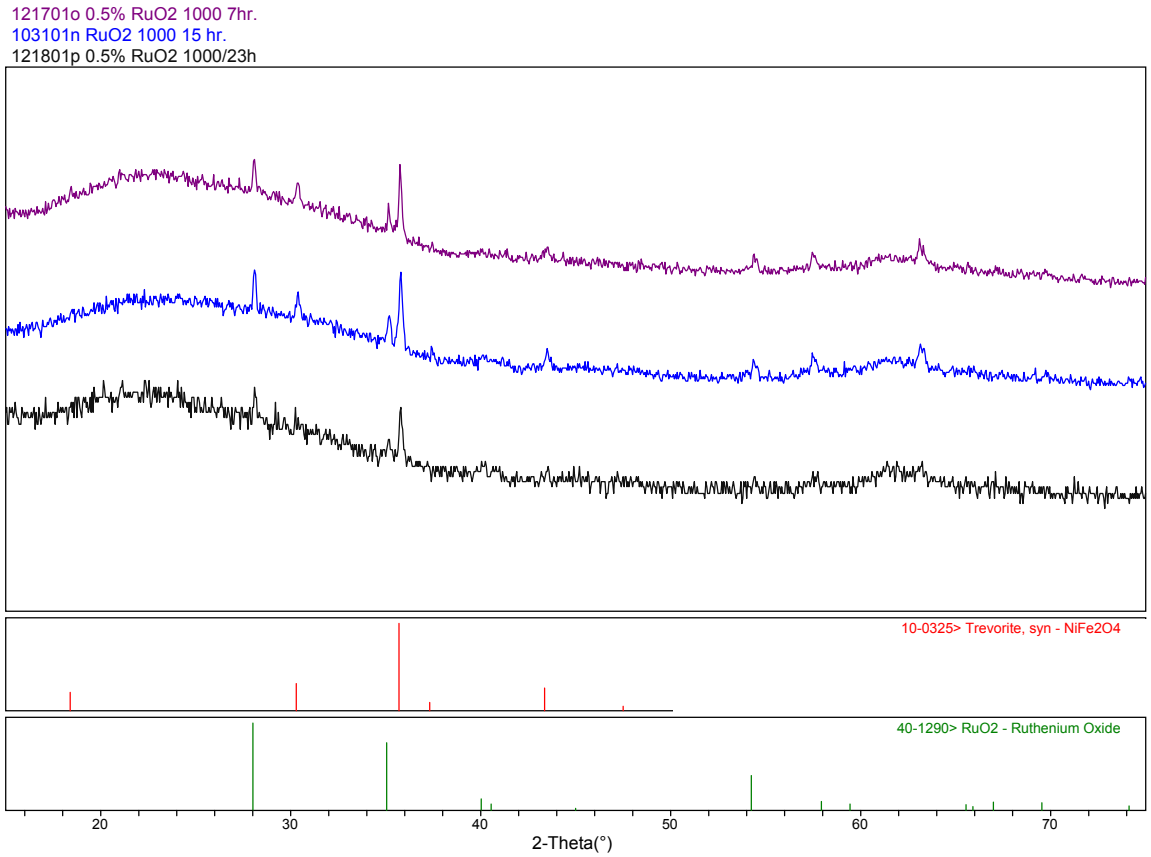

Figure 4-13. XRD of RuO_2 in MS-7 (0.5 wt.%, 1000ºC)

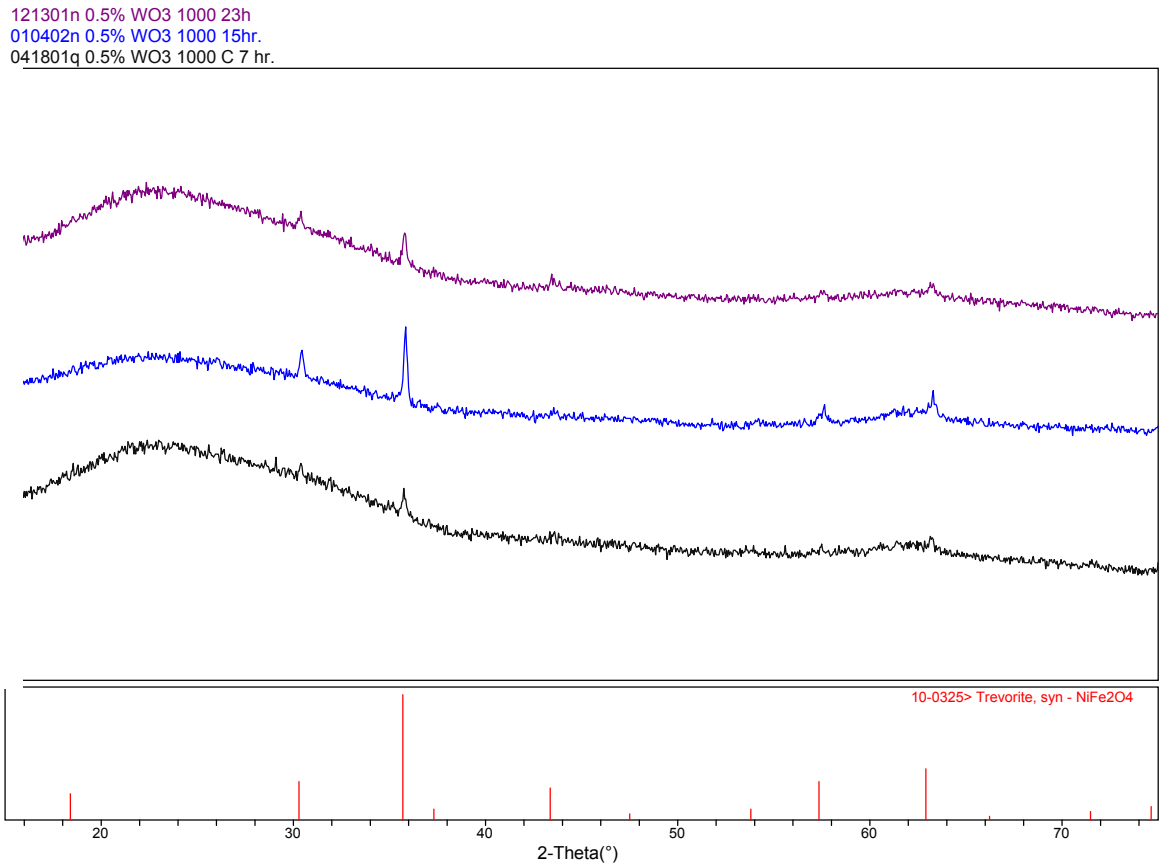

Figure 4-14. XRD of WO_3 in MS-7 (0.5 wt.%, 1000ºC)

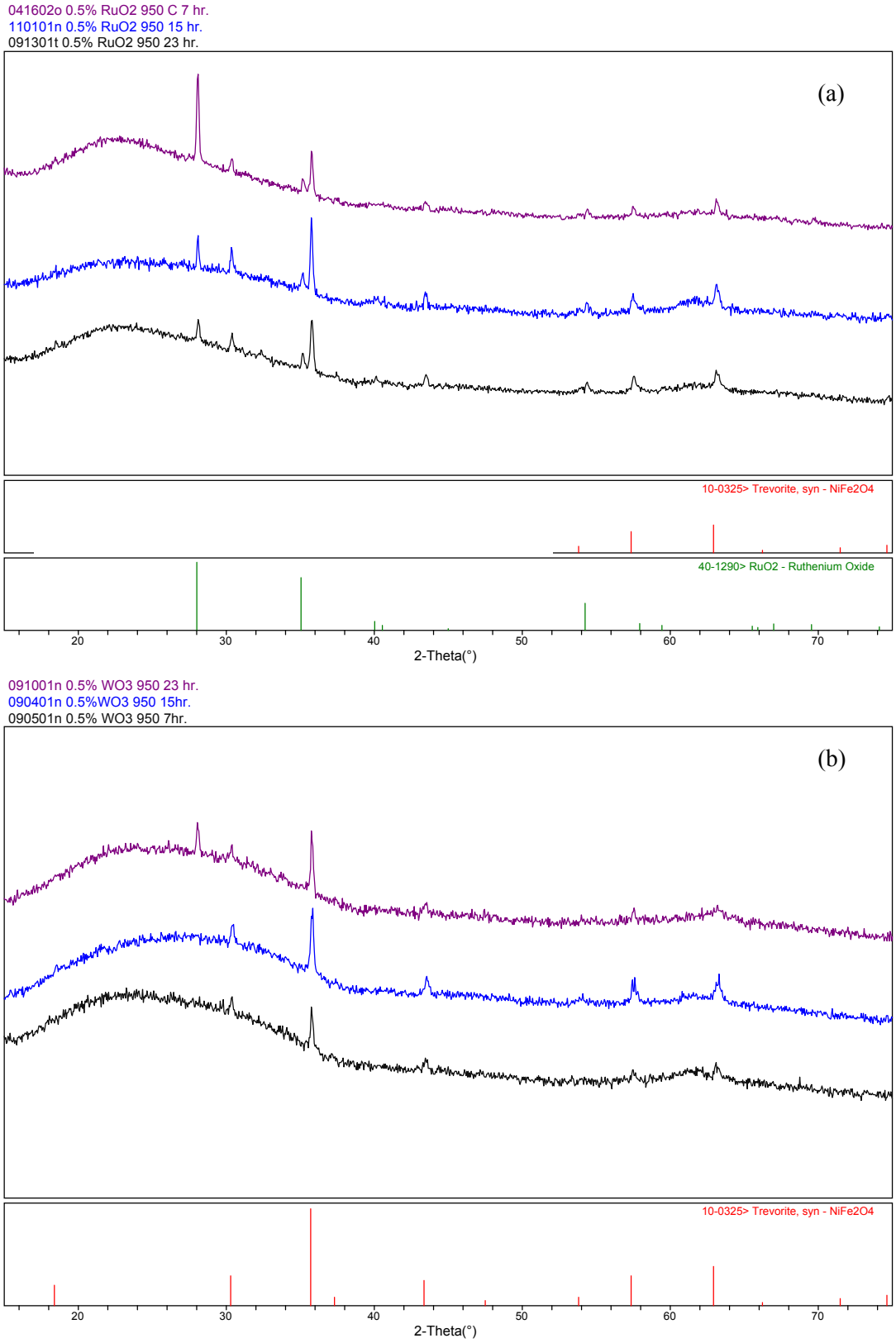

Figure 4-15. XRD of a) RuO_2 and b) WO_3 (MS-7, 0.5 wt.%, 950ºC)

4.3 Viscosity

Gradual addition of $NiCr_2O_4$ to modified would increase the spinel that crystallized from the melt, consequently increasing the viscosity of the melt. This is demonstrated in this section. Figure 4.16 shows the temperature dependence of the base modified NCAW glass. The viscosity values ranged from 1.8 Pa·s at 1356ºC to 17.3 Pa·s at 1051ºC. On addition of 1 wt.% of $NiCr_2O_4$ (Figure 4.17), the viscosity values increased slightly to 3.1 Pa·s at 1247ºC and to 58.6 Pa·s at 953ºC. On further addition (10 wt.% of $NiCr_2O_4$), the viscosity values increased significantly to 47.4 Pa·s at 1351ºC and to 209.8 Pa·s at 1050ºC. At about 1050ºC, the viscosity values were 17.3, 18.2, and 209.8 Pa·s for the base modified NCAW glass, the modified NCAW glass with 1 wt.% $NiCr_2O_4$, and the modified NCAW glass with 10 wt.% $NiCr_2O_4$, respectively.

Figure 4.19 shows the rheology of the modified NCAW glass with 10 wt.% $NiCr_2O_4$. Shear stress (Figure 4.19 (a)) corresponds to viscosity values (Figure 4.19(b)). Temperature schedule is shown for comparison. At 1350ºC, the shear stress was 10 Pa that decreased slightly to 9 Pa at 1250°C. Then the shear stress increased to 11 Pa at 1150ºC and 12 Pa at 1050ºC. The increase in shear stress was attributed to the precipitation and settling of the spinel phase.

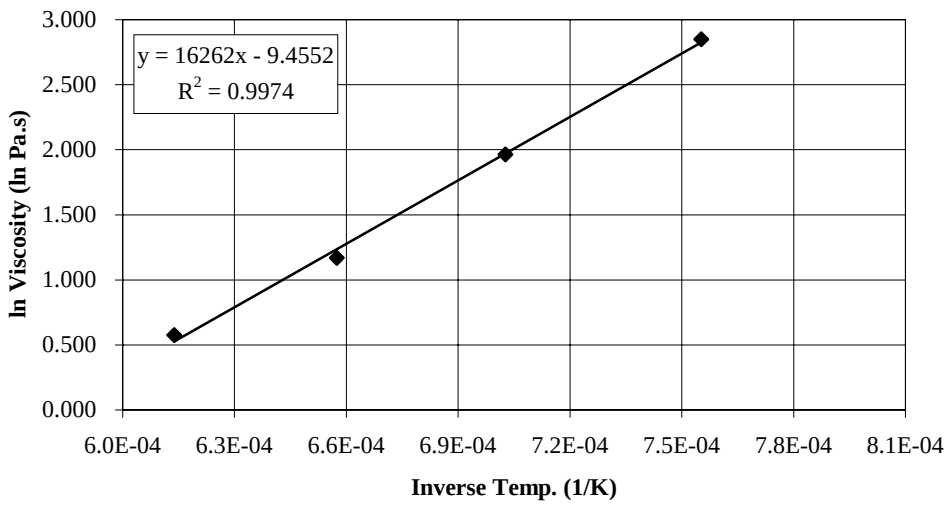

Figure 4-16. Temperature Dependence of Viscosity of Modified NCAW

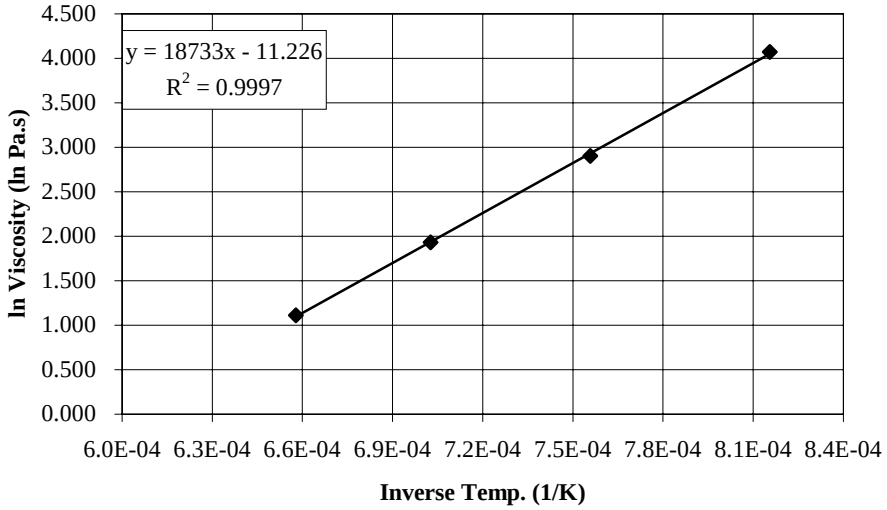

Figure 4-17. Temperature Dependence of Viscosity of Modified NCAW with 1 wt.% $NiCr_2O_4$

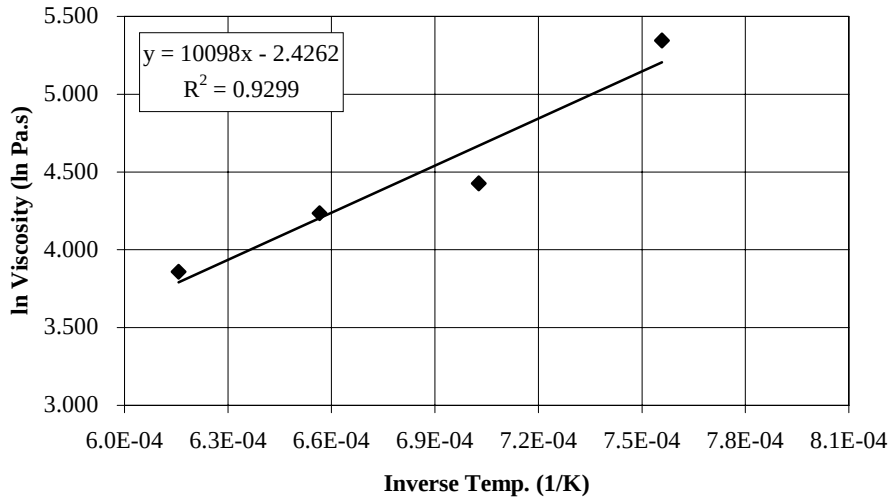

Figure 4-18. Temperature Dependence of Viscosity of Modified NCAW with 10 wt.% $NiCr_2O_4$

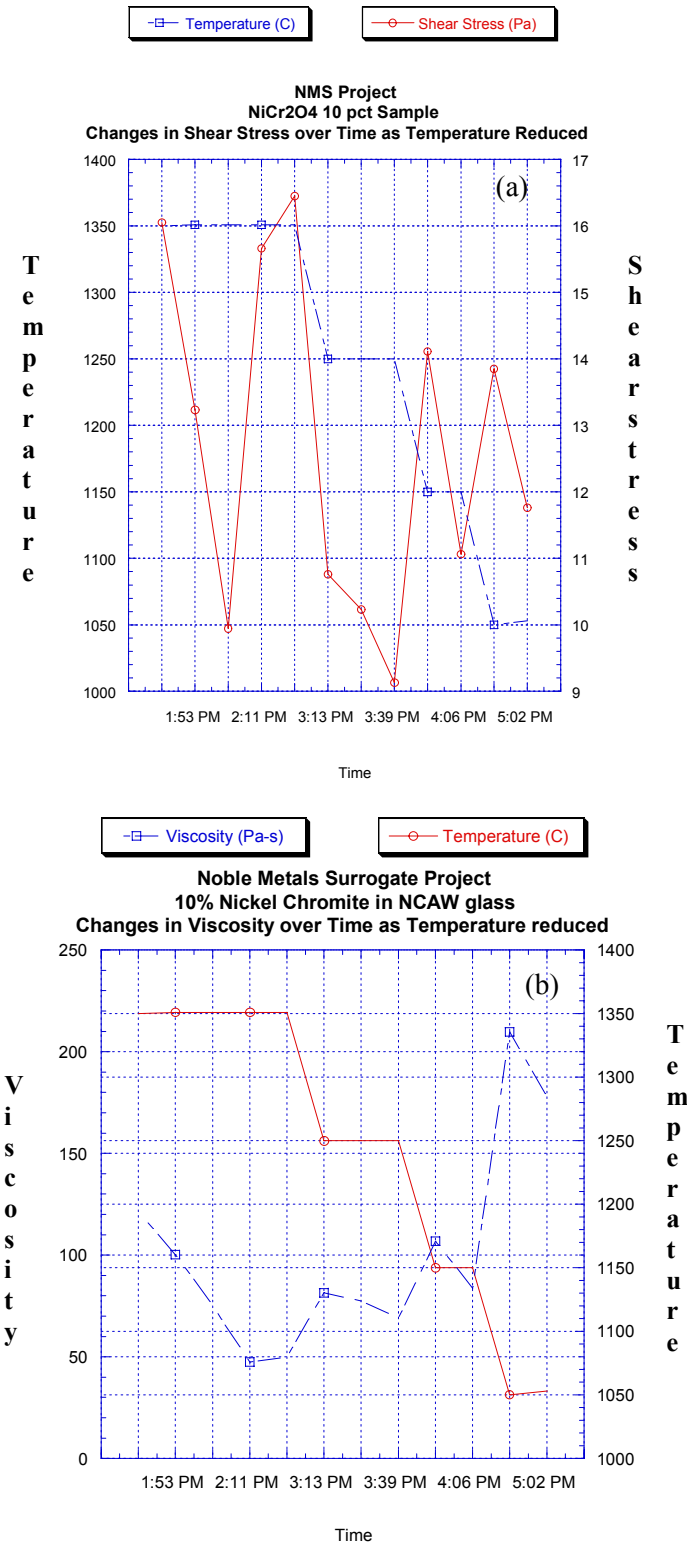

Figure 4-19. (a) Shear Stress and (b) Viscosity of Modified NCAW with 10 wt.% $NiCr_2O_4$

4.4 High Temperature Optical Microscopy

High temperature optical microscopy was used to compare the dissolution and suspension of 1 wt.% of RuO_2 (Figure 4.20) and $NiCr_2O_4$ (Figure 4.21) in MS-7 glass melt. The bright spots were due to reflections of the light from the surface of the melt. The melts showed a lot of activities, that is, moving, turning, bubbling, and convection as the temperature increased. Aggregates of RuO_2 seen at 461ºC in Figure 4.20 incorporated into the melt as the temperature increased. At 994ºC and beyond, residual fibrous suspensions were seen, indicating undissolved RuO_2 floating on the surface. In the case of $NiCr_2O_4$, aggregates incorporated into the melt as temperature increased. At 1078ºC, no suspension was seen, indicating solubility of $NiCr_2O_4$ in the melt. These observations also supported the observations of the double-crucible study (section 4.1).

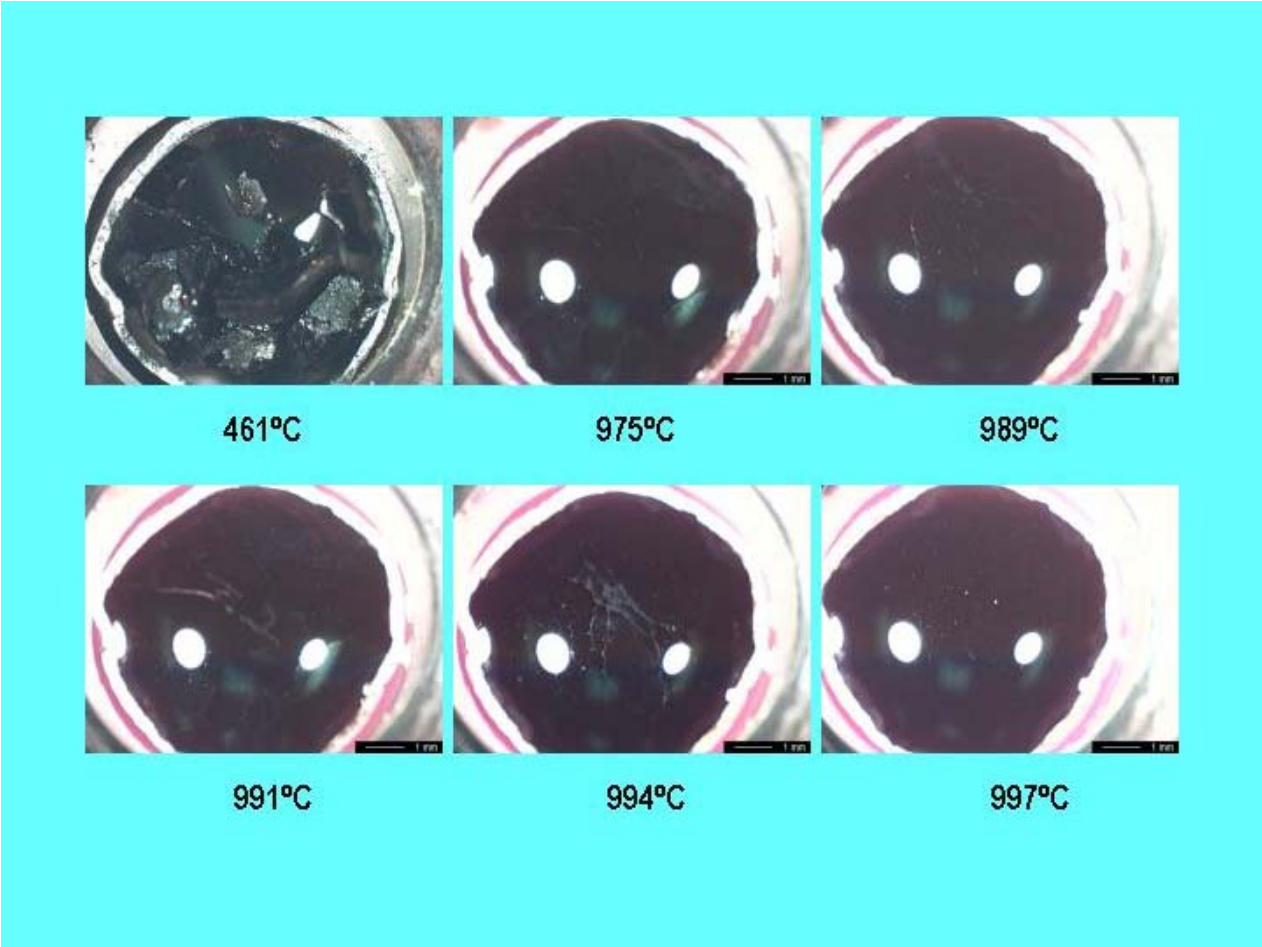

Figure 4-20. High Temperature Optical Micrographs (1 wt.% RuO_2 in MS-7)

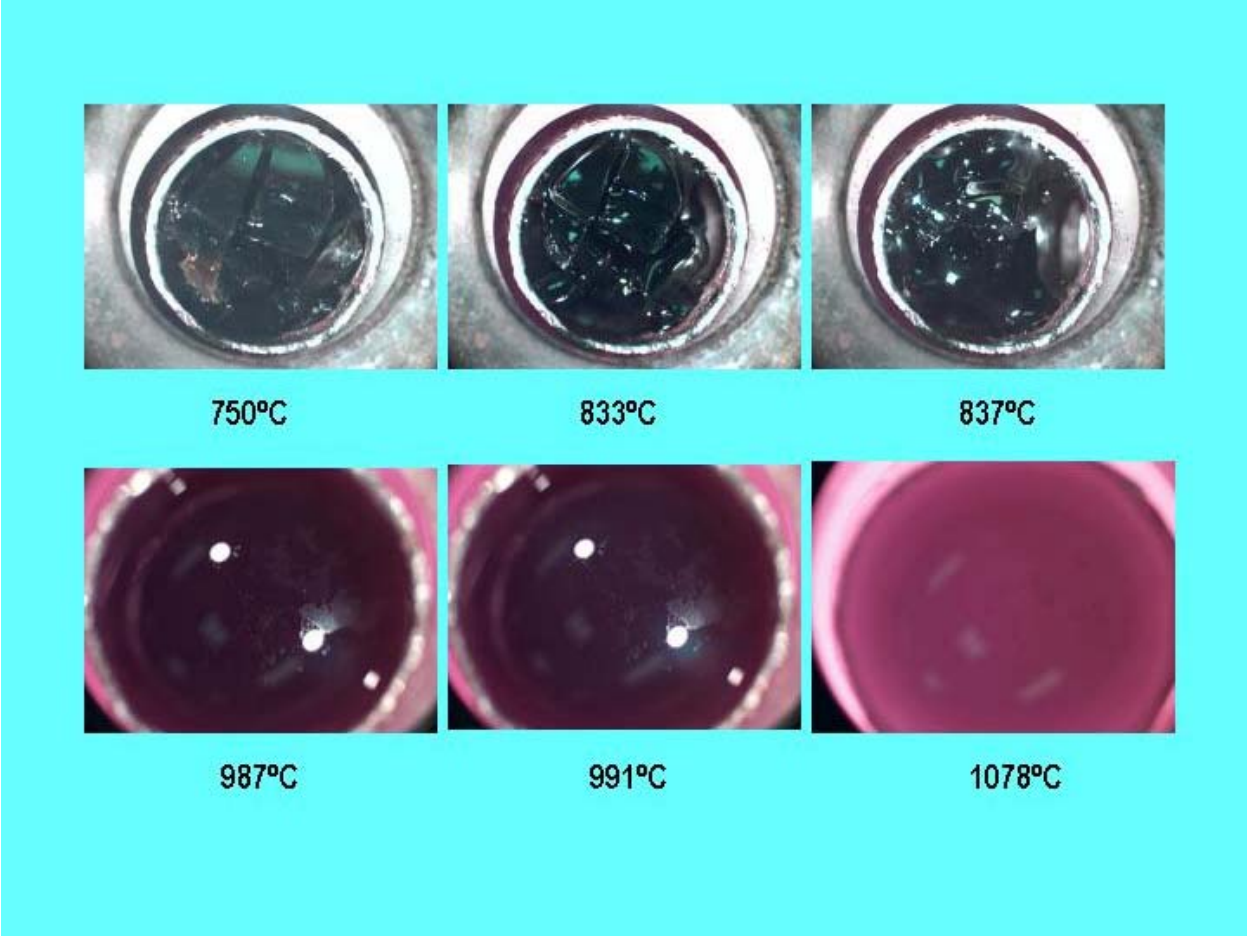

Figure 4-21. High Temperature Optical Micrographs (1 wt.% $NiCr_2O_4$ in MS-7)

4.5 Partition Studies

All partition studies used 0.5 wt.% of Ru, RuO_2, W, or WO_3. All the SEM images shown in this section (Figure 4.22 – 4.31) as well as in Appendix A (Figures A.1-A.20) are back-scattered images. In these figures, the line scans are shown on the SEM images as well as separately for clarity and comparison.

4.5.1 Ru vs. RuO_2

Figures 4.22 and 4.23 compare the addition of Ru and RuO_2 under identical test conditions (900°C/7h), respectively. In the case of Ru (Figure 4.22), an interfacial reaction layer of about 10-20 μm thickness containing Ru and spinel components (Al, Mg) was observed at the spinel-glass interface. Ru particulates crowded the glass side of this interface over 100 μm. Near the reaction layer, dislodged spinel segments were seen. In the case of RuO_2 (Figure 4.23), the reaction layer was about 5-15 μm. On the glass side of the interface, several dislodged spinel segments drifting well into the glass was seen. Ru-containing clusters were also seen in the glass side of the interfacial region.

4.5.2 W vs. WO_3

Figures 4.24 and 25 compare the addition of W and WO_3 under identical test conditions (900ºC/7h), respectively. In the case of W (Figure 4.24), an interfacial reaction layer of about 10-15 μm thickness containing W and spinel components was observed at the spinel-glass interface. On the glass side of the interface, several dislodged spinel segments drifting into the glass was seen. A few W-containing particulates were also observed. In the case of WO_3 (Figure 4.25), the interfacial layer was thicker (20-30 μm) with no dislodged spinel segments in the interfacial region.

4.5.3 Effect of Temperature of Testing

On increasing the test temperature from 900 to 1000ºC for 7h of exposure, the thickness of the interfacial reaction layer remained more or less same in the sample containing RuO_2 (Figure 26 vs. Figure 27). At 1000ºC, the dislodged spinel segments dissolved into the glass melt. Ru-containing particulates were observed in the interfacial regions. Recrystallization of spinel (sharp edges of crystals in the glass side in Figure 4.27) was observed at 1000ºC.

In the case of WO_3, increase of test temperature from 900 to 1000ºC for 7 h exposure (Figure 4.28 vs. Figure 4.29) resulted in a slightly thinner interfacial reaction layer. At 1000ºC, the spinel started dislodging and drifting into the glass side of the interfacial region. Other features remained the same.

4.5.4 Effect of Duration of Testing

On increasing the duration of the testing from 7h to 23h, RuO_2 showed the interfacial layer of more or less same thickness of about 5-15 μm, containing Ru- and spinel components (Figure 4.30). For extended period of exposures (after 19h), spinel dislodging and drifting into the glass melt was observed. Ru-rich clusters were seen in the glass side of the interfacial region.

In the case of WO_3, the reaction layer gradually thickened with increasing exposure time (Figure 4.31). Cracks along the interfacial reaction layer for 19h and 23h exposures indicated removal of the thick reaction layer due to difference in thermal expansion characteristics of the layer compared to the spinel and glass that resulted in interfacial stresses. Small segments of spinel continued to dissolve in to the glass. Recrystallization of large spinel crystals was observed for 23 h exposure.

4.5.5 Partition - RuO_2 vs. WO_3

The results presented in this section (Figures 4.22 – 4.31) and the Appendix A (Figures A.1 – A.20) revealed the similarities and differences between RuO_2 and WO_3. The similarities were:

- The glass melt reacted with the spinel forming a reaction layer at the spinel-glass interfacial region. Ru or W partitioned in spinel in this reaction layer.
- Dislodged spinel segments from the bulk spinel eventually dissolved into the glass melt.
- Ru-containing and W-rich regions were observed in the glass side of the interfacial region.
- Spinel (either $MgAl_2O_4$ or Trevorite or a combination of these two) recrystallized in the glass melt.

The differences were:

- Spinel segments started dislodging from the bulk and drifting into the glass melt early in the process with WO_3.
- The reaction layer thickened with duration of testing in the case of WO_3. Interfacial cracks indicated stresses introduced by the thickening reaction layer at the spinel-glass interfacial region.
- In the case of RuO_2, undissolved Ru-containing particles crowded the interfacial region.
- Bigger spinel crystals (sharp plates as well as nodular) recrystallized from the melt with WO_3 as compared to small crystal with RuO_2 for identical test conditions.

In spite of these differences, the basic interaction mechanism was found to identical in these cases. These results supported use of WO_3 as a suitable surrogate for RuO_2 in the test glass melt.

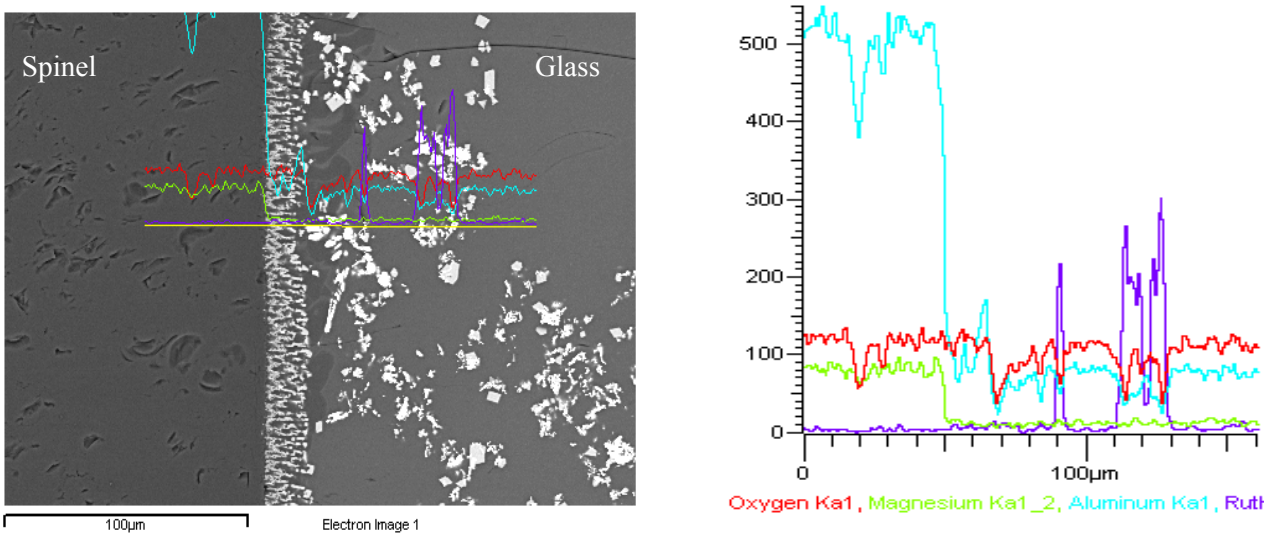

Figure 4-22. SEM (Left) – Line EDS (Right) of Ru in MS-7 (900ºC/7h)

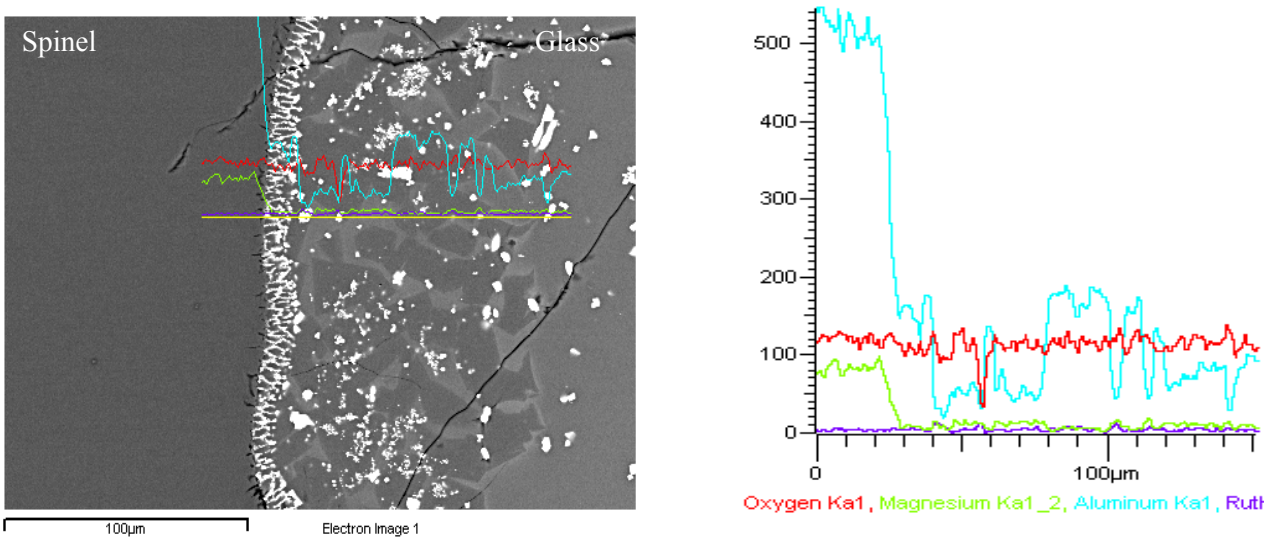

Figure 4-23. SEM (Left) – Line EDS (Right) of RuO_2 in MS-7 (900ºC/7h)

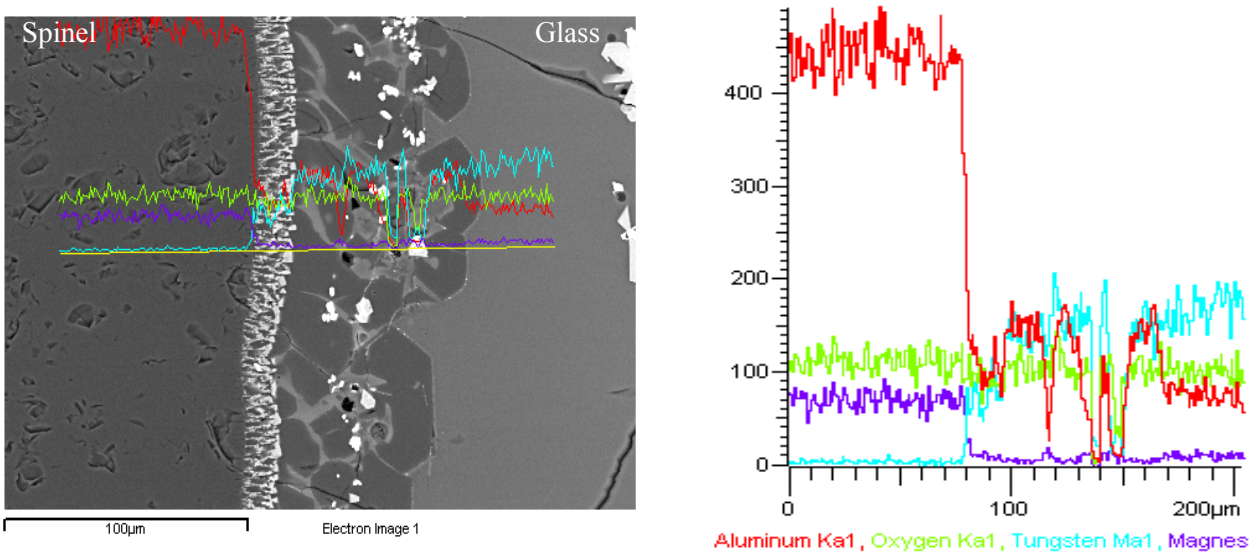

Figure 4-24. SEM (Left) – Line EDS (Right) of W in MS-7 (900ºC/7h)

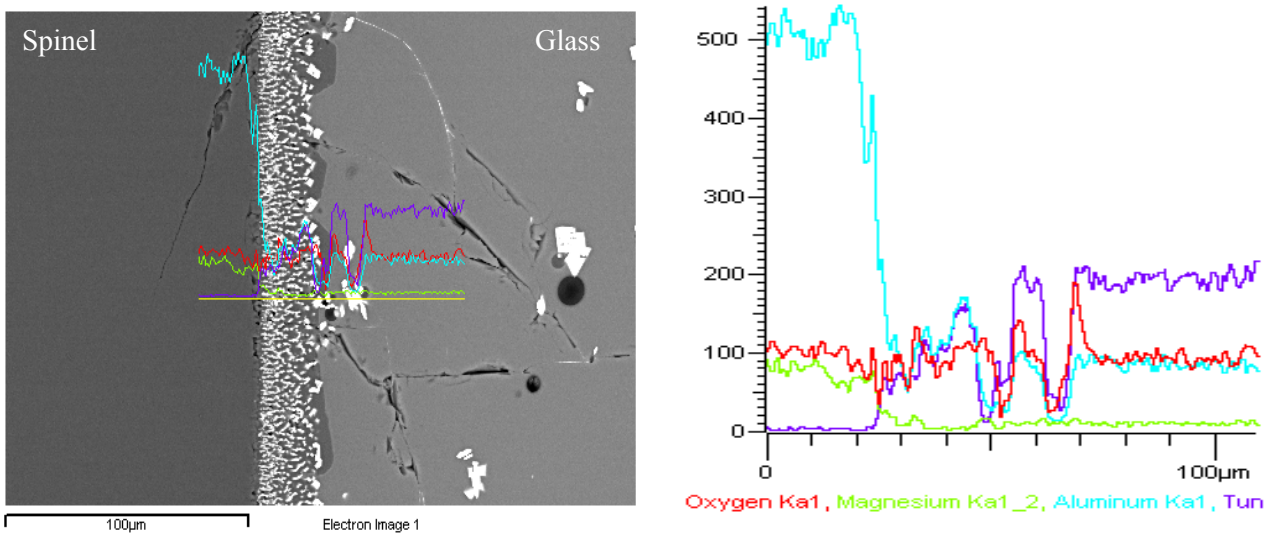

Figure 4-25. SEM (Left) – Line EDS (Right) of WO_3 in MS-7 (900ºC/7h)

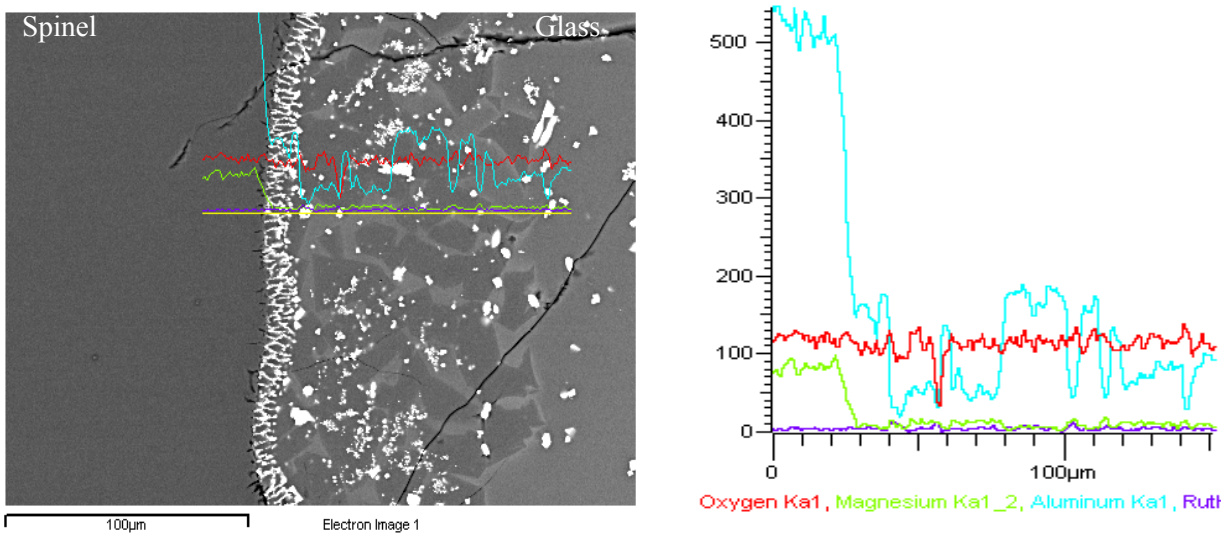

Figure 4-26. SEM (Left) – Line EDS (Right) of RuO_2 in MS-7 (900ºC/7h)

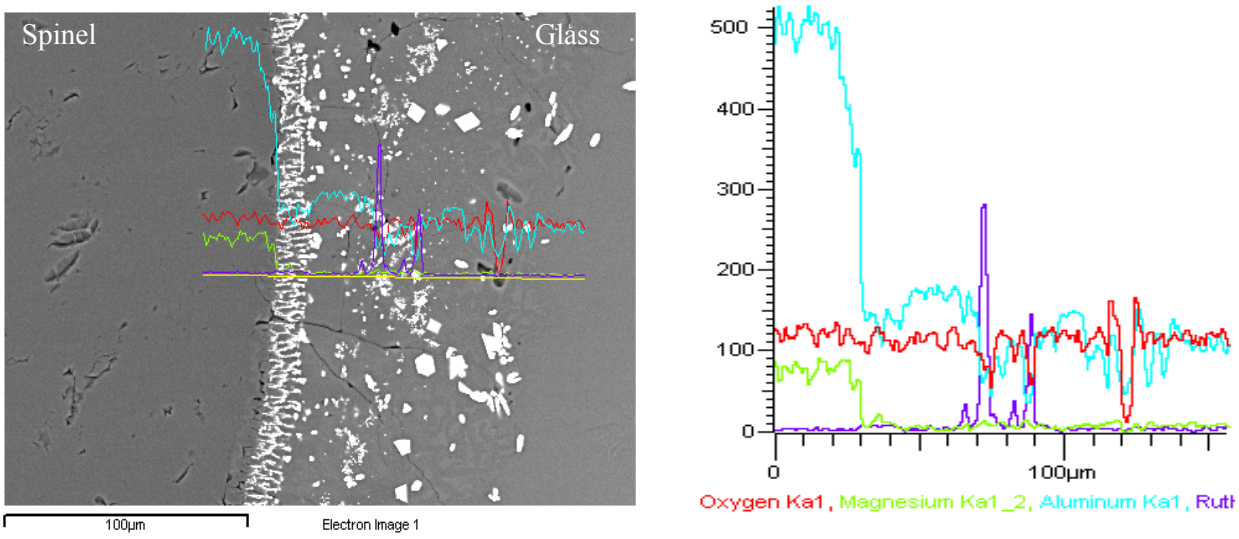

Figure 4-27. SEM (Left) – Line EDS (Right) of RuO_2 in MS-7 (1000ºC/7h)

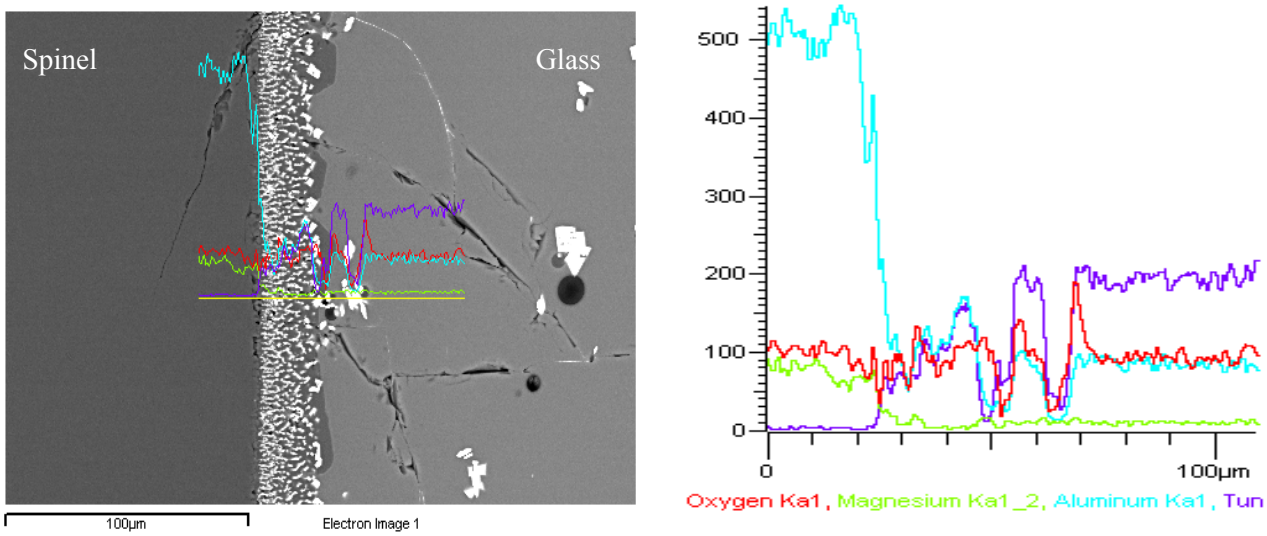

Figure 4-28. SEM (Left) – Line EDS (Right) of WO_3 in MS-7 (900ºC/7h)

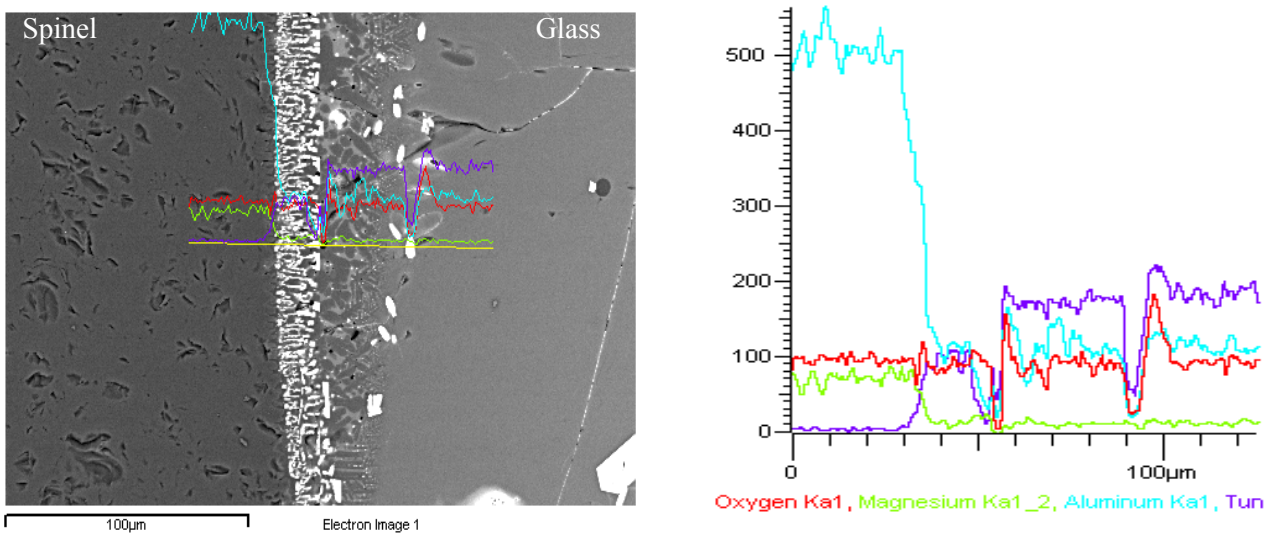

Figure 4-29. SEM (Left) – Line EDS (Right) of WO_3 in MS-7 (1000ºC/7h)

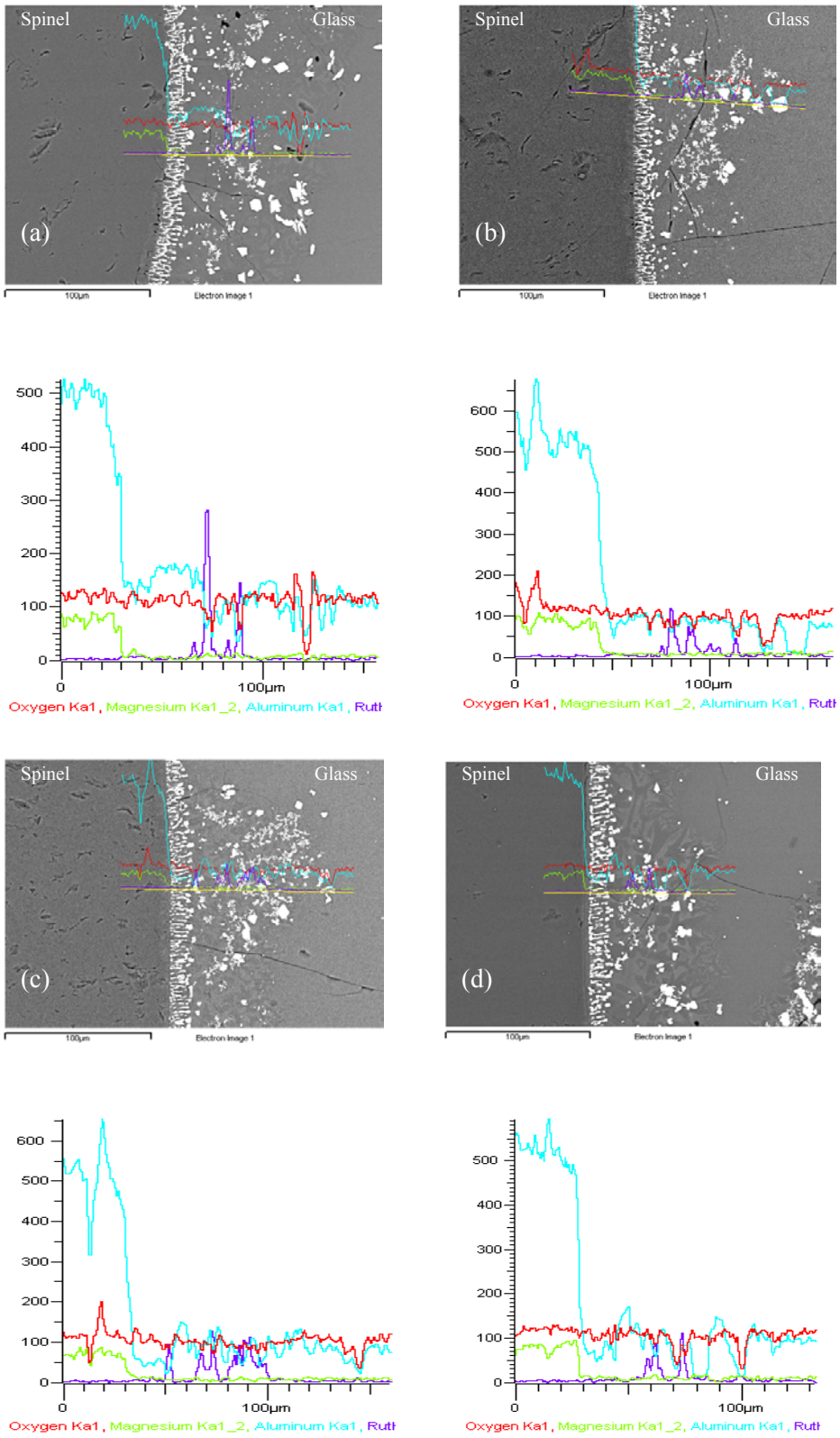

Figure 4-30. SEM (Top) – Line EDS (Bottom) of RuO_2 in MS-7 (1000ºC) for (a) 7h, (b) 15h, (c) 19h, and (d) 23h

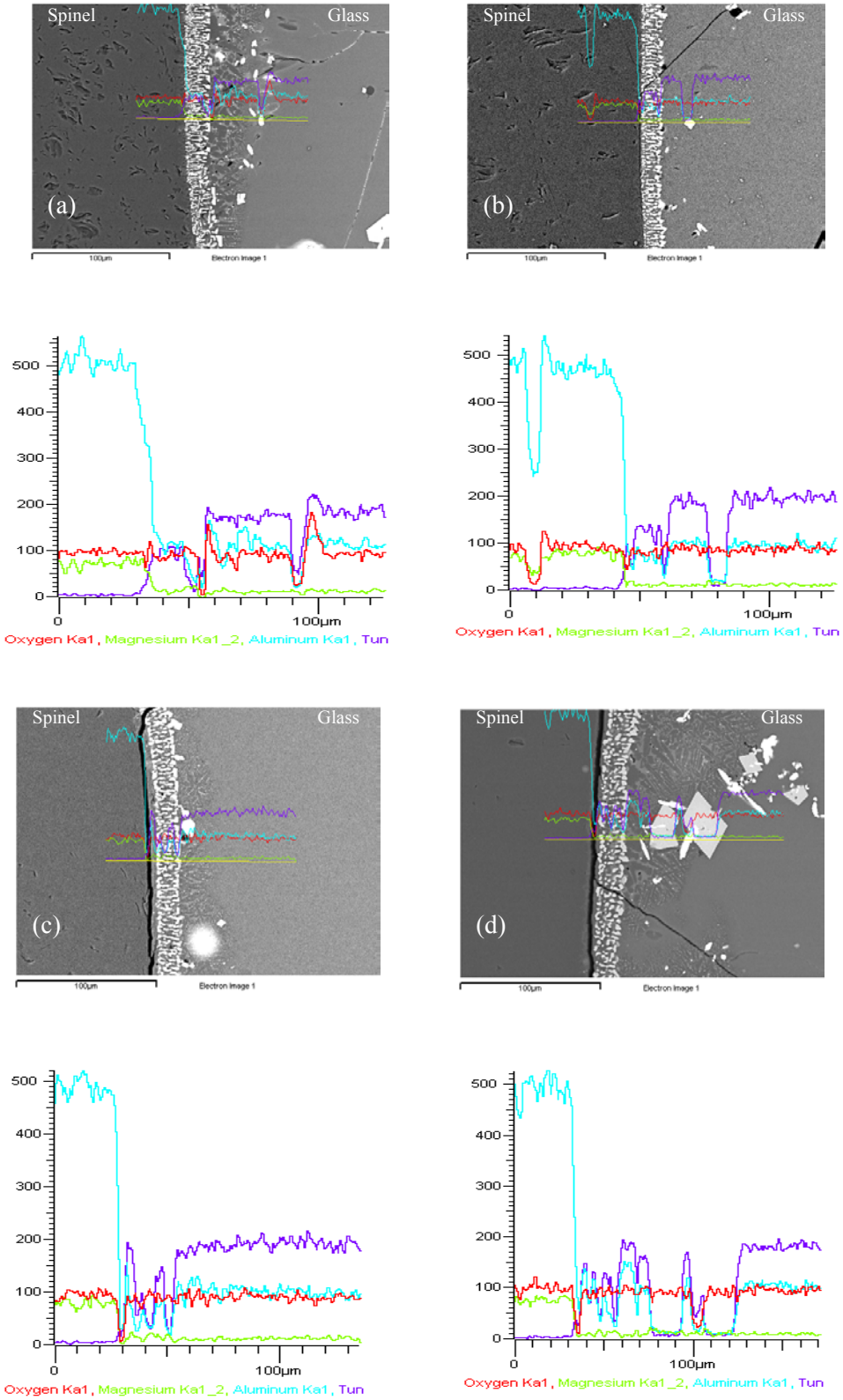

Figure 4-31. SEM (Top) – Line EDS (Bottom) of WO_3 in MS-7 (1000ºC) for (a) 7h, (b) 15h, (c) 19h, and (d) 23h

4.6 AC Conductivity Results

Figure 4.32 shows the AC conductivity of DWPF frit containing 1-10 wt. % of Inconel 600 powder, as a conductivity surrogate. Integrated DWPF Melter System (IDMS) data are shown for comparison. IDMS was run for over seven years before shutting down for post mortem analysis. The meltblobs were found at the bottom of the melter, containing significant level of the noble metals as sludge. At lower temperature (950-1050°C), the conductivity values are comparable to each other (< 100 S/m). As the temperature increased, the IDMS showed a sharp increase in conductivity.

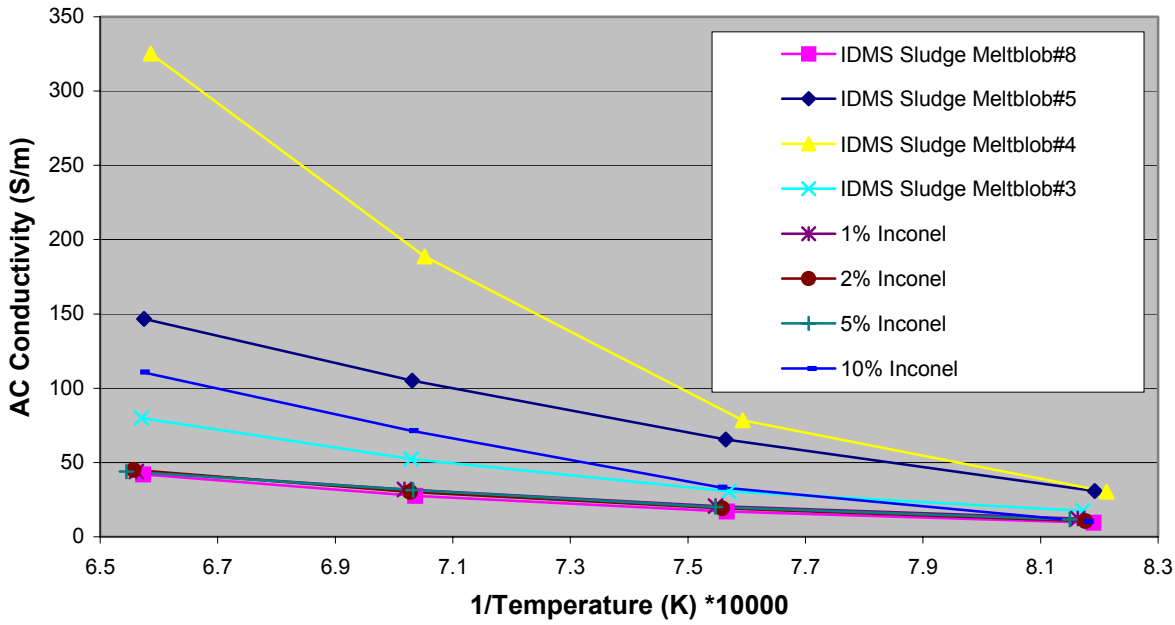

Figure 4-32 AC conductivity of DWPF frit containing Inconel 600

(Integrated DWPF Melter System (IDMS) data are shown for comparison.)

Figures 4.33 - 4.36 show the temperature dependence of AC conductivity of DWPF frit containing other conductivity surrogates, Cr_2O_3, $NiCr_2O_4$, RuO_2, and WO_3, respectively. Except the case of $NiCr_2O_4$, the additives showed a steady drop in conductivity with increase in the amount of additive until 5 wt. %. Above this limit, the conductivity increased, indicating connectivity among additive particles that establish low resistance paths for current flow in the melt. In the case of $NiCr_2O_4$, the conductivity continued to decrease with 10 wt.% addition. Cr_2O_3 showed conductivity data closely following the data of RuO_2.

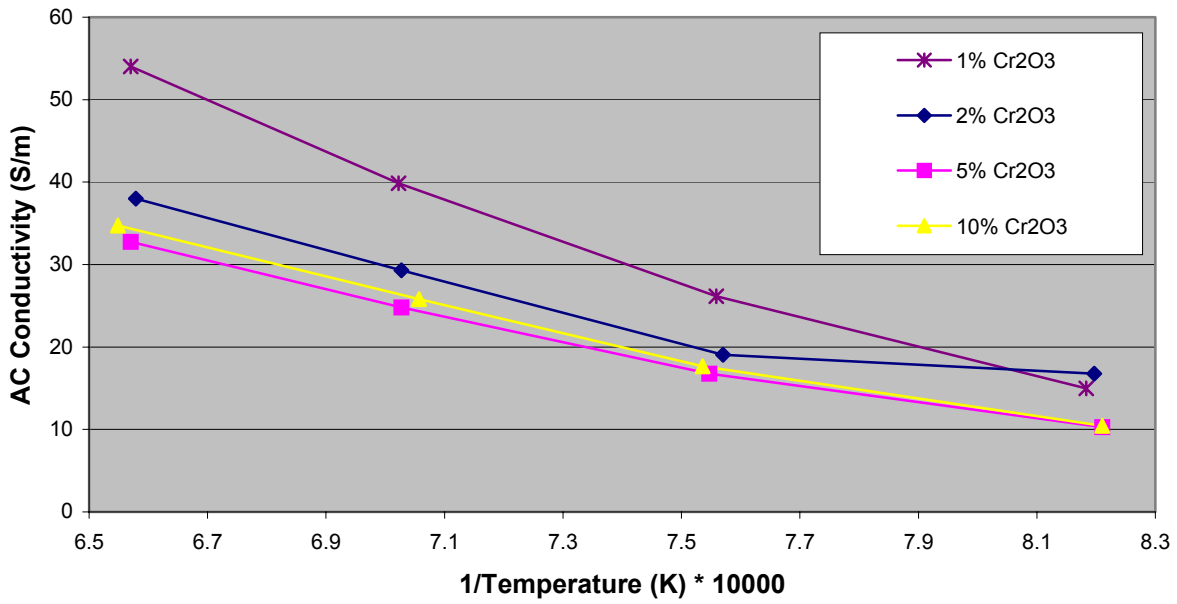

Figure 4-33 AC conductivity of DWPF frit containing Cr_2O_3

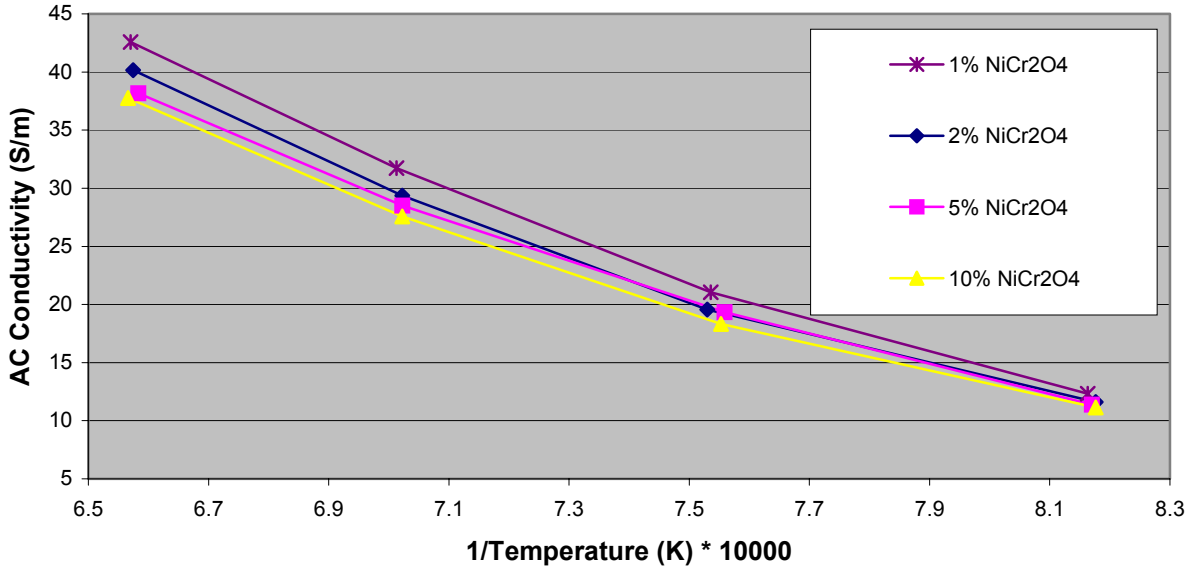

Figure 4-34 AC conductivity of DWPF frit containing $NiCr_2O_4$

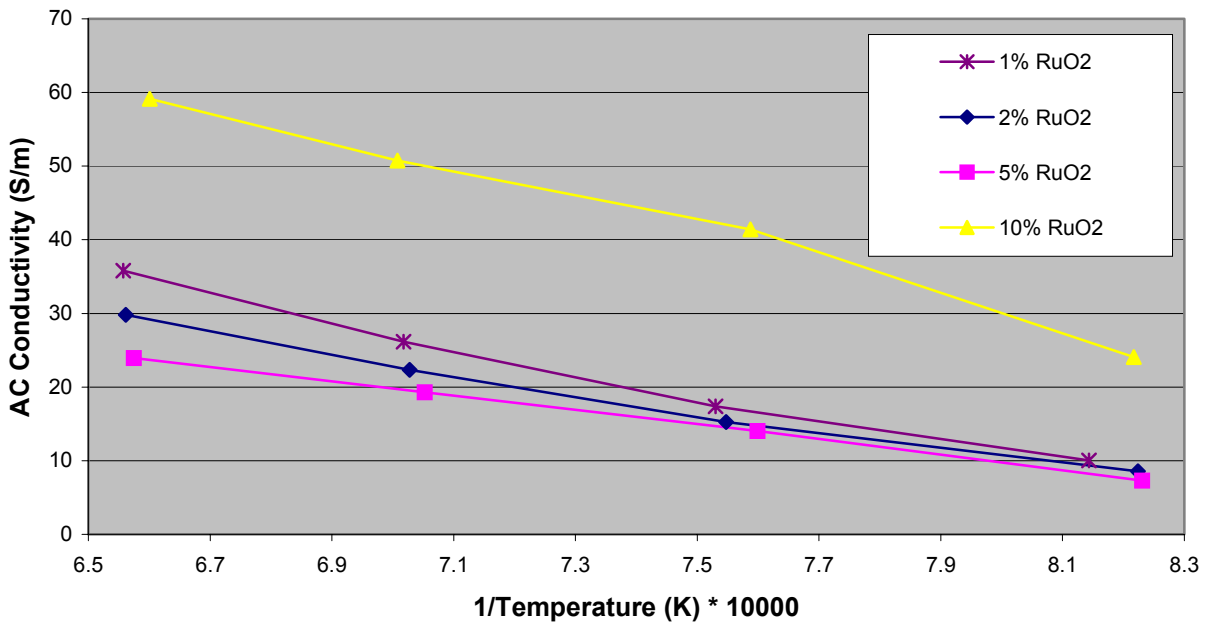

Figure 4-35 AC conductivity of DWPF frit containing RuO_2

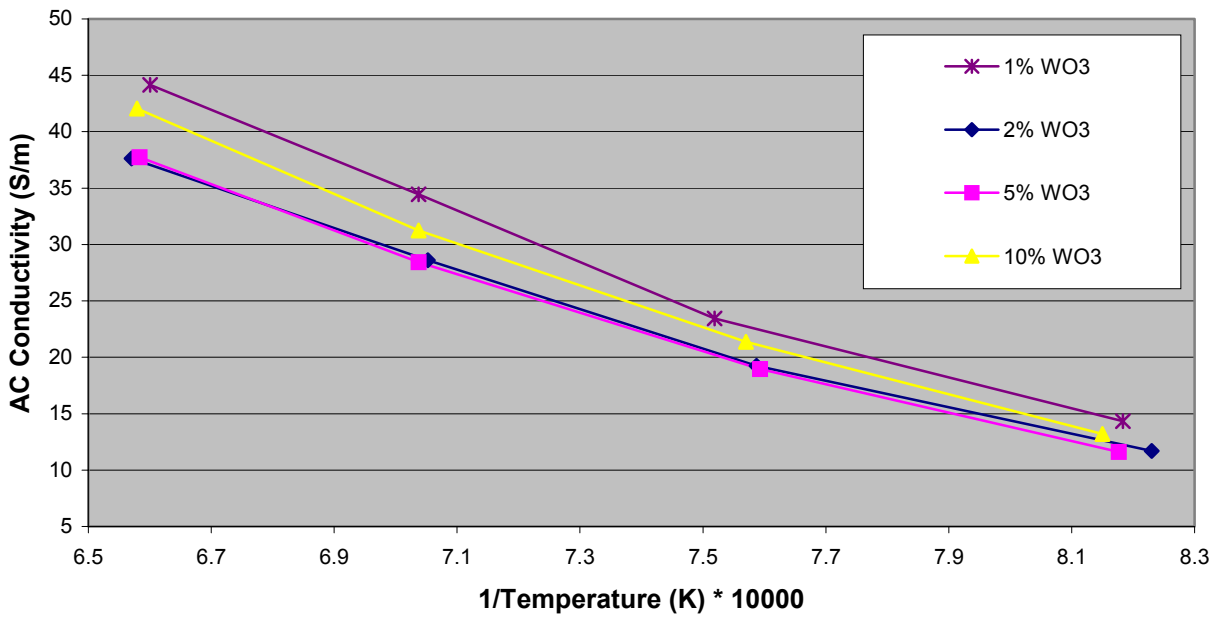

Figure 4-36 AC conductivity of DWPF frit containing WO_3

5.0 Conclusion and Recommendation

1. Limited data on noble metals solubility in silicate glass exists in the literature. Data on Ru-solubility is inconclusive. Currently, no data exists on noble metals surrogate solubility in nuclear waste glass melts. A systematic study of the solubility of noble metals (mainly Ru) as well as suitable surrogates in nuclear waste glass melts is recommended.

2. Overview of existing literature on noble metals in waste melts and melter testing indicates that RuO_2 is the most commonly detected phase present. Hence, the present investigation is focused at RuO_2 and its potential suitable surrogates.

3. Thermodynamic and density consideration supports the promise of using W-O system as a surrogate for Ru as well as RuO_2. WO_2 (12.11 g/cm^3) can act as a surrogate for Ru (12.30 g/cm^3) under reducing conditions. Alternatively, WO_3 (7.20 g/cm^3) can act as a surrogate for RuO_2 (6.97 g/cm^3) under oxidizing conditions. WO_3 is selected as the potential surrogate for RuO_2 in this investigation. Cost data also supports this selection.

4. Double-crucible settling study indicates formation of more spinel crystals have formed at 950ºC and started settling at 1000ºC, with RuO_2 as well as WO_3 in MS-7 glass. SEM, EDS, and XRD data have supported this observation. XRD data has not shown any other phase formed. Ru has been found to partition readily in the spinel phase, as compared to W.

5. Crystallization study has shown formation of Trevorite phase in the sample with addition of RuO_2 as well as WO_3. Unlike WO_3, the undissolved RuO_2 is detected by the XRD.

6. An order of magnitude increase in viscosity values has been observed as addition of $NiCr_2O_4$ (one of potential surrogates studied in this project) increased from 1 wt.% to 10 wt.% in modified NCAW glass melts. This also results in an increase in shear stress of rotating spindle in rheology testing. This data clearly establishes the consequences of increased spinel formation and accumulation.

7. High temperature optical microscopy results show floating nodular aggregates of RuO_2 at higher temperature (> 900ºC) due to its insolubility in the MS-7 melt. On the contrary, $NiCr_2O_4$ dissolved completely in the test melt.

8. Partitioning study of noble metal species (Ru and RuO_2) and the surrogate species (W and WO_3) between spinel (nonstoichiometric $MgAl_2O_4$) and model glass melt (MS-7) indicates striking similarity between RuO_2 and WO_3 in their interaction with the glass melt. Based on these results, use of WO_3 as a suitable surrogate for RuO_2 is recommended.

9. Conductivity data indicate that effect of Cr_2O_3 addition closely follow that of RuO_2 in DWPF frit.

10. In the absence of advanced data on solubility of the noble metals and surrogates, a research-scale melter (RSM) test is recommended before testing the surrogate in an engineering scale melter. RSM test will provide key processing data that will help planning the engineering scale melter test.

6.0 References

Sundaram, S. K and J. M. Perez. 2000. *Noble Metals and Spinel Settling in High Level Waste Glass Melter*s. PNNL-13347, September 2000.

Hutson, N. D. 1992. *Integrated DWPF Melter System (IDMS) Campaign Report: Hanford Waste Vitrification Plant (HWVP) Process Demonstration (U)*. WSRC-TR-92-0403, Rev. 1, Westinghouse Savannah River Company, Savannah River Technology Center, Aiken, South Carolina; Hutson, N. D., and M. E. Smith. 1992. "The Behavior and Effects of the Noble Metals in the DWPF Melter System." Proceedings of the High Level Radioactive Waste Management Conference, American Nuclear Society, La Grange Park, Illinois. 1:541-548.

Hutson, N. D. 1993. *IDMS Task Summary Report Part 1: The Behavior and Effects of the Noble Metals in the DWPF Melter System*. WSRC-TR-93-0458, Savannah River Technology Center, Aiken, South Carolina.

Hutson, N. D., J. R. Zamecnik, M. E. Smith, D. H. Miller, and J.A. Ritter. 1991. *Integrated DWPF Melter System (IDMS) Campaign Report: The First Two Noble Metals Operations (U)*. WSRC-TR-91-400, Defense Waste Processing Technology, Savannah River Laboratory, Aiken, South Carolina.

Bailer, J. C., H. J. EmelJus, T. Nyholm, and A. F. Trotman-Dickenson. 1973. *Comprehensive Inorganic Chemistry*, Vol. 5, Pergamon, New York, 1189-1209.

Mukerji, J and S. R. Biswas. 1967. "Solubility of Ruthenium in Soda-Silica Glass," *Cent. Glass Ceram. Res. Inst. Bull.*, 14, 30-34.

Biswas, S. R. and J. Mukerji. 1968. "Solubility of Ruthenium in Silicate and Phosphate Glasses," *Cent. Glass Ceram. Res. Inst. Bull.*, 15, 99-103.

Mukerji, J and S. R. Biswas. 1971. "Oxidation States of Ruthenium in Glasses," *Glass Technol.*, 12, 107-111.

Mukerji, J. 1972. "Absorption Spectra of Ruthenium in Borosilicate, Phosphate, and Aluminoborophosphate Glasses," *Glass Technol.*, 13, 135-137.

Mukerji, J. 1975. "ESR Spectra of Ruthenium in Glass," *Phys. Chem. Glasses*, 16, 61.

Schreiber, H. R., F. A. Settle, Jr., P. L. Jamison, J. P. Eckenrode, and G. W. Headley. 1986. "Ruthenium in Glass-Forming Borosilicate Melts." *J. Less Comm. Metals*, 115, 145-154.

Borisov A., H. Palme, and B. Spettle. 1994. "Solubility of Palladium in Silicate Melts: Implications for Core Formation in the Earth." *Geochim. Cosmochim. Acta.*, 58, 705-716.

Dingwell, D. B., H. St. C. Neill, W. Ertel, and B. Spettel. 1994. "The solubility and Oxidation State of Ni in Silicate Melt at Low Oxygen Fugacities: Results using a Mechanically Assisted Equilibrium Technique, *Geochim. Cosmochim. Acta.*, 58, 1967-1974.

Holzheid, A., A. Borisov, and H. Palme. 1994. "The Effect of Oxygen Fugacity and Temperature on Solubilities of Nickel, Cobalt, and Molybdenum in Silicate Melts." *Geochim. Cosmochim. Acta.*, 58, 1975-1981.

W. Ertel, H. St. C. O'Neill, D. B. Dingwell, and B. Spetel. 1996. "Solubility of Tungsten in a Haplobasaltic Melt as a Function of Temperature and Oxygen Fugacity." *Geochim. Cosmochim. Acta.*, 60(7), 1171-1180.

Capobianco, C. J. and M. J. Drake. 1990. "Partitioning of Ruthenium, Rhodium, and Palladium between Spinel and Silicate Melt and Implications for Platinum Group Element Fractionation Trends." *Geochim. Cosmochim. Acta.*, 54, 869-874.

Klouzek, J., Alton, P. Hrma, and T. Plaisted. 2001. "Crucibel Study of Spinel Settling in Molten High-Level Waste Glass." *Ceramic Transactions*, Volume 119, 301-308.

Plaisted, T., J. Alton, B. Wilson, and P. Hrma. 2001. "Effect of Minor Component Addition on Spinel Crystallization in Simulated High-Level Waste Glass." *Ceramic Transactions*, Volume 119, 291-299.

LaMont, M. and P. Hrma. 1998. "A Crucible Study of Spinel Settling in a High-Level Waste Glass." *Ceramic Transactions*, Volume 23, 343-348.

Appendix A

Additional Noble Metal Partition Data (SEM/EDS)

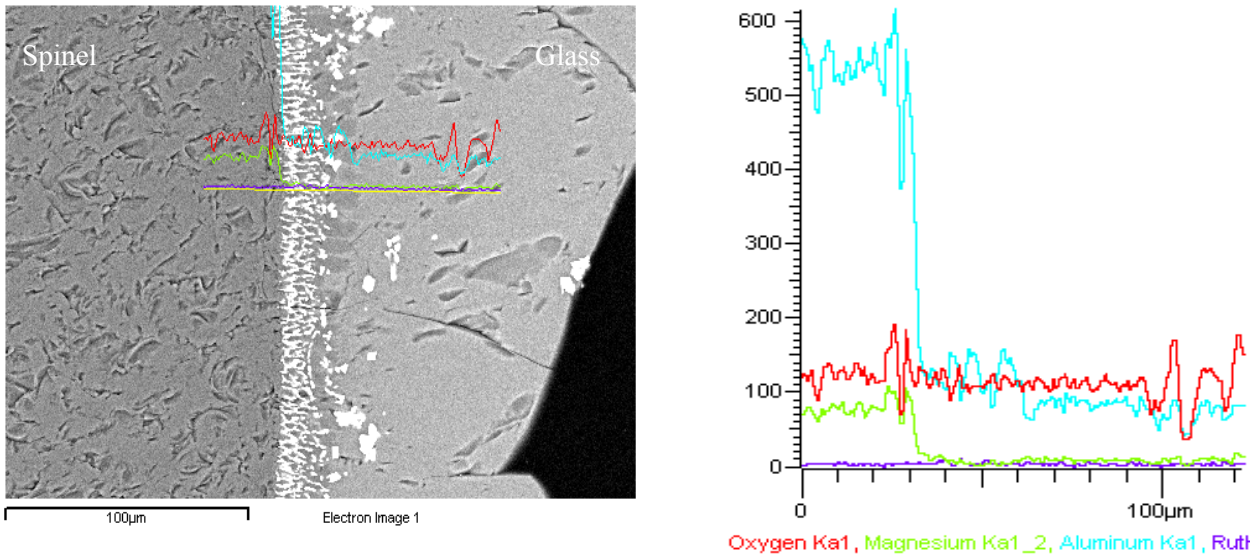

Figure A.1. SEM (Left) – Line EDS (Right) of Ru in MS-7 (900ºC/15h)

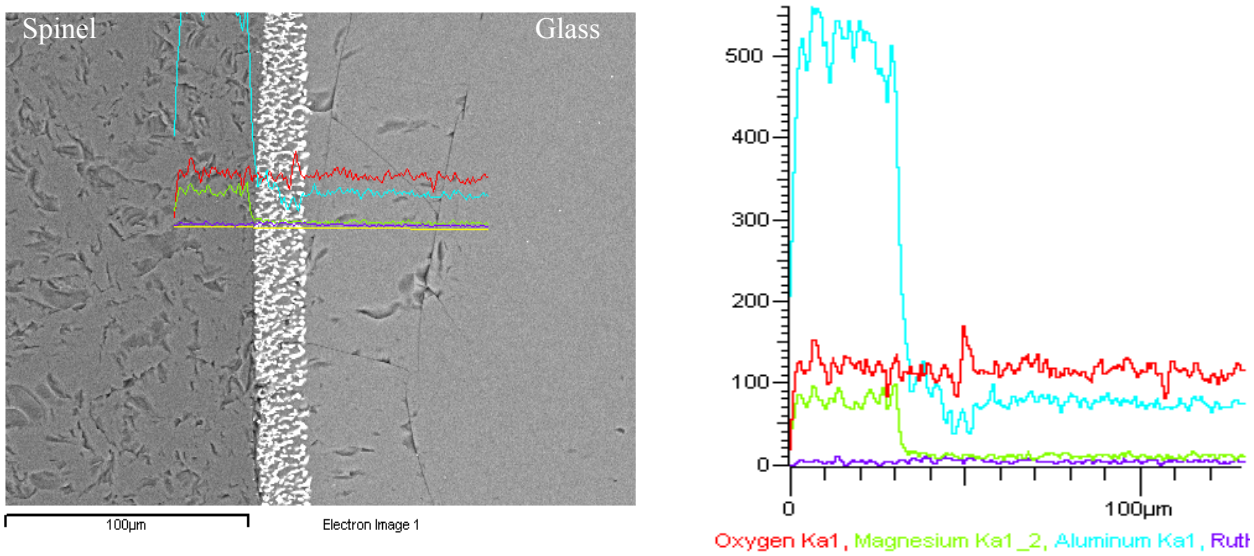

Figure A.2. SEM (Left) – Line EDS (Right) of Ru in MS-7 (900ºC/19h)

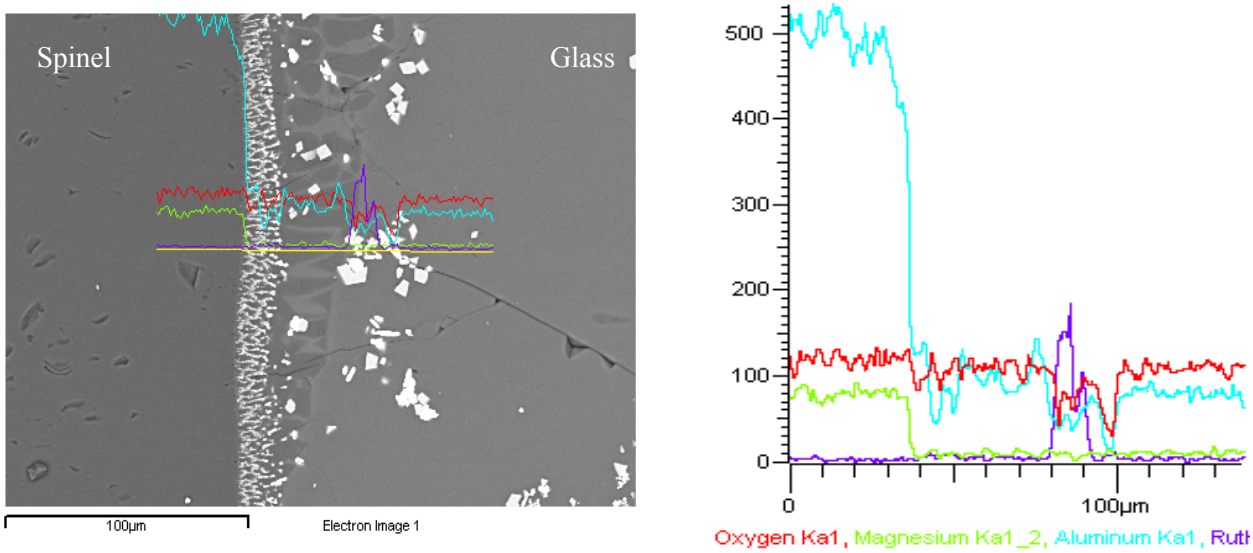

Figure A.3. SEM (Left) – Line EDS (Right) of Ru in MS-7 (900ºC/23h)

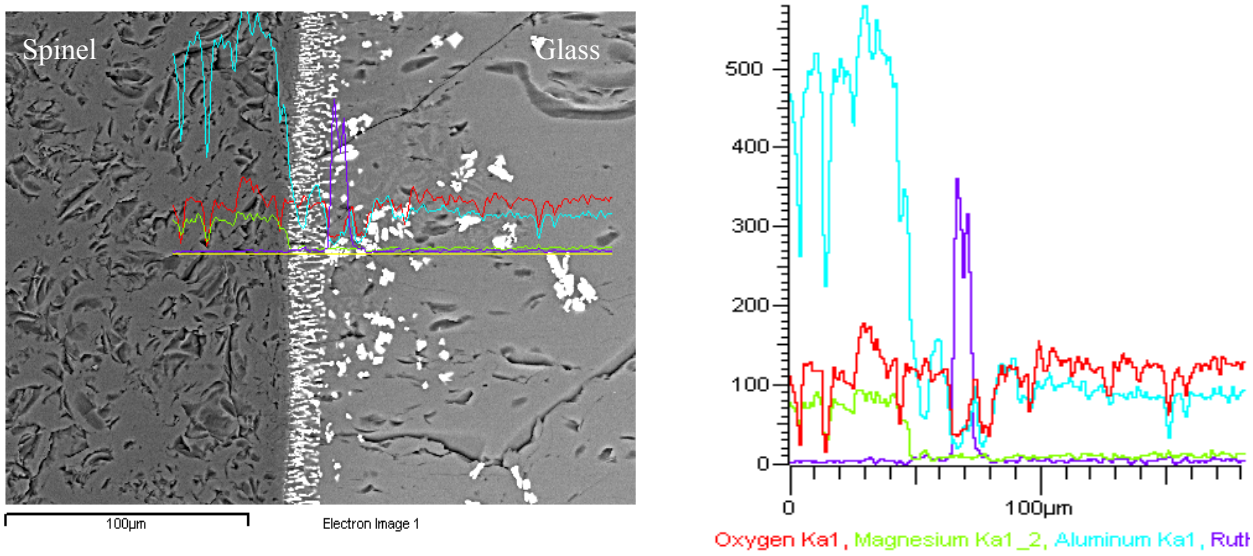

Figure A.4. SEM (Left) – Line EDS (Right) of Ru in MS-7 (1000ºC/7h)

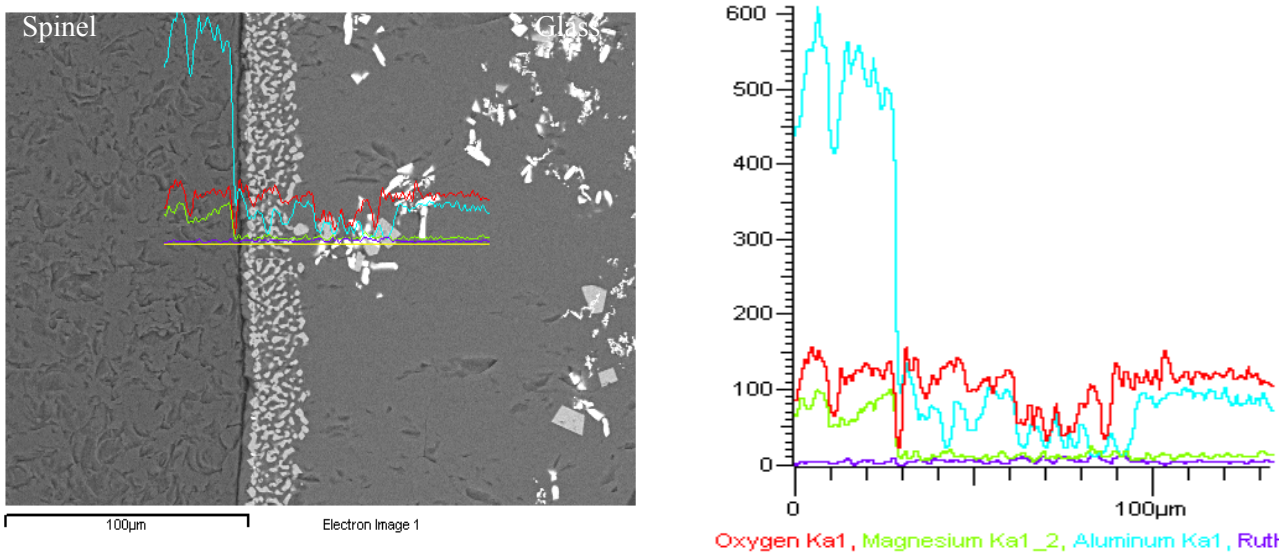

Figure A.5. SEM (Left) – Line EDS (Right) of Ru in MS-7 (1000ºC/15h)

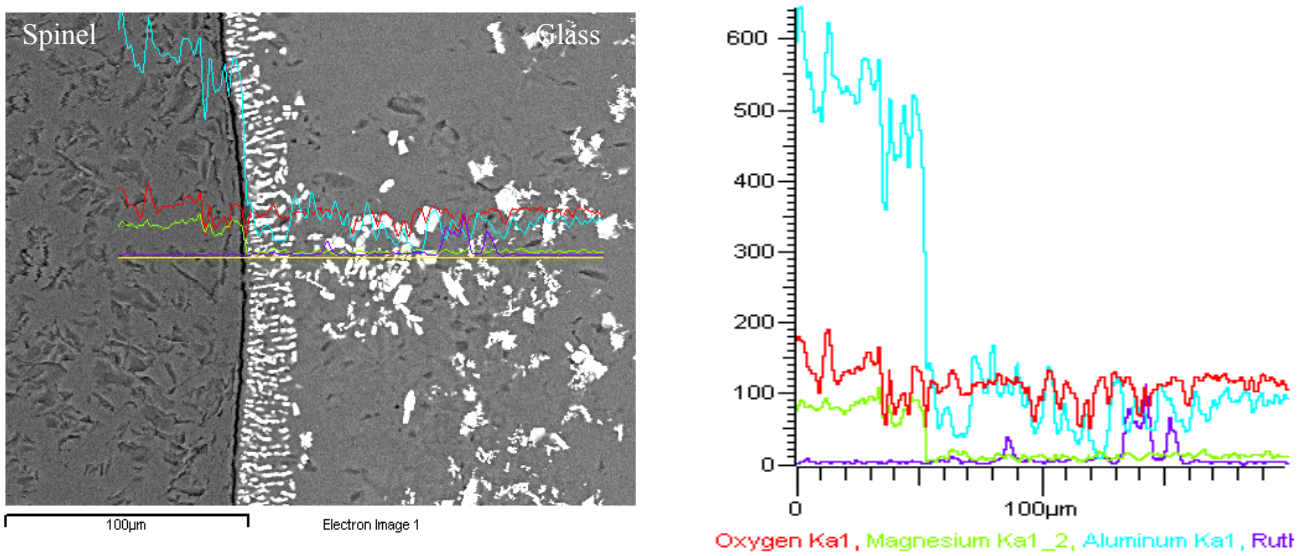

Figure A.6. SEM (Left) – Line EDS (Right) of Ru in MS-7 (1000ºC/19h)

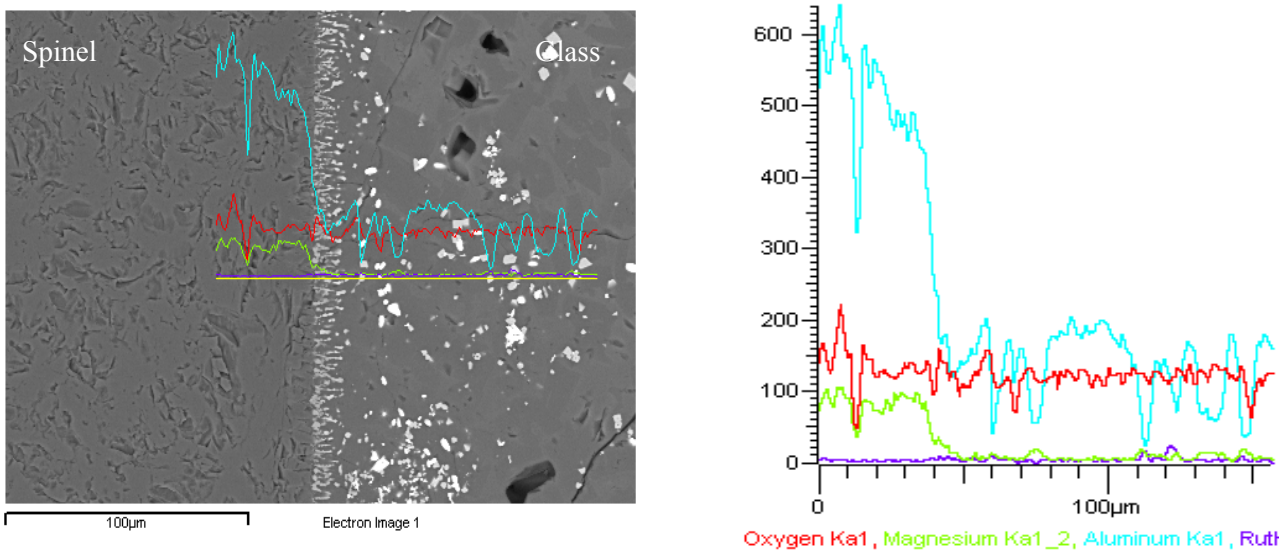

Figure A.7. SEM (Left) – Line EDS (Right) of Ru in MS-7 (1000ºC/23h)

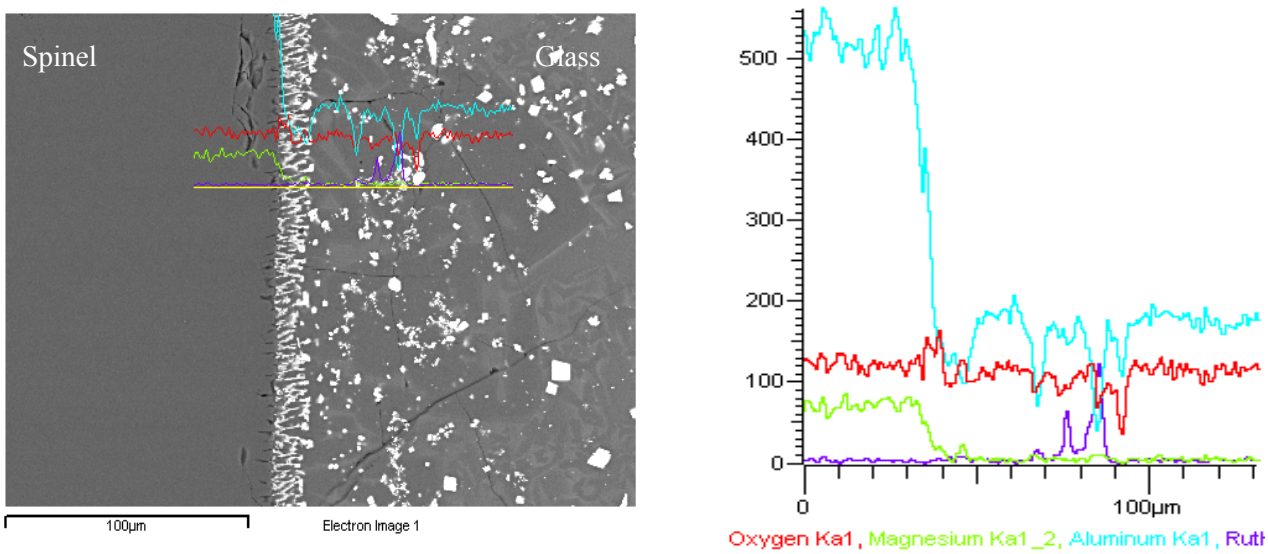

Figure A.8. SEM (Left) – Line EDS (Right) of RuO_2 in MS-7 (900ºC/15h)

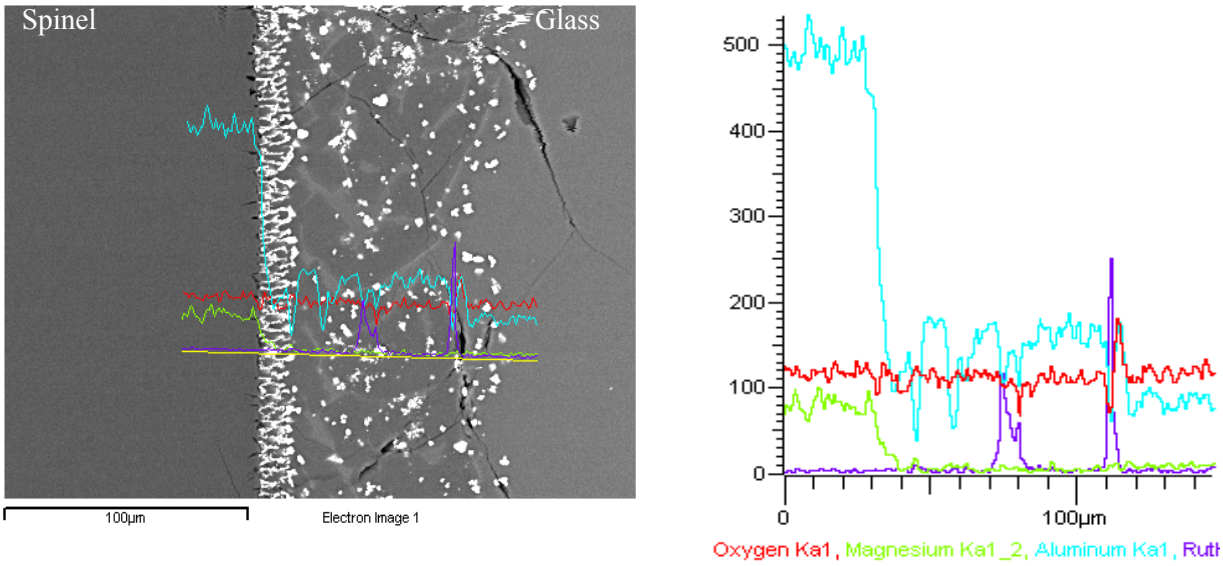

Figure A.9. SEM (Left) – Line EDS (Right) of RuO_2 in MS-7 (900ºC/19h)

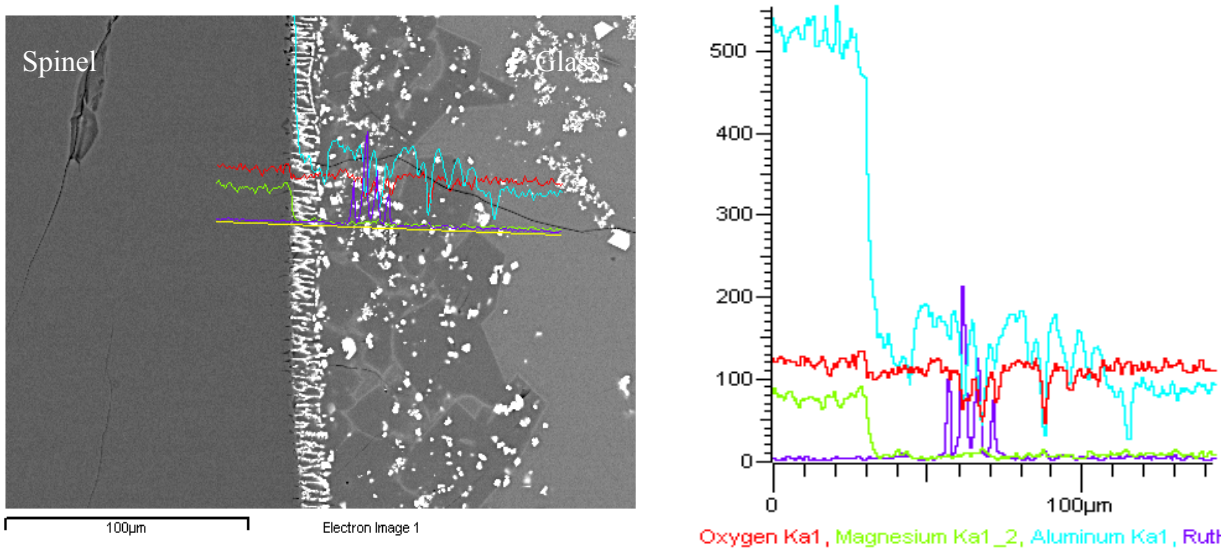

Figure A.10. SEM (Left) – Line EDS (Right) of RuO_2 in MS-7 (900ºC/23h)

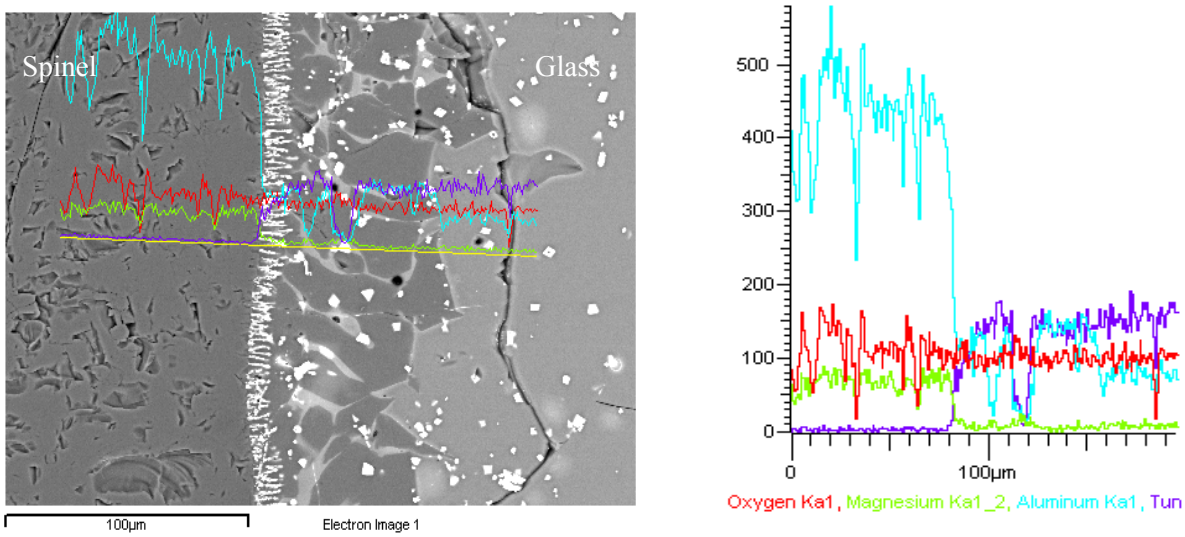

Figure A.11. SEM (Left) – Line EDS (Right) of W in MS-7 (900ºC/15h)

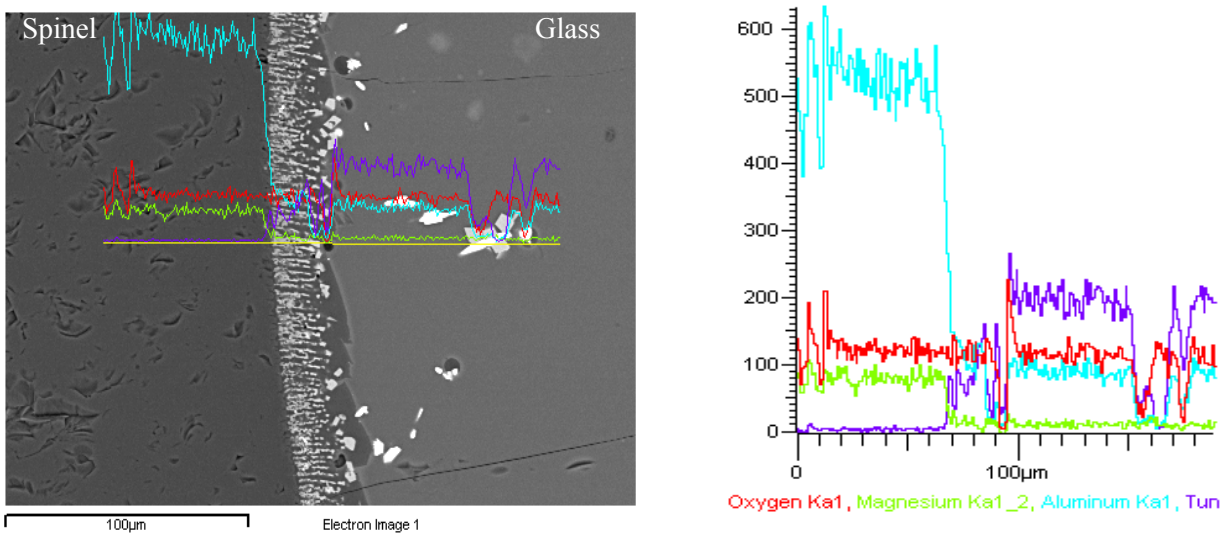

Figure A.12. SEM (Left) – Line EDS (Right) of W in MS-7 (900ºC/19h)

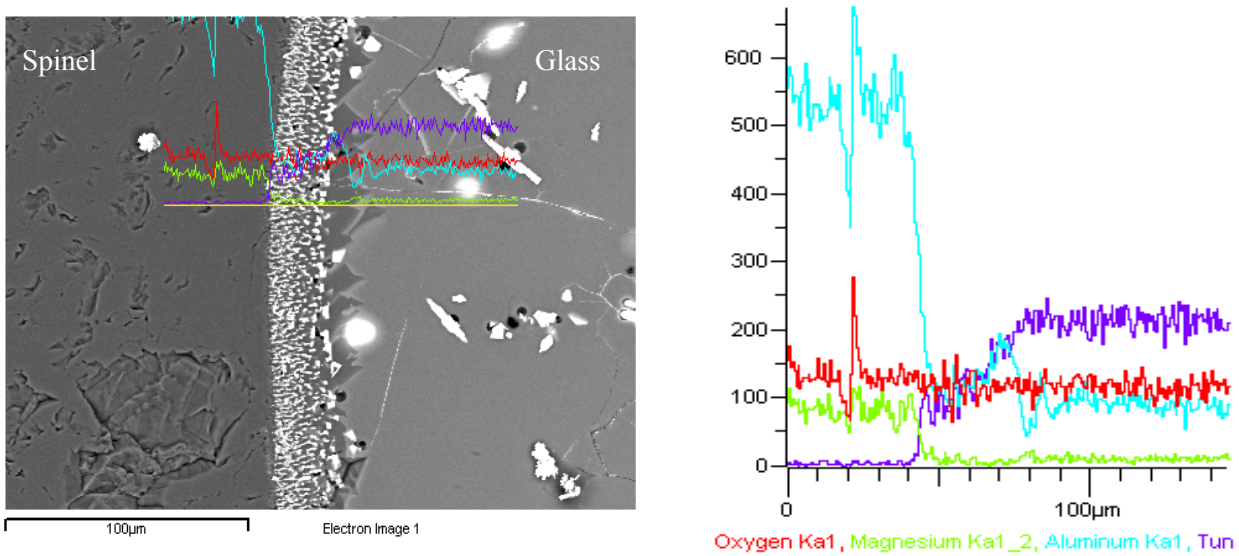

Figure A.13. SEM (Left) – Line EDS (Right) of W in MS-7 (900ºC/23h)

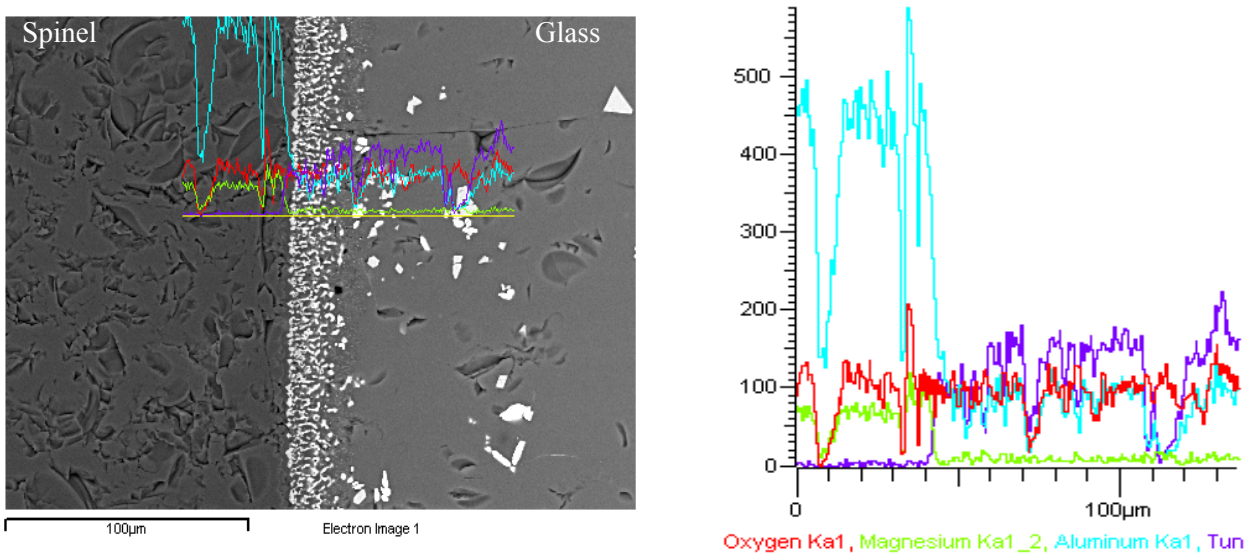

Figure A.14. SEM (Left) – Line EDS (Right) of W in MS-7 (1000ºC/7h)

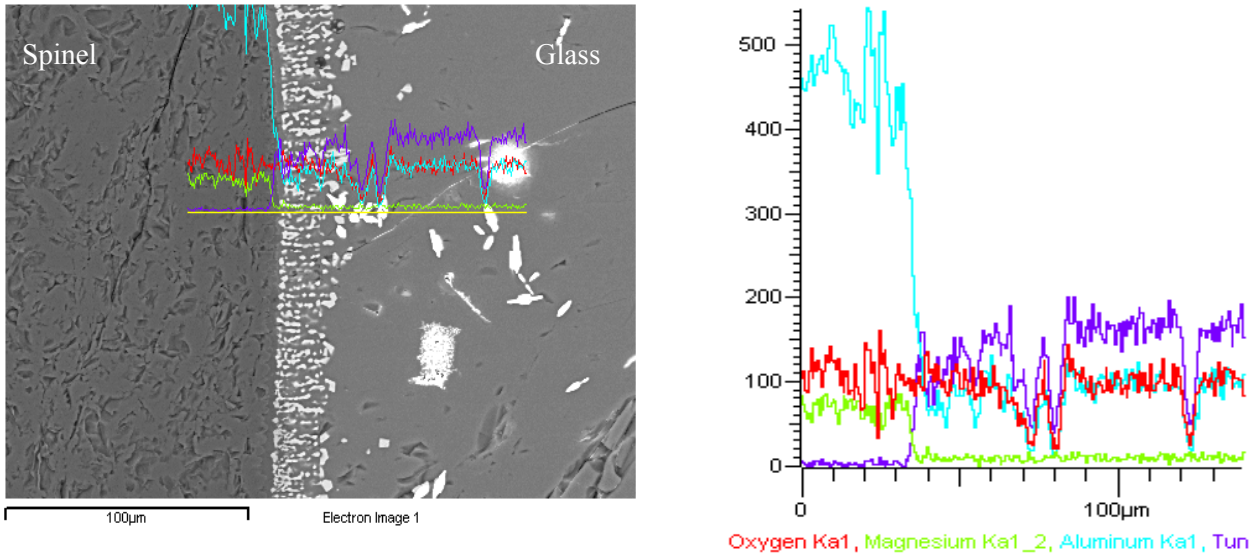

Figure A.15. SEM (Left) – Line EDS (Right) of W in MS-7 (1000ºC/15h)

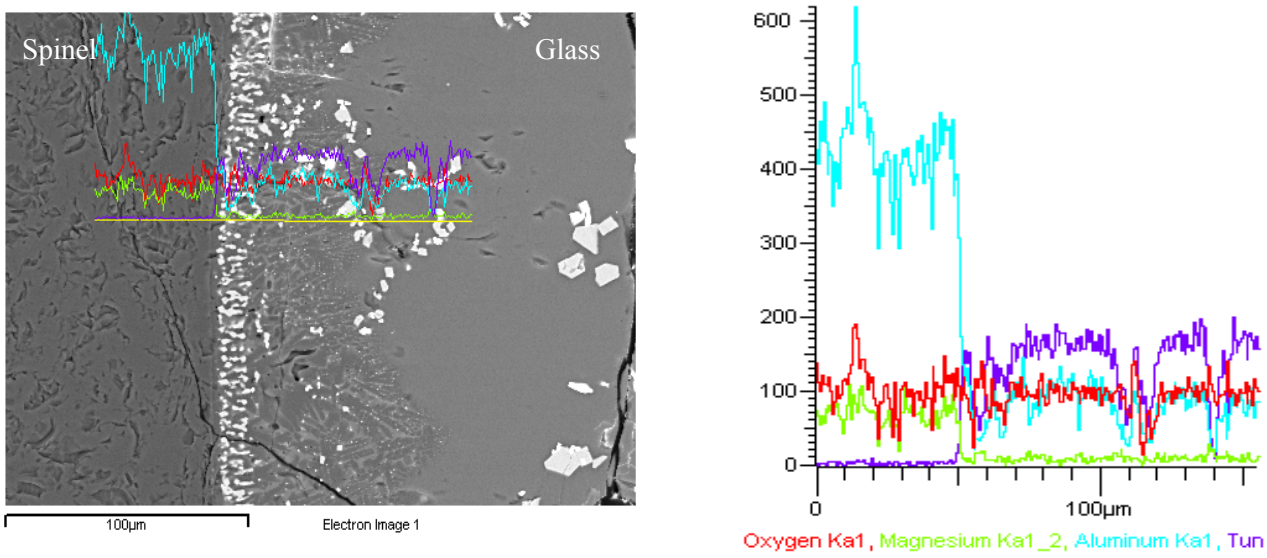

Figure A.16. SEM (Left) – Line EDS (Right) of W in MS-7 (1000ºC/19h)

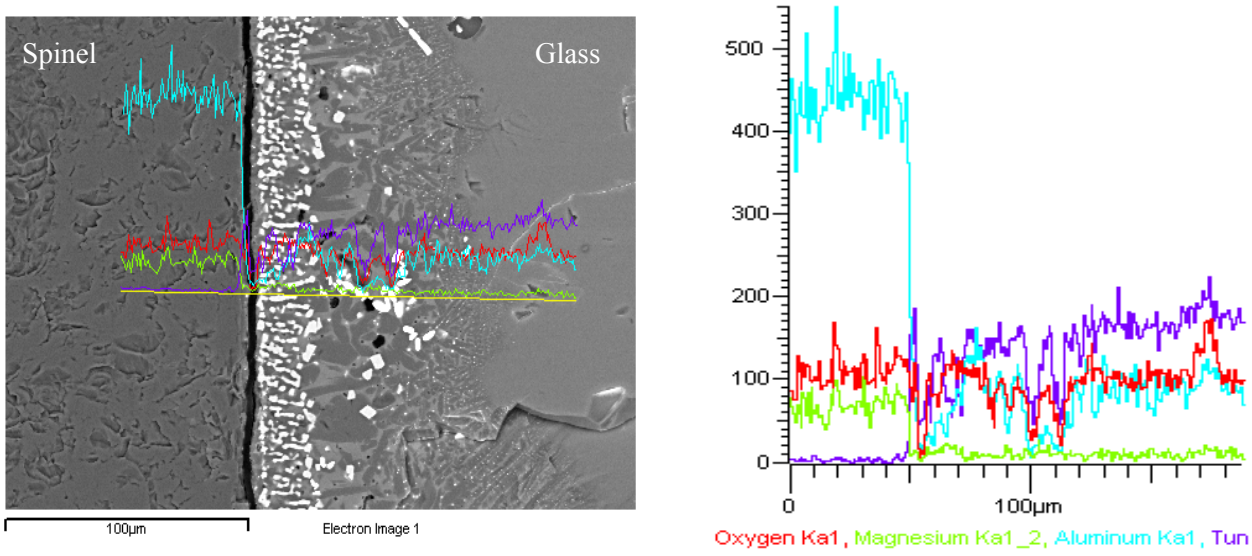

Figure A.17. SEM (Left) – Line EDS (Right) of W in MS-7 (1000ºC/23h)

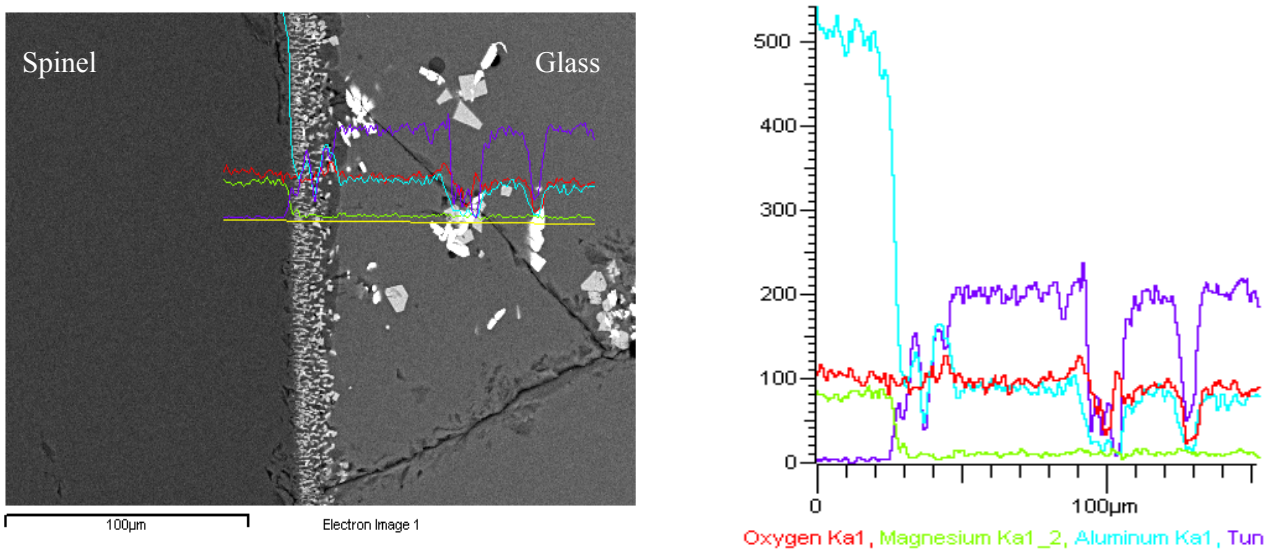

Figure A.18. SEM (Left) – Line EDS (Right) of WO_3 in MS-7 (900ºC/15h)

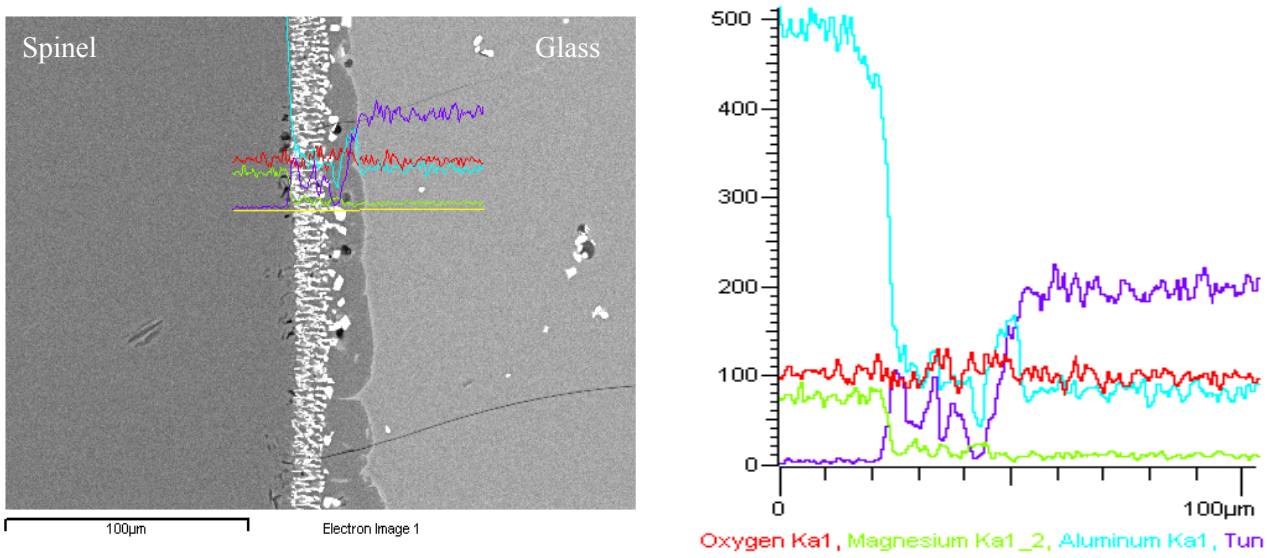

Figure A.19. SEM (Left) – Line EDS (Right) of WO_3 in MS-7 (900ºC/19h)

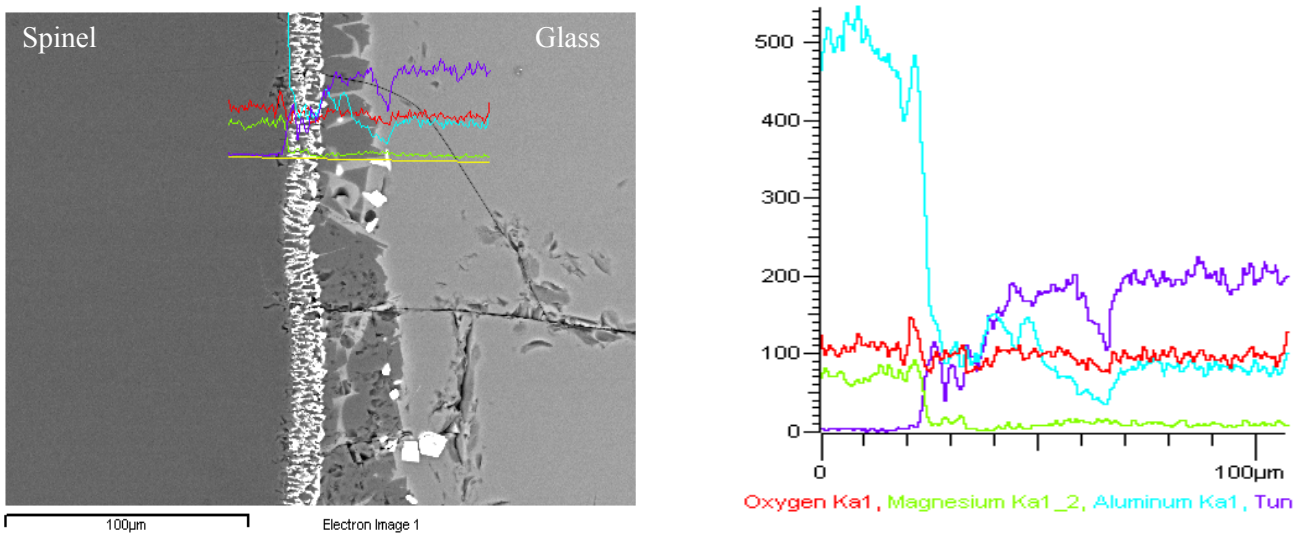

Figure A.20. SEM (Left) – Line EDS (Right) of WO_3 in MS-7 (900ºC/23h)

Distribution

No. of Copies	OFFSITE	
2	U.S. DOE / Office of Scientific and Technical Information	
1	DOE Idaho Operations Office 750 DOE Place, MSIN: 1145 Idaho Falls, ID 83402, Attn: Kieth Lockie	
15	Bechtel BWXT Idaho, Inc. (BBWI) P. O. Box 1625 Idaho Falls, ID 83415, Attn:	
	A. K. Herbst	MS 5218
	J. D. Herzog	MS 3710
	J. L. Law	MS 5218
	A. L. Olson	MS 5218
	W. B. Palmer	MS 3211
	J. Rindfleisch	MS 5218
	T. A. Todd	MS 5218
	J. H. Valentine	MS 3211
22	Westinghouse Savannah River Co. SRTC, Bldg 773-A Aiken, South Carolina 29808, Attn:	
	D. F. Bickford	999-W
	T. B. Calloway	704-1T
	William E. Daniel, Jr.	704-1T
	R. J. O'driscoll	704-30S
	R. F. Edwards	704-25S
	J. T. Gee	704-25S
	C. R. Goetzman	773-A
	E. K. Hansen	704-T
	E. W. Holtzscheiter	773-A
	D. C. Iverson	704-30S
	W. D. Kerley	704-S
	J. C. Marra	773-43A
	S. L. Marra	999-W
	D. K. Peeler	773-43A
	C. T. Randall	773-42A
	F. G. Smith	774-42A
	M. E. Smith	773-43A
	D. Witt	999-W
	J. R. Zamecnik	773-41

No. of Copies	OFFSITE	
1	ENVITCO, Inc., Attn: David M. Bennert	
2	GTS Duratek Inc., Attn: B. W. Bowan Will Eaton	
1	Southwest Research Institute, Attn: Vijay Jain	
	ONSITE	
1	DOE Richland Operations Office P. O. Box 550, MS: K8-50 Richland, Washington 99352	
	T. P. Pietrok	K8-50
1	DOE/Office of River Protection	
	R. Carreon	H6-60
1	CH2M Hill Hanford Group, Attn:	
	K. A. Gaper	L4-07
3	Washington Group	
	J. M. Perez	H4-02
	E. V. Morrey	H4-02
	C. A. Musick	H4-02
32	Pacific Northwest National Laboratory	
	W. F. Bonner	K9-14
	T. M. Brouns	K9-69
	J. L. Buelt	K9-09
	W. L. Kuhn	K7-15
	R. L. Gilchrist	K9-91
	R. W. Goles	K6-24
	L. M. Peurrung	K2-50
	G. L. Smith	K6-24
	H. D. Smith	K6-24
	S. K. Sundaram (10)	K6-24
	J. S. Tixier, Jr.	K6-24
	J. D. Vienna	K6-24
	J. H. Westsik	K9-91
	B. J. Williams (TFA)(8)	K9-69
	Tech. Report Files (2)	P8-55